KETONE PRODUCTION FROM THE THERMAL DECOMPOSITION OF CARBOXYLATE SALTS

A Dissertation

by

MICHAEL LANDOLL

Submitted to the Office of Graduate Studies of
Texas A&M University
in partial fulfillment of the requirements for the degree of

DOCTOR OF PHILOSOPHY

Approved by:

Chair of Committee,	Mark T. Holtzapple
Committee Members,	Mahmoud El-Halwagi
	Charles Glover
	Sergio Capareda
Head of Department,	Charles Glover

December 2012

Major Subject: Chemical Engineering

ABSTRACT

The MixAlco™ process uses an anaerobic, mixed-culture fermentation to convert lignocellulosic biomass to carboxylate salts. The fermentation broth must be clarified so that only carboxylate salts, water, and minimal impurities remain. Carboxylate salts are concentrated by evaporation and thermally decomposed into ketones. The ketones can then be chemically converted to a wide variety of chemicals and fuels.

The presence of excess lime in the thermal decomposition step reduced product yield. Mixtures of calcium carboxylate salts were thermally decomposed at 450 °C. Low lime-to-salt ratios (g $Ca(OH)_2$/g salt) of 0.00134 and less had a negligible effect on ketone yield. In contrast, salts with higher lime-to-salt ratios of 0.00461, 0.0190, and 0.272 showed 3.5, 4.6, and 9.4% loss in ketone yield, respectively. These losses were caused primarily by increases in tars and heavy oils; however, a three-fold increase in hydrocarbon production occurred as well. To predict ketone product distribution, a random-pairing and a Gibbs free energy minimization model were applied to thermal decompositions of mixed calcium and sodium carboxylate salts. Random pairing appears to better predict ketone product composition.

For sodium and calcium acetate, two types of mixed sodium carboxylate salts, and two types of mixed calcium carboxylate salts, activation energy (E_A) was determined using three isoconversional methods. For each salt type, E_A varied significantly with conversion. The average E_A for sodium and calcium acetate was 226.65 and 556.75 kJ/mol, respectively. The average E_A for the two mixed sodium carboxylate salts were

195.61, and 218.18 kJ/mol. The average E_A for the two mixed calcium carboxylate salts were 232.78, and 176.55 kJ/mol. In addition, three functions of conversion were employed to see which one best modeled the experimental data. The Sestak-Berggren model was the best overall. Possible reactor designs and configurations that address the challenges associated with the continuous thermal decomposition of carboxylate salts are also presented and discussed.

Methods of fermentation broth clarification were tested. Flocculation showed little improvement in broth purity. Coagulation yielded broth of 93.23% purity. Filtration using pore sizes from 1 μm to 240 Daltons increased broth purity (90.79 to 98.33%) with decreasing pore size.

DEDICATION

This work is dedicated to my loving family, especially my parents, Patrick and Karen Landoll. I am who I am because of them.

ACKNOWLEDGEMENTS

I would like to thank my advisor and committee chair, Dr. Holtzapple, for his help and support throughout my research and studies here at Texas A&M University. I would also like to thank my committee members, Dr. El-Halwagi, Dr. Glover, and Dr. Capareda, for their guidance and support throughout the course of this research.

Appreciation is given to Dr. Melinda Wales and Dr. John Dunkleman, for their help with my projects, papers, and experiments; Dr. Benjamin Wilhite, Dr. Juergan Hahn, and Dr. Jubo Zhang for their help with experiment design and data analysis; and Dr. Viet Pham and Dr. Mahmoud El-Halwagi for their help with Aspen Plus. Special thanks are given to Dr. Capareda and the BETA laboratory for use of their gas analysis instrumentation, to Dr. Dan Shantz and Dr. Karen Wooley for the use of their TGA instruments, and to Randy Marek for his time, effort, and help with the fabrication and repair of equipment and use of his machine shop.

I also want to extend my gratitude to Dr. Cesar Granda, Dr. Aaron Smith, Dr. Kyle Ross, John Tjaden, John and Rae Spencer, and all the people of Terrabon, Inc. of Houston, TX who generously provided support for this research, use of their equipment and instruments, and for their help with projects

I am grateful for all of the people who helped me pursue an education, get my B.S. in chemistry at Cameron University, and encouraged me to do research and go to graduate school. Thanks also goes to all the friends I have made over these past years in Bryan/College Station, my colleagues, and the department faculty and staff in the Artie

McFerrin Department of Chemical Engineering for making my time at Texas A&M University a great experience. Special thanks to my parents, Patrick and Karen Landoll, and my family for their encouragement and love. Finally, thanks to my Lord and my God, through Him all things are possible.

TABLE OF CONTENTS

Page

Page

LIST OF FIGURES

Page

Page

Page

Page

LIST OF TABLES

Page

Page

1. INTRODUCTION AND LITERATURE REVIEW

Fossil fuels (e.g., petroleum, natural gas, and coal) currently meet most global energy needs; however, growing demand for these depleting resources [1] causes price instability and shortages. Also, fossil fuel combustion causes global warming, acid rain, and pollution [2, 3]. To meet the growing energy needs and help reduce U.S. dependence on foreign oil with a domestic fuel supply, renewable and non-polluting "green" energy sources are becoming increasingly important. Converting biomass into biofuels as a "green" energy source does not cause net increase in atmospheric carbon dioxide [4, 5] because biomass growth removes the same amount of carbon dioxide from the atmosphere that was released during biofuel combustion [2]. The two most common biofuels are bioethanol and biodiesel, which are made from starchy grains and seed oils, respectively.

Lignocellulosic biomass is the largest biological renewable energy source in the world, with a production of ~200×10^9 tons/year [6, 7]. To unlock the potential of lignocellulose, which is much more abundant and less costly than other forms of biomass, new technologies are required. One promising option is the carboxylate platform, which produces liquid fuels from lignocellulose [8].

An example of the carboxylate platform is the MixAlco™ process, which converts biomass to liquid fuels and industrial chemicals. It reduces dependence on fossil fuels, provides an alternative to more expensive renewable energy resources, and is more easily scaled down than thermochemical techniques. The MixAlco™ process

(Figure 1-1) is a biomass-to-energy technology that biologically converts biomass (e.g., lignocellulose, lipids, proteins, carbohydrates) into carboxylate salts via anaerobic mixed-acid fermentation. The carboxylate salts are concentrated and chemically converted into chemicals, solvents, and fuels (e.g., ketones, alcohols, gasoline) [9-11]. In the fermentation step, biomass is fermented by a mixed culture of microorganisms to produce carboxylic acids. After the fermentation step, metal hydroxide, carbonate, or bicarbonate buffers are added to convert the acids to their corresponding carboxylate salts, which are then precipitated via a dewatering process. The salts are thermally decomposed to form ketones (e.g., acetone), hydrogenated to produce mixed alcohols (e.g., isopropanol), and catalytically converted to hydrocarbons (e.g., gasoline, jet fuel). This continuous and versatile process produces liquid fuels that can be fully used by existing engines, uses nearly any biomass feedstock (minimizing market distortions and food scarcity), has low capital and operating costs, does not require sterile operating conditions or added enzymes, and has already reached the demonstration level of development.

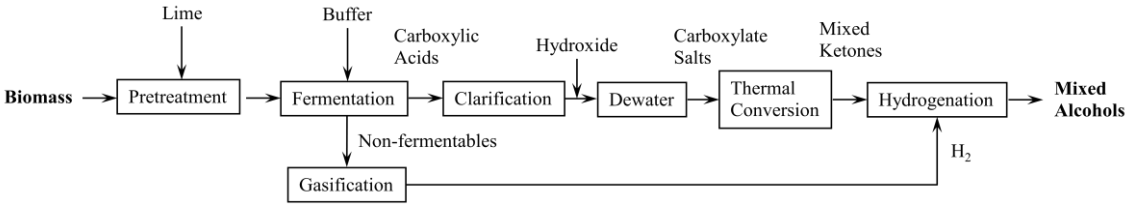

Figure 1-1. MixAlco™ process diagram.

This research focuses on the thermal decomposition of the carboxylate salts to ketones as shown in Equation 1-1.

$$RCOOM + R'COOM \xrightarrow{\Delta} RCOR' + M_2CO_3 \quad (1\text{-}1)$$

R can be any hydrocarbon group and M can be any metal (generally, any alkali metal or half of any alkaline earth metal). For purposes of this research, M can be either a sodium ion or half of a calcium ion and R can be any one of the groups associated with the nine carboxylic acids produced from MixAlco™ fermentations [12-14]. This reaction was first observed by Eugene Melchior Peligot who thermally decomposed calcium acetate to yield acetone [15]. Later, Williamson demonstrated the same reaction with other calcium carboxylate salts, as well as mixtures of calcium carboxylate salts, which yielded mixtures of corresponding ketones. Since then, the thermal decomposition of numerous carboxylate salts has been studied [16]. The ketone yield from the thermal decomposition of various individual and mixed carboxylate salts has been studied in a variety of environments [17-21]. Several researchers have even studied reaction mechanisms using tracer isotopes [22-31]. These studies have resulted in a multitude of proposed mechanisms, none of which are soundly conclusive. Various mechanisms have been proposed involving carbanions [29, 31] (Equations 1-2 and 1-3), carbonium ions [24, 25] (Equation 1-4), free radicals [22, 23, 28] (Equation 1-5), and a four-center intermediate [27] (Equation 1-6), also known as a concerted mechanism. Unfortunately, none of the proposed mechanisms fully explain the data, leading some investigators to propose that decomposition proceeds by more than one mechanism [25].

$$\begin{aligned} RCOOM &\rightarrow R^- + CO_2 + M^+ \\ R'COOM + R^- &\rightarrow R'COR + MO^- \\ M^+ + MO^- &\rightarrow M_2O \end{aligned} \qquad (1\text{-}2)$$

$$\begin{aligned} RCH_2COOM &\rightarrow RC^-HCOOM + H^+ \\ RC^-HCOOM + R'COOM &\rightarrow R'CCHCOOM + MO^- \\ & \qquad\qquad\qquad\quad \| \ | \\ & \qquad\qquad\qquad\quad O \ R \\ R'CCHCOOM + H^+ &\rightarrow R'CCH_2R + CO_2 + M^+ \\ \| \ | \qquad\qquad & \qquad\quad \| \\ O \ R \qquad\qquad & \qquad\quad O \\ M^+ + MO^+ &\rightarrow M_2O \end{aligned} \qquad (1\text{-}3)$$

$$\begin{aligned} RCOOM &\rightarrow RC^+O + MO^- \\ R'COOM + RC^+O &\rightarrow R'COR + CO_2 + M^+ \\ M^+ + MO^- &\rightarrow M_2O \end{aligned} \qquad (1\text{-}4)$$

$$\begin{aligned} RCOOM &\rightarrow R\cdot + \cdot COOM \\ R'COOM + R\cdot &\rightarrow R'COR + \cdot OM \\ \cdot COOM + \cdot OM &\rightarrow M_2CO_3 \end{aligned} \qquad (1\text{-}5)$$

$$\begin{array}{l} \quad O \\ \quad \| \\ R\text{-}C\text{-}OM \\ \quad \vdots \ \vdots \\ R'\text{-}C\text{-}OM \\ \quad \| \\ \quad O \end{array} \quad \rightarrow \quad \begin{array}{l} \quad O \\ \quad \| \\ RCR' + M_2CO_3 \end{array} \qquad (1\text{-}6)$$

Models of this thermal decomposition reaction must be developed to make this step in the MixAlco™ process a viable unit operation that can be scaled up for commercial use, optimized, and have the flexibility necessary to accommodate different

types of carboxylate salts. In addition, how the decomposition is affected by impurities commonly found in MixAlco™ salts must also be characterized.

This study looks at the following areas:

- Accurately modeling product composition from the thermal decomposition of carboxylate salts with and without additives.
- Defining kinetic parameters and developing a mechanism(s), that describes the thermal decomposition of individual and mixed carboxylate salts.
- Developing simple methods for determining kinetic parameters.
- Developing reactors to decompose salts in a continuous fashion on a commercial scale.

1.1. Legal disclaimer

MixAlco™ is a registered trademark of Terrabon, Inc. Unless otherwise noted in this document, inclusion of such trademark in this document does not imply support or endorsement by Terrabon, Inc.

2. THERMAL DECOMPOSITION OF MIXED CALCIUM CARBOXYLATE SALTS: EFFECTS OF LIME ON KETONE YIELD*

2.1. Introduction

In the MixAlco™ process, lignocellulosic biomass is first pretreated with calcium hydroxide (lime) to increase digestibility and is then fermented by a mixed culture. Carboxylic acids (e.g., acetic, propionic, and butyric acid) are the desired products of the fermentation. Calcium carbonate buffers the fermentation pH between 5.8 and 6.2; thus, the corresponding carboxylate salts (e.g., calcium acetate, propionate, and butyrate) are formed. The fermentation broth is clarified and then dewatered, which involves evaporating all volatiles in the broth, leaving the precipitated solids. After dewatering, the remaining solids are mostly calcium carboxylate salts with small amounts of cells, extracellular proteins, and minerals.

*Reprinted from Biomass and Bioenergy, 35, Landoll M, Holtzapple MT, Thermal decomposition of mixed calcium carboxylate salts: effects of lime on ketone yield, 3592–3603, Copyright (2011), with permission from Elsevier.

The carboxylate salts are thermally decomposed to yield their corresponding ketones, as shown in Equation 2-1.

$$(RCOO^{-})\ Ca^{2+}\ (R'COO^{-}) \xrightarrow{\Delta} RCOR' + CaCO_3 \qquad (2\text{-}1)$$

To fully convert the acids to their corresponding salts, additional lime is added before the dewatering step. If not enough lime is added, the un-ionized acids that are not converted to salts will be lost to the vapor phase during evaporation. At about pH 8, the carboxylic acids completely convert to their corresponding salts. At a commercial scale, the simplest way to ensure sufficient lime addition is to add a slight excess of lime, which then becomes incorporated into the remaining solids. Young [32] stated that thermal decomposition of calcium acetate in the presence of free lime decreased acetone yield. Other sources state that thermal decomposition of carboxylate salts in the presence of lime yields higher amounts of hydrocarbons, thereby decreasing ketone yield [16, 21, 33]. This competing reaction is shown in Equation 2-2.

$$(RCOO^{-})\ Ca^{2+}\ (R'COO^{-}) + Ca(OH)_2 \xrightarrow{\Delta} RH + R'H + 2\ CaCO_3 \qquad (2\text{-}2)$$

For the purpose of this study, R and R’ in both equations can be any one of nine groups associated with the nine carboxylic acids listed in Table 2-1.

Table 2-1. Acid and corresponding salt profiles of reagent-grade salts.

Carbon Number	Acid	Acid (wt. %)	Salt (wt. %)
2	Acetic	54.69	56.77
3	Propionic	14.71	14.57
4	Isobutyric	0.94	0.90
4	Butyric	11.12	10.66
5	Isovaleric	0.70	0.66
5	Valeric	6.39	5.97
6	Caproic	8.03	7.37
7	Heptanoic	2.90	2.62
8	Octanoic	0.52	0.47

To develop a viable process, it is necessary to address the following questions: Does the presence of excess lime in mixed carboxylate salts affect the ketone yield upon thermal decomposition? If so, how sensitive is the ketone yield to the presence of lime and what byproducts are produced? To answer these questions, mixtures of reagent-grade calcium carboxylate salts were thermally decomposed with varying amounts of lime to determine if there were any changes in ketone yield and product composition. The use of reagent-grade salts eliminated reactions associated with impurities found in fermentation salts allowing changes in the ketone yield to be attributed to the presence of excess lime. The reagent-grade salt composition closely mimicked that of salts from fermentation broth. For comparison, fermentation salts were employed in one sample run. In this section, any solid mixture composed of mostly calcium carboxylate salts will be described as *feed salts*.

2.2. Materials and methods

2.2.1. Preparation of salts

Reagent-grade feed salts were prepared by mixing the corresponding reagent-grade carboxylic acids with equimolar amounts of calcium hydroxide in deionized water resulting in a solution of pH 8. The composition of the acids and corresponding salts were verified by gas chromatography (Table 2-1). These acid and corresponding salt profiles are typical of what has been reported for anaerobic mixed-culture fermentation [12-14]. A 2-L aliquot of this solution was taken and evaporated in a glass beaker. The dry solids (reagent-grade feed salts) were collected and weighed. To additional 2-L aliquots, excess lime was added to make solutions of pH 9, 10, 11, and 12. These solutions were also evaporated in glass beakers and the remaining reagent-grade feed salts were collected and weighed. Another 2-L aliquot of pH 8 solution was evaporated and 20% excess lime (0.2 g $Ca(OH)_2$/g feed salt) was added to the remaining reagent-grade feed salts. Fermentation feed salts were prepared using clarified broth from a MixAlco™ fermentation (Terrabon, Inc, Houston, TX). Clarification was performed using a proprietary process involving flocculant and a decanter centrifuge. The broth was adjusted to pH 9 by adding excess lime and then evaporated to collect the fermentation feed salts (see Table 2-2). For each solution, the amount of excess lime per amount of carboxylic salt (lime-to-salt ratio) was calculated (Table 2-3).

Table 2-2. Acid and corresponding salt profile of fermentation feed salts.

Carbon number	Acid	Acid (wt. %)	Salt (wt. %)
2	Acetic	48.87	50.92
3	Propionic	12.44	12.38
4	Isobutyric	0.91	0.87
4	Butyric	21.92	21.10
5	Isovaleric	1.25	1.17
5	Valeric	6.65	6.24
6	Caproic	6.80	6.26
7	Heptanoic	0.93	0.84
8	Octanoic	0.23	0.20

Table 2-3. Salt content and lime-to-salt ratio for feed salts from each solution.

Solution	Type	Salt Content (g salt/g solid)	Lime-to-Salt Ratio (g $Ca(OH)_2$/g salt)
pH 8	Reagent grade	0.862	0
pH 9	Reagent grade	0.860	0.000672
pH 10	Reagent grade	0.860	0.00134
pH 11	Reagent grade	0.861	0.00461
pH 12	Reagent grade	0.845	0.0190
20% Lime	Reagent grade	0.697	0.272
pH 9	Fermentation broth[c]	0.795	0.000672

[c] Fermentation feed salts provided by Terrabon, Inc.

2.2.2. Apparatus

Figure 2-1 is a schematic of the apparatus. Reactions occurred in a 2-L stirred reactor (Parr 4501, Parr Instrument Co., Moline, IL). As Figure 2-2 illustrates, the reactor head contained five ports. Port 1 was connected to the holding chamber. Port 2 was connected to a pressure gauge for pressure measurement. Port 3 was connected to a ball valve for pressure relief. Port 4 was connected to a series of three condensers (Figure 2-3). Port 5 was the thermal well for the thermocouple. Figure 2-4 shows the details of the holding chamber. It was equipped with a screw conveyor, which acted as a loading mechanism to deliver feed salts into the reactor. It also contained a unique "fan valve" to keep the feed salts in the vessel until the desired temperature in the reactor was reached. The fan valve consisted of a stationary plate mounted to the housing of the feeder and a rotating seal plate attached to the center shaft of the screw conveyor. Before feed salts were placed into the feeder, the rotating seal plate was set to a position that completely covered the opening of the stationary plate. In this way, feed salts were kept in the feeder. When the screw conveyor was turned on, the seal plate rotated and feed salts flowed through the opening of the stationary plate. Figure 2-5 shows the fan function in detail.

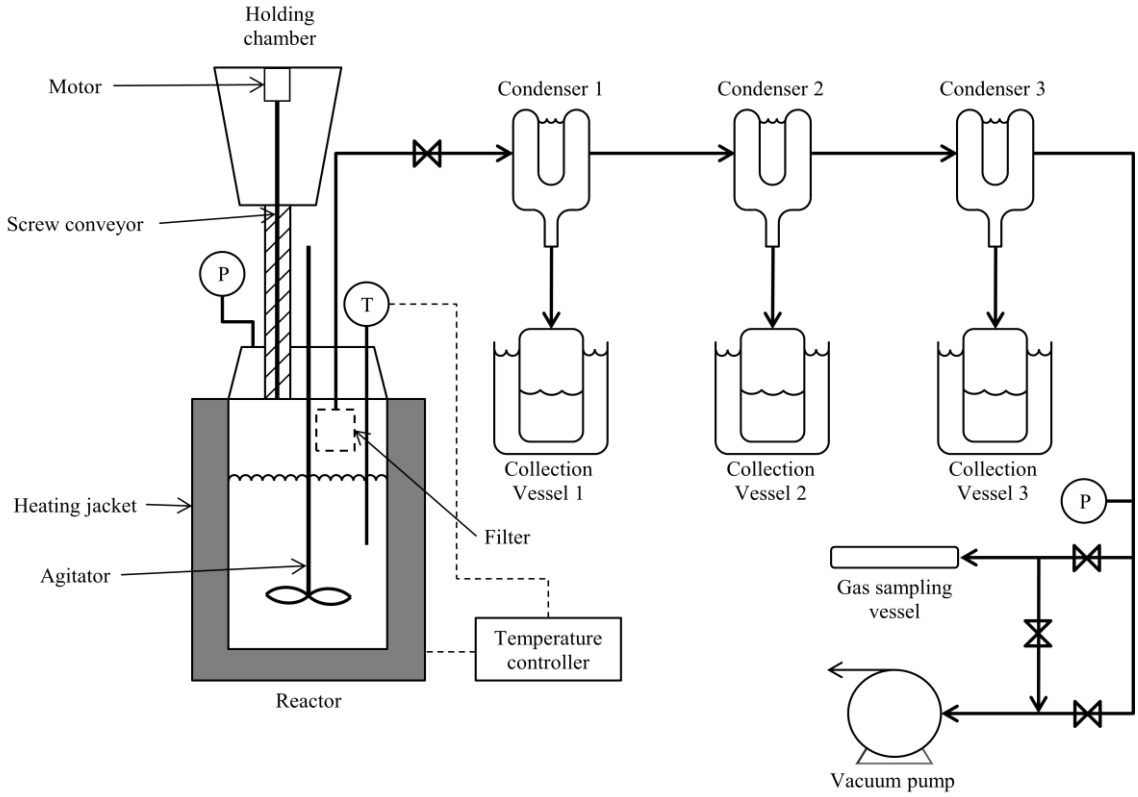

Figure 2-1. Schematic of apparatus used to thermally decompose feed salts and collect products.

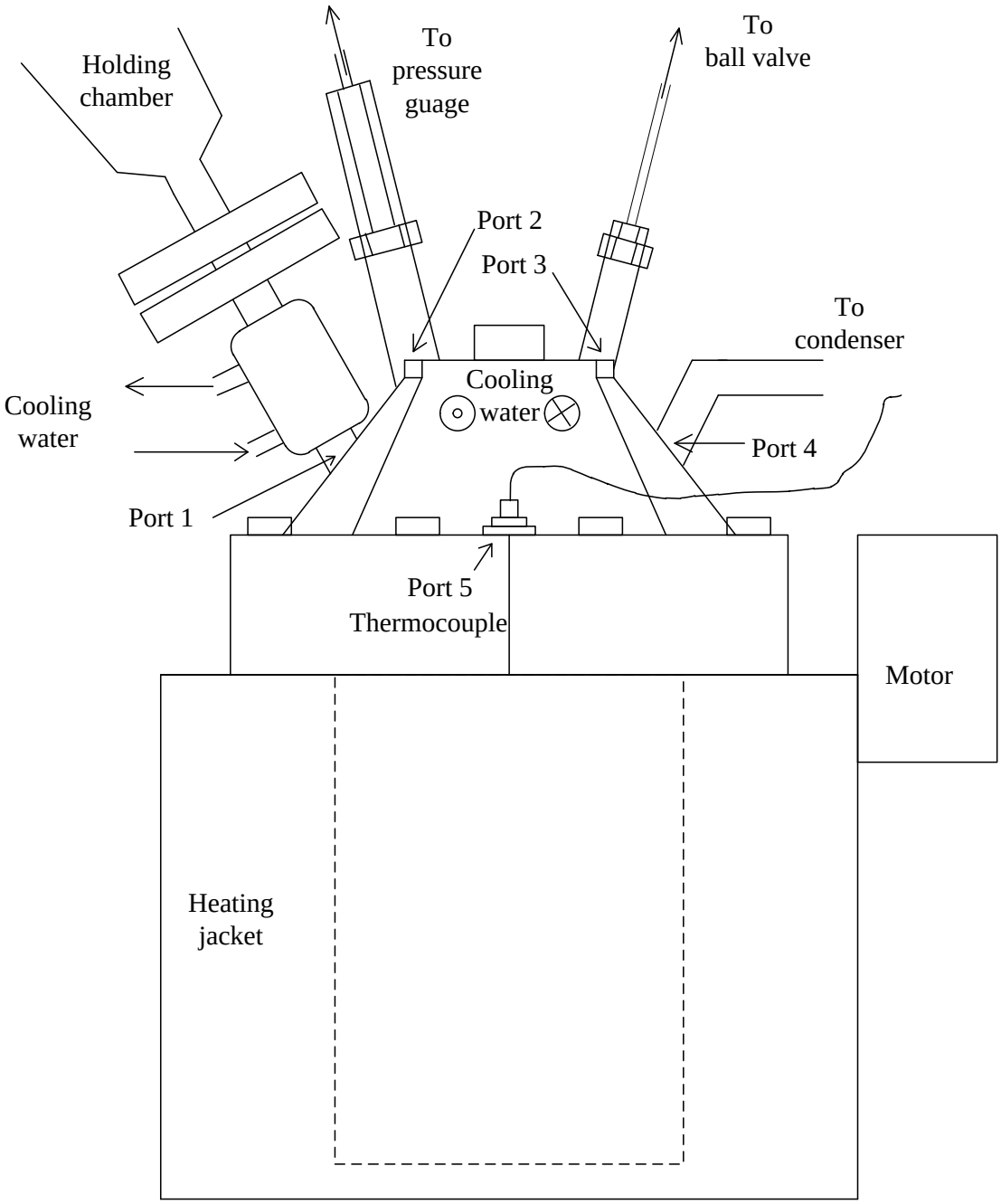

Figure 2-2. Parr 4501 reactor.

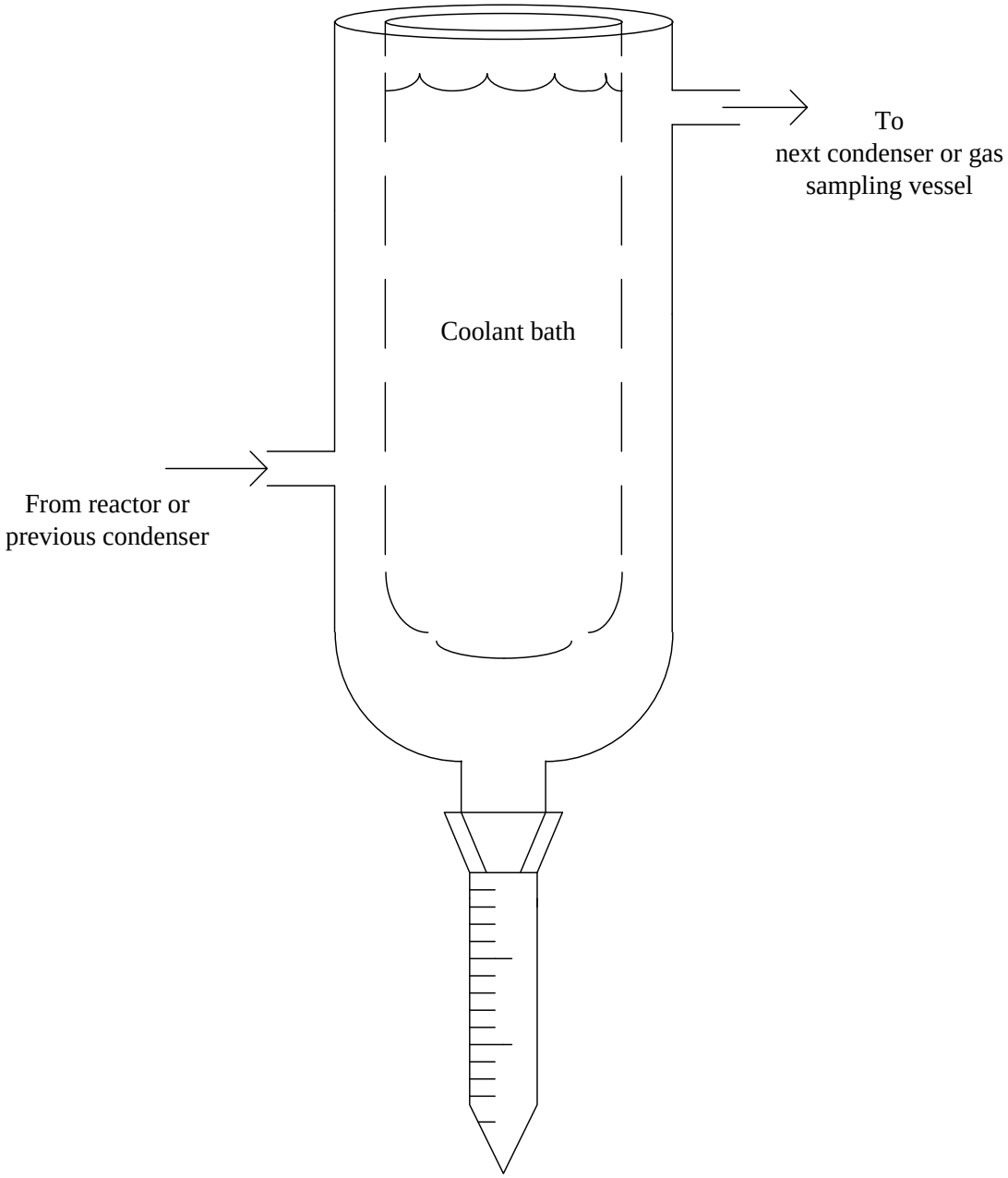

Figure 2-3. Condenser and graduated collection tube (collection vessel).

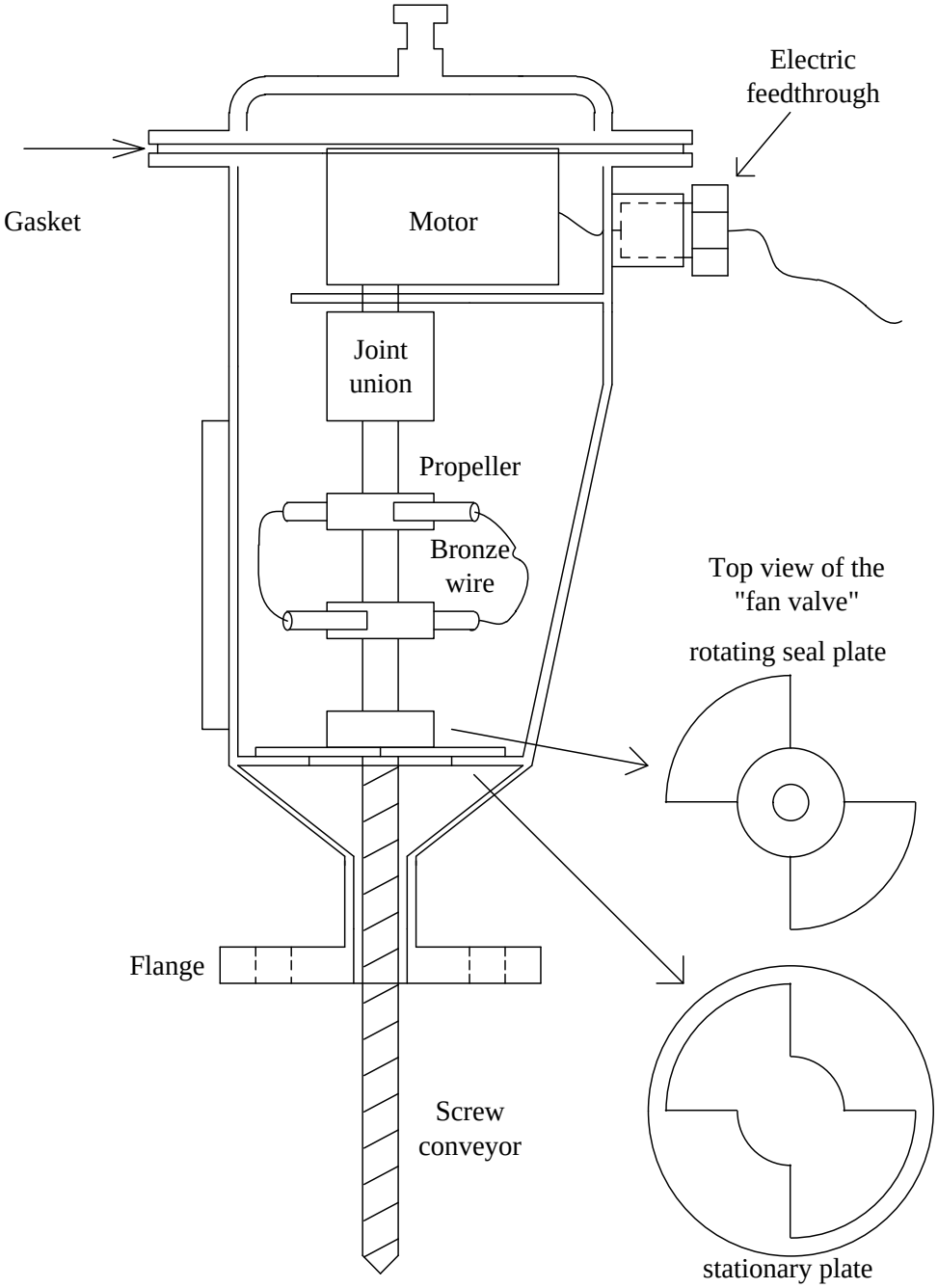

Figure 2-4. Holding chamber.

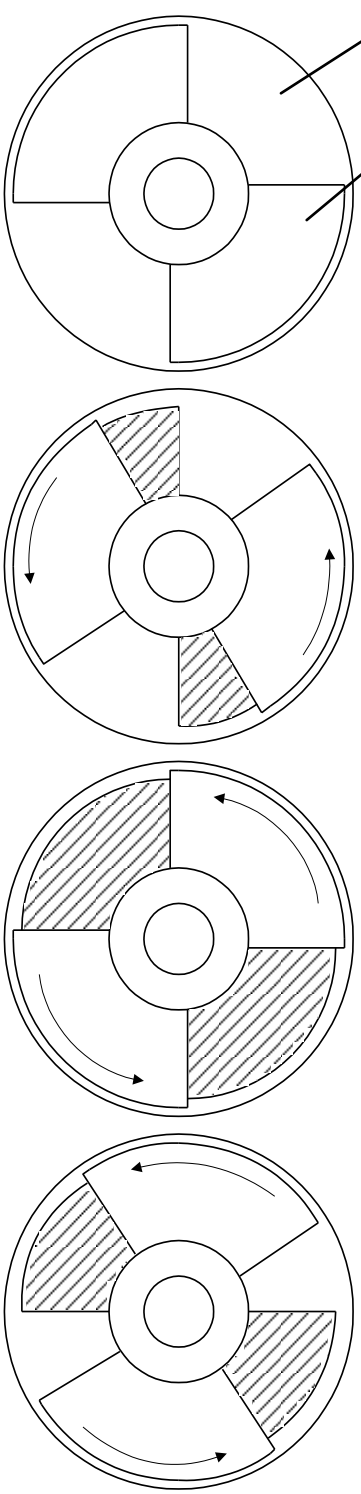

Phase 1. Before the screw conveyor was turned on, the rotating seal plate completely covered the opening of the stationary plate.

Phase 2. The conveyor was turned on. The seal plate rotated with the screw conveyor revealing the opening in the stationary plate. Feed salt loading commenced. The shaded area represents the opening.

Phase 3. The seal plate rotated to the position that provided the maximum opening area for feed salt loading.

Phase 4. The rotating seal plate started to cover the opening again. Then the rotating seal plate returned to Phase 1 and the process was repeated until the screw conveyor was turned off.

Figure 2-5. Phases of the "fan valve" (top view).

The reactor had a 100-µm porous stainless steel filter (Figure 2-6) fitted to the outlet that retained solid particles but allowed vapor to pass through. It was set inside the reactor at the mouth of Port 4. Glass beads were used in the reactor to ensure adequate mixing and to provide thermal mass to help maintain the temperature during delivery of feed salts. Temperature was maintained with a 1500-W heating jacket connected to an Omega C9000A temperature controller and Type-K thermocouple. Port 4 of the reactor was connected by a ¼-in stainless steel tube to three glass condensers (Figure 2-3) (Ace Glass, #8757-35) in series. The first had ice/water (0 °C), the second had dry ice/isopropanol (–78 °C), and the third had liquid nitrogen (–196 °C). Because of the large range in molecular weights of the product vapors, multiple condensing stages were necessary to ensure maximum product condensation while minimizing solid formation on the condenser surfaces. Each condenser had its own collection vessel for catching condensate, which was immersed in the same cooling media as was used in the condenser to keep the condensate from re-vaporizing. The last condenser exited to a gas sampling vessel and vacuum pump (Welch DuoSeal #1400B-01), both of which could be sealed from the system with valves.

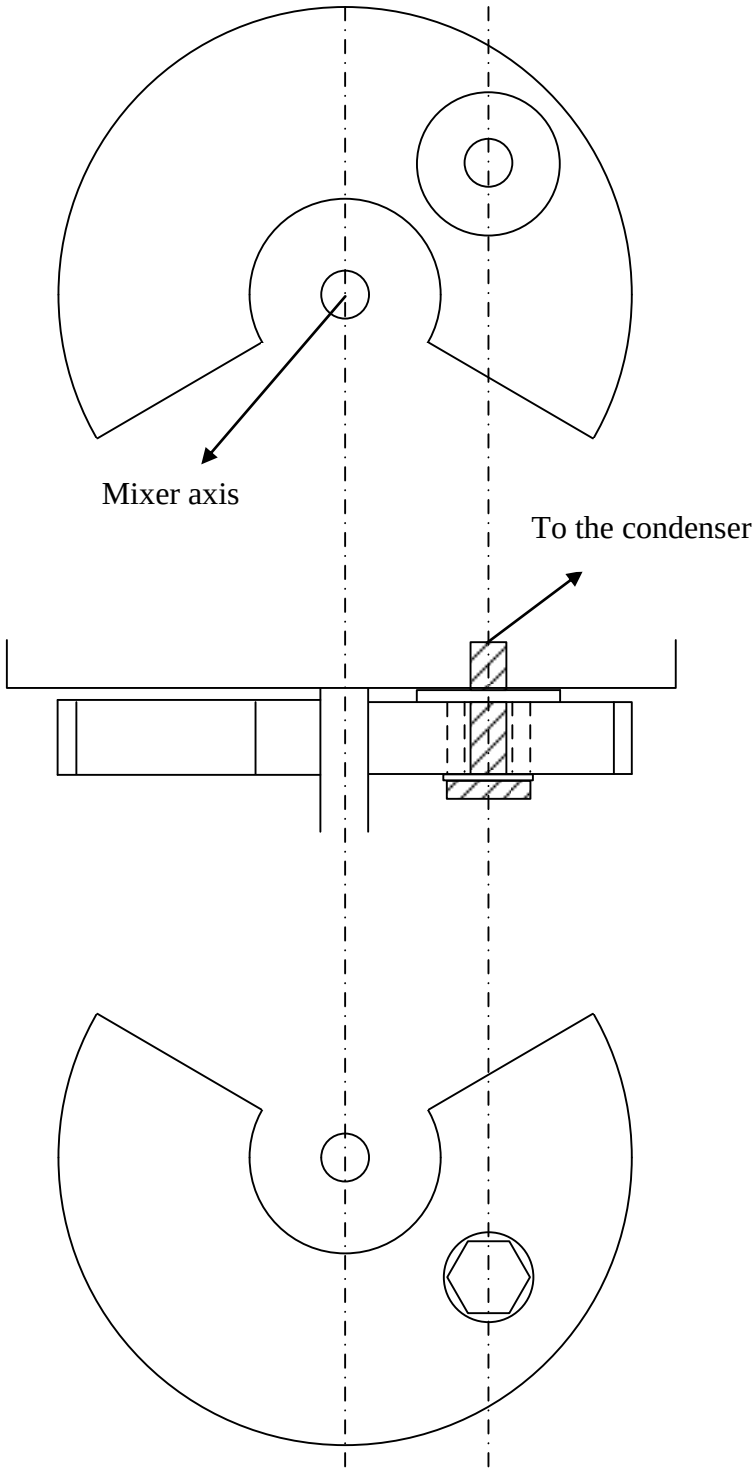

Top view of the filter and the relative position of the mixer axis.

Side view of the filter when it is connected to the reactor head.

Bottom view of the filter and the relative position of the mixer axis.

Figure 2-6. Sintered filter.

2.2.3. Thermal decomposition of feed salts

Charges of prepared feed salts with constant moisture content were weighed (average weight 25 g). In a typical run, 1450 g of borosilicate glass beads (VWR Scientific Product, # 89091-366) were placed in the reactor and the charge of feed salts was placed in the holding chamber. The reactor was sealed and the vacuum pump evacuated the system (~0.4 kPa). The three cooling media were added to their respective condensers and collection vessels. The temperature controller maintained the reactor at 450 °C (±5 °C). Once at temperature, the screw conveyor was turned on to deliver the charge of feed salts into the reactor and the valve to the vacuum pump was closed. After 90 min elapsed, the temperature controller was turned off and the reactor cooled. The condensers came to room temperature and the valve on the gas sampling vessel was closed and removed for gas analysis. The liquid product was removed from the collection vessels and the non-aqueous fraction was decanted. Both the aqueous and non-aqueous fractions were weighed and analyzed. When the reactor had cooled to near room temperature, the residual solids were weighed and dissolved with 200.0 mL of 3-M H_3PO_4 and 300.0 mL of deionized water. Residual solids not dissolved in the solution were filtered using an Advantec MFS #5C filter. The filtrate was analyzed via gas chromatography to determine the amount of unreacted salts in the residual solids. The average mass balance closure was 98.3%. The average fractional conversion was 0.881. Fermentation feed salts were thermally decomposed at Terrabon, Inc. using a similar apparatus and experimental conditions.

2.2.4. Solids analysis

Calcium carboxylate salts are hygroscopic, usually forming a monohydrate in the presence of water vapor [34]. All feed salts were dried to a constant moisture content at 105°C for at least 24 h and placed in a desiccator. Samples of feed salts were weighed (0.3 g) and dissolved with 2 mL of 3-M phosphoric acid. The mixture was then diluted to 10 mL with deionized water. Solutions of both dissolved feed salts and dissolved residual solids were mixed with equal parts of a 1.162 g/L solution of 4-methyl-valeric acid (internal standard) and 3-M phosphoric acid. Acid analysis was performed using an Agilent 7890A gas chromatography (GC) system equipped with a flame ionization detector (FID), and an Agilent DB-FFAP: J&W 123-3232 column. Injection volume was 0.2 µL and inlet temperature was 230 °C. Carrier gas was helium at 103 kPa (gauge) at a flow rate of 3.78 mL/min. The temperature profile was 40 °C for 2 min, ramped to 200 °C at 20 °C/min, and held for 2.5 min. Outlet temperature was 230 °C. The run lasted for 12.5 min. Carboxylate salt compositions and the amount of salts per amount of solid (salt content) were calculated from the acid compositions of the solutions reported by the GC for each lime-to-salt ratio (Table 2-3) and for all residual solids.

The amount of carboxylate salts delivered into the reactor was calculated based on the measured salt content. The amount of carboxylate salts thermally decomposed was calculated by subtracting the amount of carboxylate salts delivered from the amount of carboxylate salts in the residual solids. In addition to non-decomposed carboxylate salts, other components in the residual solids included calcium carbonate (from the primary reaction), lime, quicklime, and tars and heavy oils (from product degradation).

On a theoretical basis, the amount of calcium carbonate was calculated from the amount of carboxylate salts decomposed. The presence of tars and heavy oils was observed by visual inspection and the quantity was estimated using a mass balance.

$$\begin{aligned}\text{Tars \& heavy oils (g)} = \text{Salts decomposed (g)} - \text{Liquid product (g)} \\ - \text{Gas product (g)} - CaCO_3\ \text{(g)}\end{aligned} \tag{2-3}$$

No attempt was made to determine the composition of the tars and heavy oils, nor the quantity of lime or quicklime.

2.2.5. Liquid analysis

Condensate samples were diluted 10:1 with reagent-grade methanol and analyzed using an Agilent 7890A GC system coupled to an Agilent 5975C mass spectroscopy detector (MS). Injection volume was 0.2 µL and inlet temperature was 280 °C. Carrier gas was helium at 48.3 kPa (gauge) at a flow rate of 1 mL/min. An Agilent HP-5MS 5% Phenyl Methyl Silox column was used at a temperature profile of 40 °C for 5 min, ramped to 250 °C at 10 °C/min, and held for 5 min. Outlet temperature was 230 °C. The run lasted for 31 min. Components determined by MS with a match quality of less than 50 were classified as "unknown liquids." Water content of condensate samples was determined using a Mettler Toledo V20 series Karl Fisher volumetric titrator (titrant: Fisher Chemical, Aqualine Complete 5K #AL2250R-1; solvent: Fisher Chemical, Aqualine Matrix K #AL2300R-1). Water content was subtracted from the total liquid product to determine amounts of all other liquid components.

2.2.6. Gas analysis

Gas sampling vessels were filled with helium to 34.5 kPa (gauge) at a measured temperature. Gas samples were analyzed using a SRI 8610C GC equipped with helium

ionization and thermal conductivity detectors. The sample loop was 0.1 µL. Carrier gas was helium at 186 kPa (gauge) at a flow rate of 20 mL/min. Restek Molecular 13X 80/100 mesh and ShinCarbon ST, 100/200 mesh columns were used at a temperature profile of 65 °C for 6 min, ramped to 200 °C at 16 °C/min, and held for 7 min. The run lasted for 21.5 min. Volume percentages (% v/v) reported by the GC for each gas component was converted to grams using the ideal gas law.

2.3. Theory/calculations

Random pairing of R groups is a simple model to predict the mole fractions of the ketone products (x_{ij}^{K}) and is the only model to predict product composition found in the literature. Ludlam [18] used it to predict mole fractions of ketones resulting from the thermal decomposition of a binary mixture of calcium carboxylate salts. Because random pairing assumes that the kinetic rate for the production of each ketone is equal, the mole fraction of each ketone is simply the product of the mole fractions of the two R groups that compose each ketone. The formulas and calculations used in random pairing are detailed in Section 3.3.

Alternatively, rather than using a kinetic model, product composition could be modeled on the basis of thermodynamic stability. Gibbs free energy minimization finds the product composition with the lowest Gibbs free energy. Reactant and product species as well as initial amounts must be defined. The product composition with the lowest Gibbs free energy is found using an element balance around all reaction species. Unlike the random-pairing model, non-expected products can be included in Gibbs free energy minimization as well. Gibbs free energy minimizations were performed using Aspen

Plus, V7.2 (Aspen Technology, Inc.) using the NRTL properties method. The input summary of the simulation is included in Appendix A.

Using nine different R groups, 45 different combinations of "expected ketones" can be produced (i.e., all ketones that would be produced if only the reaction described in Equation 2-1 occurred). Any other ketones or compounds produced from thermal decomposition that were not predicted by the random-pairing model are considered "non-expected products." For Gibbs free energy minimization, amounts of calcium acetate, propionate, butyrate, and valerate were used in proportions that simulate reagent-grade feed salts. Parameters necessary for Gibbs free energy minimization were not available for the remaining calcium carboxylate salts used in the experiment. Using four different R groups, 10 different combinations of expected ketones can be produced.

2.4. Results and discussion

Figure 2-7 shows a negative correlation between the yield of expected ketones and the lime-to-salt ratio of the feed salts. There was no statistically significant correlation ($p = 0.443$) between the first three lime-to-salt ratios (0, 0.000672, and 0.00134) and the expected ketone yield, indicating that the expected ketone yield is not affected, with statistical significance, by a lime-to-salt ratio of 0.00134 or less. This is expected because at a lime-to-salt ratio of 0.00134 or less there is not enough lime present for the reaction in Equation 2-2 to have a measureable impact on the expected ketone yield. A negative correlation ($p = 0.067$) occurred when a lime-to-salt ratio of 0.00461 was included in the statistical analysis. A stronger negative correlation ($p = 0.008$) occurred when all six lime-to-salt ratios were included. At a lime-to-salt ratio of

0.00461, 0.0190, and 0.272 there was a 3.5, 4.6, and 9.4% loss in base-line expected ketone yield, respectively. This indicates that the expected ketone yield decreases, with statistical significance, at lime-to-salt ratios above 0.00134.

Table 2-4 gives yields of all expected ketones for each lime-to-salt ratio of the reagent-grade feed salts and the fermentation feed salts. Only expected ketones that were produced are listed. Analysis of non-expected product yields (Table 2-5) shows an increase in the production of hydrocarbons during thermal decomposition as the lime-to-salt ratio increases. Gaseous hydrocarbon production remained relatively constant for lime-to-salt ratios of 0.0190 and less. At a lime-to-salt ratio of 0.272, methane, ethane, and ethene production increased by a factor of 2.5, 15, and 3, respectively. Production of liquid hydrocarbons (aromatics, olefins, and paraffins) also increased as the ratio of excess lime increased; up to a factor of 5 at a lime-to-salt ratio of 0.272. Although overall hydrocarbon production increased with higher lime-to-salt ratios, its increase did not account for the majority of the decrease in expected ketone yield. Figure 2-8 shows that the majority of the expected ketone yield loss resulted from increased production of tars and heavy oils. It also shows that production of non-expected ketones remained fairly constant whereas production of oxygenates and syngas (H_2 + CO) decreased slightly as the lime-to-salt ratio increased.

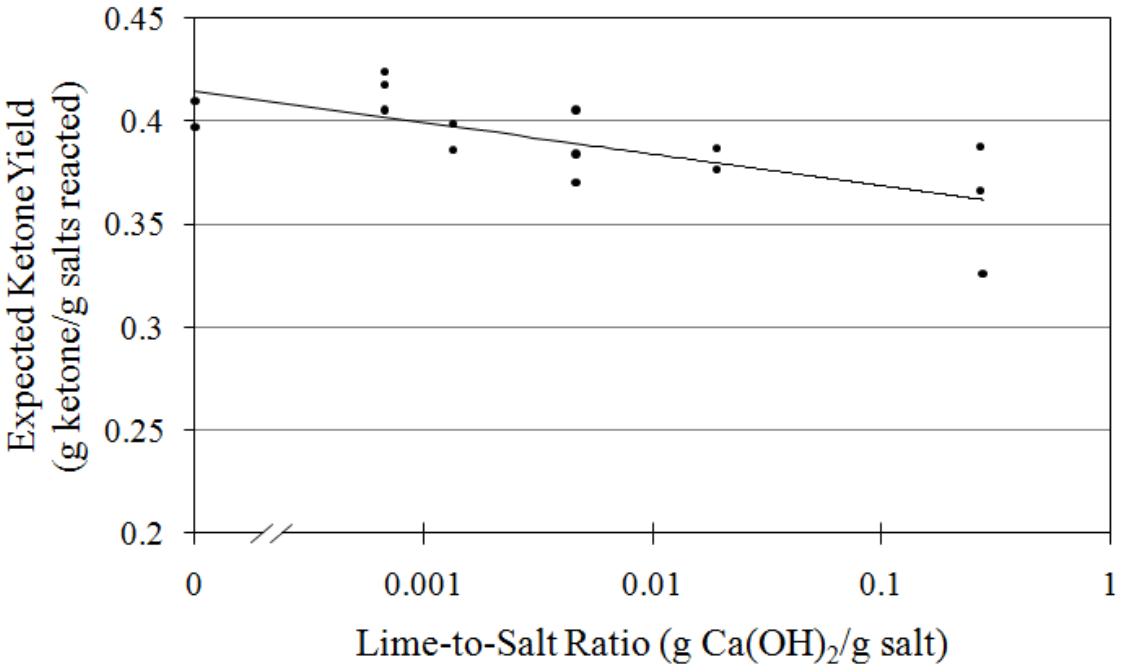

Figure 2-7. Yield of expected ketones for each lime-to-salt ratio.

Table 2-4. Expected ketone yield analysis.

		Lime-to-Salt Ratio (g $Ca(OH)_2$/g salt)						
		0	0.000672	0.00134	0.00461	0.0190	0.272	(0.000672)[c]
Compound Name	Carbon #	Yield[d] (g/g salt reacted) × 10^3						
2-propanone	3	73.10	71.81	90.55	98.35	44.67	84.40	45.48
2-butanone	4	82.18	65.41	62.15	64.15	65.19	58.41	34.06
3-methyl-2-butanone	5	4.761	5.379	4.001	3.762	5.839	1.804	2.649
2-pentanone	5	68.03	69.91	57.56	54.23	71.80	53.16	68.51
3-pentanone	5	10.57	12.47	7.391	7.900	13.88	7.465	6.130
2-methyl-3-pentanone	6	1.841	–	1.152	1.407	2.070	0.7440	0.6284
4-methyl-2-pentanone	6	3.831	4.936	3.503	1.003	5.561	2.292	2.647
2-hexanone	6	40.16	46.09	37.78	35.24	47.36	34.38	31.73
3-hexanone	6	14.38	20.30	13.37	12.59	21.61	13.63	28.83
2,4-dimethyl-3-pentanone	7	0.4602	–	–	–	–	0.2259	–
2-methyl-3-hexanone	7	0.2015	–	–	0.2862	0.9316	–	1.077
5-methyl-3 hexanone	7	0.7112	1.069	0.6226	0.5709	1.191	0.4717	0.8079
2-heptanone	7	50.17	48.28	51.71	45.95	46.06	46.94	38.55
3-heptanone	7	7.783	9.688	7.852	7.230	9.744	7.804	10.28
4-heptanone	7	4.499	6.404	5.327	4.632	6.348	5.249	29.67
2,5-dimethyl-3-hexanone	8	–	0.3768	–	–	–	–	–

Table 2-4. Continued

		Lime-to-Salt Ratio (g $Ca(OH)_2$/g salt)						
		0	0.000672	0.00134	0.00461	0.0190	0.272	(0.000672)[c]
Compound Name	Carbon #	Yield[d] (g/g salt reacted) × 10^3						
2-methyl-3-heptanone	8	0.2433	0.3067	0.2608	0.2498	0.3750	0.1451	0.8204
2-methyl-4-heptanone	8	0.3383	0.5550	0.3940	0.3503	0.5519	0.2762	1.481
2-octanone	8	16.29	15.44	18.38	16.90	11.30	15.68	6.464
3-octanone	8	8.713	10.98	9.816	9.603	8.201	9.081	11.25
4-octanone	8	4.281	6.492	5.252	5.114	4.895	4.753	18.50
2,6-dimethyl-4-heptanone	9	–	0.2191	0.1506	0.2091	–	0.0967	–
2-methyl-3-octanone	9	–	0.2780	–	0.2400	0.2387	0.1290	0.3393
2-methyl-4-octanone	9	–	0.2093	–	0.1678	0.2835	–	0.5301
2-nonanone	9	0.9587	0.9528	1.229	1.173	0.7352	0.8735	0.7684
3-nonanone	9	2.305	2.916	2.944	2.809	2.243	2.442	1.693
4-nonanone	9	5.431	8.287	7.036	7.142	6.113	5.912	25.97
5-nonanone	9	–	–	–	–	0.1150	–	0.2495
2-methyl-3-nonanone	10	–	–	–	–	0.2835	–	–
2-methyl-4-nonanone	10	0.1674	0.1256	–	0.1343	0.2430	–	0.4910
3-decanone	10	–	0.1256	0.2259	0.2765	0.2835	–	0.6661
4-decanone	10	–	–	0.3142	–	–	0.2016	–

Table 2-4. Continued

		Lime-to-Salt Ratio (g $Ca(OH)_2$/g salt)						
		0	0.000672	0.00134	0.00461	0.0190	0.272	(0.000672)[c]
Compound Name	Carbon #	Yield[d] (g/g salt reacted) × 10^3						
5-decanone	10	2.932	4.567	4.076	4.260	3.518	3.221	13.01
6-undecanone	11	1.339	2.291	1.715	2.459	1.612	1.450	11.51
6-dodecanone	12	0.2510	1.052	0.3232	0.5990	0.4380	0.7417	4.909
6-tridecanone	13	–	–	–	–	–	–	1.430
7-tridecanone	13	–	–	–	–	0.0810	–	–
Total ketone		405.94	416.90	395.08	389.00	383.76	361.98	401.13
Theoretical yield (%)		91.77	94.25	89.32	87.94	86.76	81.83	88.97

[c] Fermentation feed salts provided by Terrabon, Inc.
[d] Reported values have been multiplied by 10^3.

Table 2-5. Non-expected product yield analysis.

	Lime-to-Salt Ratio (g $Ca(OH)_2$/g salt)						
	0	0.000672	0.00134	0.00461	0.0190	0.272	(0.000672)[c]
Compound	Yield[d] (g/g salt reacted) × 10^3						
Non-expected ketones	4.328	6.951	8.728	6.933	7.782	8.184	33.56
Other oxygenates							
Acids	0.1424	0.4187	0.3890	0.4049	0.0788	–	3.766
Aldehydes	–	–	–	–	–	–	0.6284
Esters	0.7423	–	–	0.9397	–	–	–
Ethers	0.5164	–	2.688	4.162	1.256	–	0.2693
Alcohols	–	1.123	0.121	1.046	0.9316	0.1830	1.526
Hydrocarbons							
Aromatics	–	–	–	–	0.1215	–	3.905
Olefins	0.1291	0.2371	0.7907	0.1673	0.04051	0.8064	2.885
Paraffins	–	–	–	0.4028	0.2835	0.1142	0.8528
Methane	7.4	10.6	5.3	8.1	4.1	18	n/a
Ethane	0.18	0.38	0.56	0.44	–	4.8	n/a
Ethene	0.19	0.41	0.05	0.35	–	0.65	n/a

Table 2-5. Continued

	Lime-to-Salt Ratio (g $Ca(OH)_2$/g salt)						
	0	0.000672	0.00134	0.00461	0.0190	0.272	(0.000672)[c]
Compound	Yield[d] (g/g salt reacted) × 10^3						
Other							
Hydrogen	0.79	0.96	0.45	0.31	0.29	1.0	n/a
Carbon monoxide	3.5	2.2	0.99	1.0	0.56	0.91	n/a
Carbon dioxide	8.3	9.2	10	6.9	–	1.8	n/a
Tars and heavy oils	17.3	2.3	25.5	28.1	50.3	52.1	184
Unknown liquids	4.511	5.059	2.891	5.391	3.654	2.477	16.04
Total non-expected products	**48.1**	**39.9**	**58.7**	**64.7**	**69.3**	**91.1**	**247.4**

[c] Fermentation feed salts provided by Terrabon, Inc.
[d] Reported values have been multiplied by 10^3.

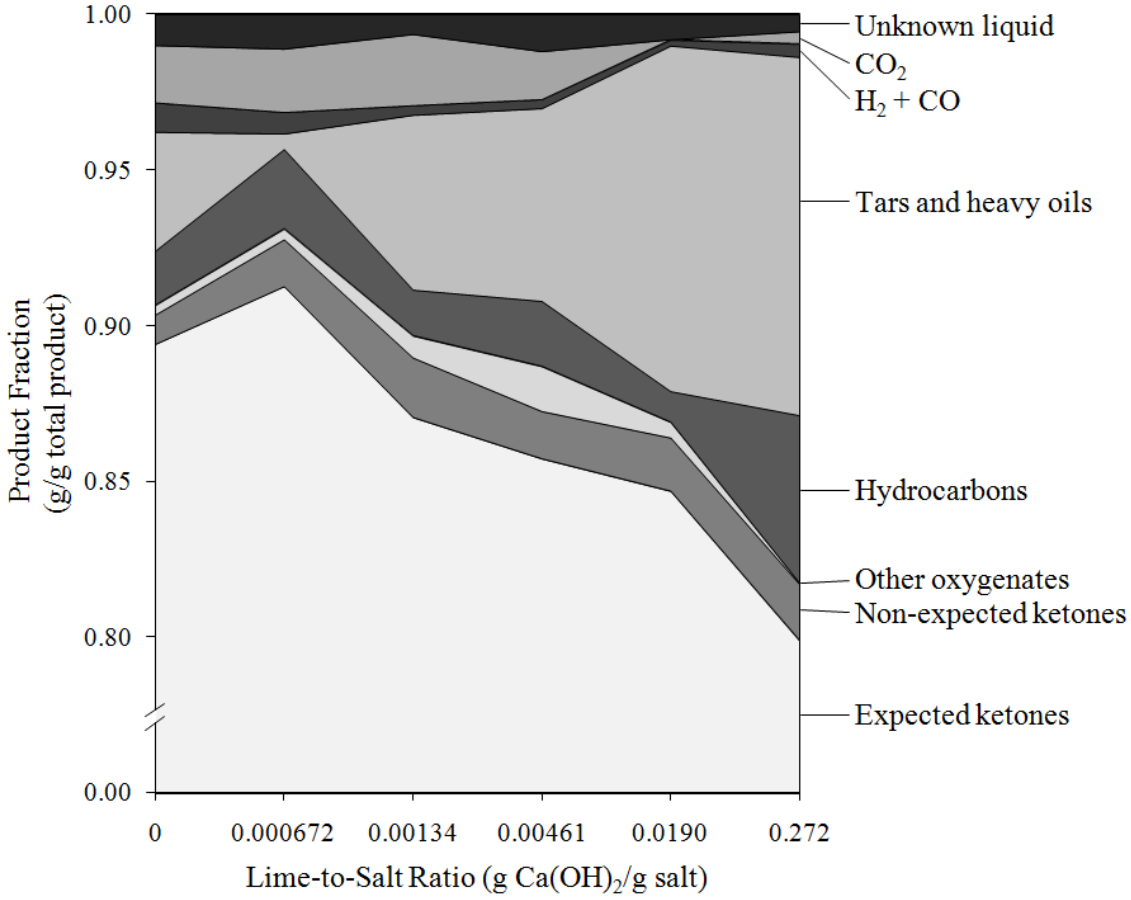

Figure 2-8. Distribution of products from thermal decomposition of reagent-grade feed salts.

It is assumed that all carbon dioxide produced was the result of ketone degradation, because calcium carbonate does not decompose at the reactor temperature (450°C) [35]. Ketone degradation was kept to a minimum by rapidly cooling the product as it exited the reactor and by maintaining a vacuum (~0.4 kPa). Analysis of gas samples revealed small amounts of oxygen, which could have reacted with the products to form carbon dioxide. Degradation of some of the ketones themselves could have also led to carbon dioxide production [36-38]. Production of carbon dioxide decreased as the lime-to-salt ratio increased. At 325 °C, lime begins decomposing to calcium oxide (quick lime) and water vapor [35]. As calcium carboxylate salts decompose into ketones and calcium carbonate, lime simultaneously decomposes into quicklime and water vapor. Quick lime absorbs carbon dioxide to form calcium carbonate until equilibrium pressure (0.0024 kPa at 450° C) is reached [39]. Lime also absorbs carbon dioxide in the presence of water vapor to form calcium carbonate [40]. These are the two most likely causes for the decrease in carbon dioxide. Similarly, Duruz [41] found that adding hydroxide to the thermal decomposition of sodium propionate greatly destabilized the reaction, with decomposition occurring at much lower temperatures. The production of hydrocarbons was increased and the production of carbon dioxide decreased. By contrast, there was no increase in the production of tars and heavy oils.

It can only be speculated as to why increased lime increased the production of tars and heavy oils. It is assumed that the tars and heavy oils result from ketone degradation, which occurs at the reactor temperature [42, 43]. Visual inspection [18] of the thermal decomposition of feed salts indicates that they become viscid and semi-

transparent, but not quite liquid, indicating that the crystals must melt before decomposition occurs [34]. However, as the crystal melts, the reaction occurs so quickly that the ketone vapor and solid calcium carbonate evolve before the entire crystal melts, thus the feed salts cannot become completely liquid. Thermal decomposition of feed salt particles most likely resembles a heterogeneous shrinking core. The surface of the unreacted layer melts, forming a liquid film. Decomposition occurs in this film, leaving behind a solid layer of calcium carbonate. Because excess lime and quicklime are also solids at the decomposition temperature, they could form a solid matrix that impedes newly formed ketones from exiting the liquid film into the vapor space, thus allowing for higher rates of ketone degradation.

From the fermentation feed salts, total expected ketone yields were comparable to those from reagent-grade feed salts with a lime-to-salt ratio of 0.00134. This shows that a lime-to-salt ratio above 0.00134 has a larger effect on expected ketone yield loss than impurities normally found in fermentation feed salts. Yields of tars and heavy oils, liquid hydrocarbons, acids, and non-expected ketones from fermentation feed salts were approximately 10, 18, 13, and 5 times larger than those from reagent-grade feed salts, respectively. Thermal decomposition products of fermentation feed salts also contained nitrogen, sulfur, and phosphorous impurities. Gas product analysis was not available for thermal decomposition of the fermentation feed salts. The increased production of non-expected products from thermal decomposition of fermentation feed salts could result from degradation of expected ketones caused by the presence of impurities, or from

thermal decomposition of the impurities themselves. Most likely, it is a combination of both.

From the experiment, expected ketones with the same carbon number were summed and compared to their respective random-pairing sums for each lime-to-salt ratio and the fermentation feed salts (Figure 2-9). The same was done for the expected ketones from the Gibbs free energy minimization. Because some of the carboxylate salts used in the experiment could not be included in the Gibbs free energy minimization, a direct comparison to experimental data could not be made. Instead, Gibbs free energy minimization sums were compared to respective random-pairing sums (Figure 2-10).

The random-pairing model predicts an exponential distribution of expected ketone carbon numbers with a maximum at carbon number 3. In contrast, the experimental data from reagent-grade feed salts have a plateau from carbon numbers 3–5 or in some cases a maximum at carbon number 5. Carbon numbers above 5 follow trends similar to those of random pairing. In addition, experimental values with carbon numbers of 6 and 7 exceed their random-pairing values for every lime-to-salt ratio. For the fermentation salts, carbon number distributions are shifted as well, but with a maximum at carbon numbers of 6 or 7. There also appears to be larger-than-expected amounts of ketones with larger carbon numbers (9–12).

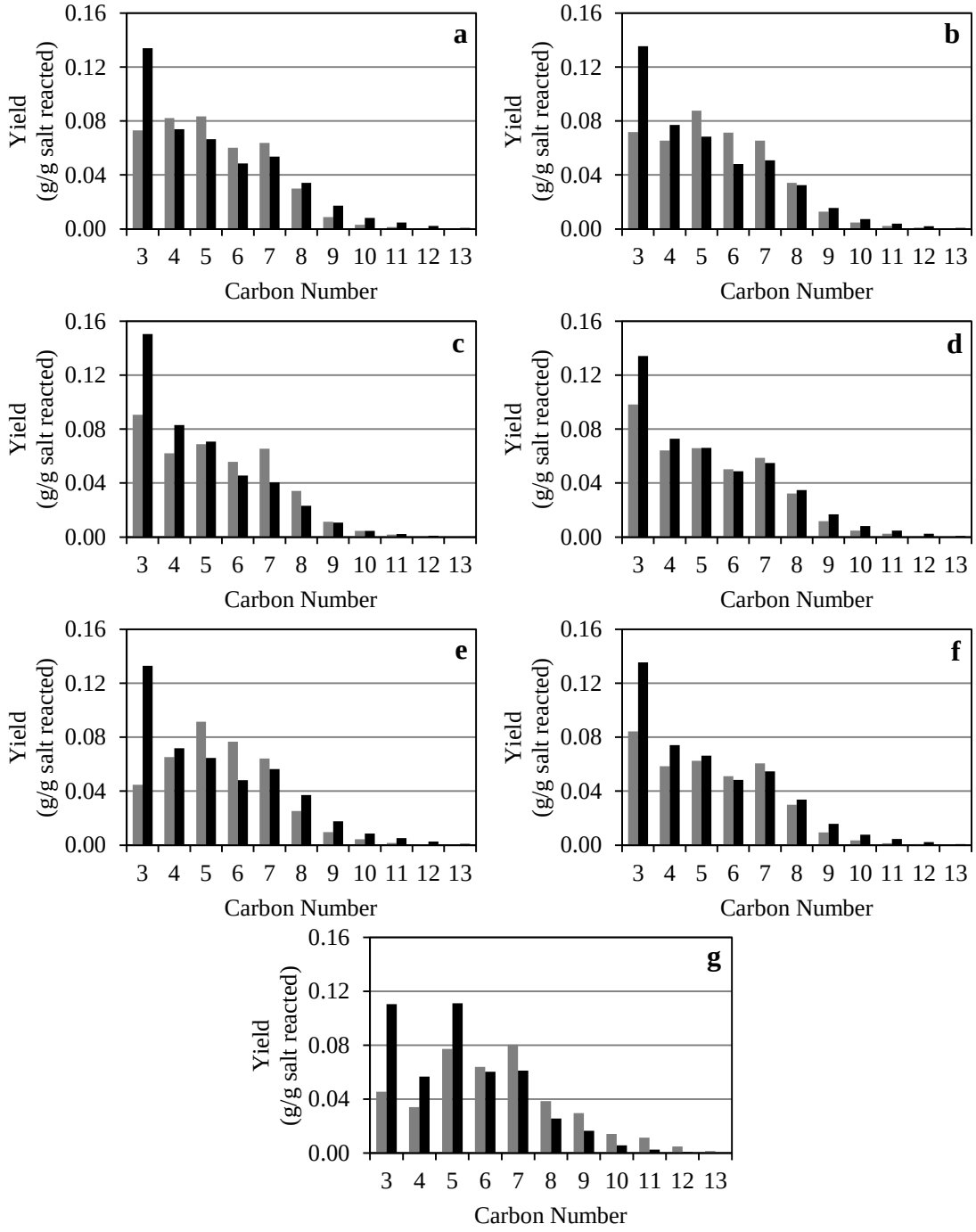

Figure 2-9. Comparison of experimental and random pairing carbon number distributions of expected ketones for each lime-to-salt ratio (■ Experimental ■ Random pairing); (a) 0.000, (b) 0.000672, (c) 0.00134, (d) 0.00461, (e) 0.0190, (f) 0.272, (g) 0.000672 (fermentation feed salts).

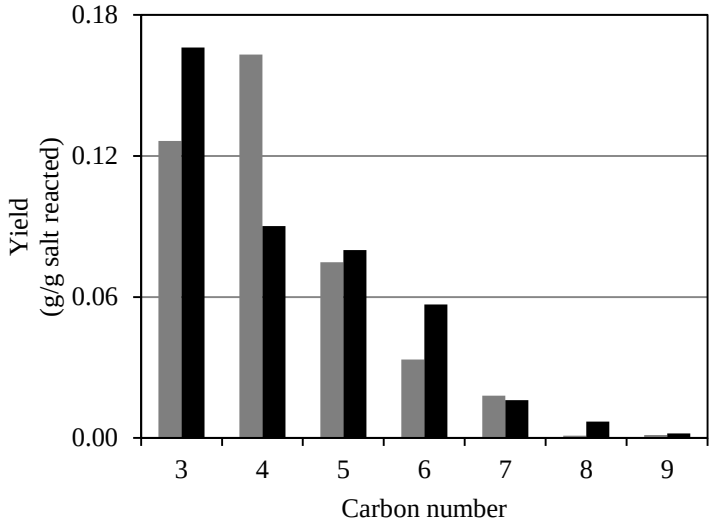

Figure 2-10. Comparison of Gibbs free energy minimization and random pairing carbon number distributions of expected ketones from reagent-grade salts (■ Gibbs free energy minimization ■ Random pairing).

One potential explanation for the lower-than-predicted amount of carbon number 3 (i.e., acetone) is that the degradation rate of acetone is higher than other expected ketones, which would account for the shift in carbon number distribution. However, when considering the small percentage of total non-expected products, this seems unlikely. Moreover, ketones with larger carbon numbers are more fragile and would be expected to have higher degradation rates, which is observed in expected ketones from reagent-grade feed salts with carbon numbers larger than 8. It is more likely that thermal decomposition is not best modeled by random paring. Perhaps this model could be improved if weighted coefficients were assigned to each pair when calculating the mole fractions for each expected ketone. This would account for the fact that some ketones are

kinetically favored over others during decomposition. These coefficients would most likely be specific to given reaction conditions.

The Gibbs free energy minimization model predicts expected ketones with carbon numbers from 3–9. It predicts a maximum at carbon number 4 instead of 3, which is predicted by random pairing. Expected ketones with a carbon number of 5 and higher follow trends similar to those in the experimental results with the exception of carbon number 8.

For the reagent-grade experiments shown in Figure 2-9, the pattern is distinctive which makes the reagent-grade salts an ideal choice for comparing the two models. Fermentation salts were excluded from the comparison because the high level of impurities introduces unnecessary complexity. The trends predicted by random pairing (i.e., an exponential distribution starting at carbon number 3) are not consistent with the experimental data. The shift in maximum carbon number in the Gibbs free energy minimization is more similar to the experimental data.

This study provides the first evidence that Gibbs free energy minimization may be a better model for predicting ketone profiles than random pairing. A model that considers both the thermodynamic and kinetic aspects of the thermal decomposition, as well as the production of by-products, would most likely follow experimental data the best. Future studies should explore this in more depth.

2.5. Conclusions

Upon dewatering, the pH of fermentation broth may be as high as 10 without statistically significant expected ketone yield losses during thermal decomposition.

Above pH 10 (i.e., feed salts with lime-to-salt ratios higher than 0.00134), larger amounts of tars and heavy oils and hydrocarbons are produced upon thermal decomposition. This increased production of non-expected products causes losses in expected ketone yields, the majority of which come from tars and heavy oils. In the thermal decomposition of fermentation feed salts, the production of non-expected ketones, acids, hydrocarbons, tar and heavy oils, and other impurities are much higher because of impurities in the fermentation feed salts. To a first approximation, the random-pairing model predicts expected ketone yields from the thermal decomposition of calcium carboxylate salts; however, there is significant disagreement particularly at low carbon numbers. Perhaps better agreement with experimental data can be achieved by using weighting factors to account for ketones that are kinetically favored. Gibbs free energy minimization is an alternative approach that follows the experimental data more closely than those of random pairing. Experimental data show that carbon numbers of 4–8 are favored, with 5 being the maximum.

3. MODELING PRODUCT COMPOSITON AND YIELD FROM THE THERMAL DECOMPOSITION OF CARBOXYLATE SALTS

3.1. Introduction

In the MixAlco™ process, carboxylate salts are thermally decomposed to yield their corresponding ketones, as shown in Equation 3-1.

$$M^+(RCOO^-) + M^+(R'COO^-) \xrightarrow{\Delta} RCOR' + M_2CO_3 \quad (3\text{-}1)$$

The cation (M^+) depends upon the buffering agent used in the fermentation and can be monovalent or divalent. At a commercial scale, it is necessary to predict the product composition and yield for a variety of carboxylate salt compositions. Two models (random pairing and Gibbs free energy minimization) were compared by their ability to predict the product composition of thermally decomposed salts. In addition, product yields from the thermal decomposition of each carboxylate salt mixture were measured and compared. Two types of carboxylate salts, one with monovalent (sodium) cations and one with divalent (calcium) cations, were examined. For both types of carboxylate salts, three mixtures with varying compositions of acetate, propionate, butyrate, and valerate were used for this study. One mixture contained mostly low-molecular-weight salts (i.e., acetate and propionate), another contained equimolar amounts of acetate, propionate, butyrate, and valerate salts, and the other contained mostly high-molecular-weight salts (i.e., butyrate and valerate). Using these six different carboxylate salt mixtures, the effectiveness of both models could be assessed for the thermal decomposition of carboxylate salts with different cations and various carboxylate salt

compositions. All carboxylate salt mixtures contained reagent-grade components to eliminate effects of impurities commonly found in fermentation salts.

3.2. Materials and methods

3.2.1. Preparation of salts

For each of the three salt profiles, acid solutions were prepared by mixing the individual reagent-grade carboxylic acids. In this section, any mixture composed of calcium or sodium carboxylate salts will be described as either *calcium salts* or *sodium salts*. To make the three calcium salt mixtures, aliquots from each of the three acid solutions were taken and mixed with stoichiometric amounts of calcium hydroxide in deionized water resulting in a solution of pH 8. Similarly, the three sodium salt mixtures were prepared by mixing aliquots of the three acid solutions with stoichiometric amounts of sodium carbonate in deionized water resulting in a solution of pH 8. The mixtures were evaporated in glass beakers and the dry solids (calcium and sodium carboxylate salts) were collected and weighed. Each of the salt mixtures was ground with mortar and pestle and dried in an oven at 105 °C for at least 24 h. Salt compositions were verified by gas chromatography (Table 3-1).

Table 3-1. Salt profile of each carboxylate salt mixture.

		Salt composition			
	Salt Content	Acetate	Propionate	Butyrate	Valerate
Salt mixture	(g salt/g solid)	(mol %)			
Low-MW Ca salts	0.892	40.53	30.27	19.29	9.91
Equimolar Ca salts	0.866	23.56	23.93	25.28	27.23
High-MW Ca salts	0.881	10.44	20.34	29.59	39.64
Low-MW Na salts	0.934	40.89	27.93	20.44	10.75
Equimolar Na salts	0.924	24.81	24.22	25.08	25.90
High-MW Na salts	0.951	9.36	19.01	30.11	41.52

3.2.2. Thermal decomposition of carboxylate salts

The apparatus used to thermally decompose the carboxylate salts was the same as described in Section 2.2.2. It was modified by removing the holding chamber and plugging Port 1 because the holding chamber was not necessary for this study. Charges of prepared carboxylate salts with constant moisture content were weighed. The average charge of calcium salts was 67 g and the average charge of sodium salts was 57 g. In a typical run, 1500 g of borosilicate glass beads (VWR Scientific Product, # 89091-366) were placed in the reactor and the charge of carboxylate salts was added on top of the glass beads. The reactor was sealed and the vacuum pump evacuated the system (~0.4 kPa). The three cooling media were added to their respective condensers and collection vessels. The heating jacket was turned on and the temperature controller maintained the reactor at 450 °C (±5 °C) for the calcium salts and 470 °C (±5 °C) for the sodium salts. Once the reactor temperature reached 200 °C, the valve to the vacuum pump was closed. After 180 min elapsed, the temperature controller was turned off and the reactor cooled. The condensers came to room temperature and the valve on the gas sampling vessel was closed and removed for gas analysis. The liquid product was removed from the collection vessels and the non-aqueous fraction was decanted. Both the aqueous and non-aqueous fractions were weighed and analyzed. When the reactor had cooled to near room temperature, the residual solids were weighed and were then dissolved with 350.0 mL of 3-M H_3PO_4 and 150.0 mL of deionized water. Residual solids not dissolved in the solution were filtered with a 0.2-µm cellulose acetate filter (VWR International, #28145-477). Via gas chromatography, the filtrate was analyzed to determine the amount of

unreacted salts in the residual solids. The average mass balance closure was 98.8% for the calcium salts and 98.9% for the sodium salts. The average fractional conversion was 0.909 for the calcium salts and 0.903 for the sodium salts.

A Carbolite HTR 11/75 rotary reactor furnace with a viewing panel was used to visually inspect the thermal decomposition of one calcium and sodium salt sample. Samples (30 g) were placed in the reaction vessel and a purge gas of N_2 at a flow rate of 50 mL/min was used for all runs. All runs in the rotary reactor furnace used a heating rate of 10 °C/min.

Differential scanning calorimetry (DSC) was performed on one sample of the calcium and sodium salts using a Mettler Toledo Polymer DSC, located in room 405W in the 1959 Wing of the Chemistry Building at Texas A&M University, using a purge gas of N_2 at a flow rate of 50 mL/min. Sample sizes were approximately 10 mg and the heating rate used for each run was 10 °C/min.

3.2.3. Solids analysis

All carboxylate salts were dried to a constant moisture content at 105°C for at least 24 h and placed in a desiccator. Samples of carboxylate salts were weighed (0.15 g) and dissolved with 1–3 mL of 3-M phosphoric acid. The mixture was then diluted to 10 mL with deionized water. Solutions of both dissolved carboxylate salts and dissolved residual solids were mixed with equal parts of a 1.162 g/L solution of 4-methyl-valeric acid (internal standard) and 3-M phosphoric acid. Acid analysis was performed using an Agilent 7890A gas chromatography (GC) system equipped with a flame ionization detector (FID), and an Agilent DB-FFAP: J&W 123-3232 column. Injection volume was

0.2 µL and inlet temperature was 230 °C. Carrier gas was helium at 103 kPa (gauge) at a flow rate of 3.78 mL/min. The temperature profile was 40 °C for 2 min, ramped to 200 °C at 20 °C/min, and held for 2.5 min. Outlet temperature was 230 °C. The run lasted for 12.5 min. Carboxylate salt compositions and the amount of salts per amount of solid (salt content) were calculated from the acid compositions of the solutions reported by the GC for each carboxylate salt mixture (Table 3-1) and for all residual solids.

The amount of carboxylate salts delivered into the reactor was calculated based on the measured salt content. The amount of carboxylate salts thermally decomposed was calculated by subtracting the amount of carboxylate salts delivered from the amount of carboxylate salts in the residual solids. In addition to non-decomposed carboxylate salts, other components in the residual solids included calcium or sodium carbonate (from the primary reaction) and tars and heavy oils (from product degradation). On a theoretical basis, the amount of calcium carbonate was calculated from the amount of carboxylate salts decomposed. The presence of tars and heavy oils was observed by visual inspection and the quantity was estimated using a mass balance.

$$\begin{aligned}\text{Tars \& heavy oils (g)} = {} & \text{Salts decomposed (g)} - \text{Liquid product (g)} \\ & - \text{Gas product (g)} - CaCO_3\ \text{(g)}\end{aligned} \tag{3-2}$$

No attempt was made to determine the composition of the tars and heavy oils.

3.2.4. Liquid analysis

Condensate samples were analyzed using an Agilent 7890A GC system coupled to an Agilent 5975C mass spectroscopy detector (MS). Injection volume was 0.2 µL and inlet temperature was 280 °C. Carrier gas was helium at 48.3 kPa (gauge) at a flow rate of 1 mL/min. An Agilent HP-5MS 5% Phenyl Methyl Silox column was used at a

temperature profile of 40 °C for 5 min, ramped to 250 °C at 10 °C/min, and held for 5 min. Outlet temperature was 230 °C. The run lasted for 31 min. Components determined by MS with a match quality of less than 50 were classified as "unknown liquids." Water content of condensate samples was determined using a Mettler Toledo V20 series Karl Fisher volumetric titrator (titrant: Fisher Chemical, Aqualine Complete 5K #AL2250R-1; solvent: Fisher Chemical, Aqualine Matrix K #AL2300R-1). Water content was subtracted from the total liquid product to determine amounts of all other liquid components.

3.2.5. Gas analysis

Gas sampling vessels were filled with helium to 34.5 kPa (gauge) at a measured temperature. Gas samples were analyzed using a Wasson ECE GC equipped with two flame ionization detectors (FID) and two thermal conductivity detectors (TCD) and nine proprietary columns. Injection volume was 1.0 mL. The oven temperature profile was 50 °C for 3 min, ramped to 120 °C at 10 °C/min, then ramped to 160 °C at 5 °C/min, and held for 2.5 min. Outlet temperature was 250 °C. The run lasted 20 min. Volume percentages (% v/v) reported by the GC for each gas component were converted to grams using the ideal gas law.

3.3. Theory/calculations

Random pairing of R groups is a simple model to predict the mole fractions of the ketone products (x_{ij}^{K}) and is the only model to predict product composition found in the literature. Ludlam [18] used it to predict mole fractions of ketones resulting from the thermal decomposition of a binary mixture of calcium carboxylate salts. Because

random pairing assumes that the kinetic rate for the production of each ketone is equal, the mole fraction of each ketone is simply the product of the mole fractions of the two R groups that compose each ketone. Because the mole fraction of each R group is equal to the mole fraction of the carboxylic salt from which it comes

$$x_{ij}^{K} = x_i^{S} \cdot x_j^{S} \tag{3-3}$$

where x_i^S and x_j^S are mole fractions of any of the carboxylate salts used in the thermal decomposition. The number-average molecular weight ($\overline{M}^K$) of the total ketone mixture is calculated by summing the products of each permutation of x_{ij}^K and its corresponding molecular weight (M_{ij}^K).

$$\overline{M}^K = \sum_{i=1}^{9}\sum_{j=1}^{9} x_{ij}^K M_{ij}^K = \left[\frac{\text{Total grams of ketone}}{\text{Total moles of ketone}}\right] \tag{3-4}$$

The weight fraction (w_{ij}^K) of each ketone permutation is

$$w_{ij}^K = \frac{x_{ij}^K M_{ij}^K}{\overline{M}^K} \tag{3-5}$$

The weight fraction ($\hat{w}_a^K$) of the a^{th} ketone is

$$\hat{w}_a^K = \begin{cases} 2(w_{ij}^K) & \text{if } i>j \\ w_{ij}^K & \text{if } i=j \\ 0 & \text{if } i<j \end{cases} \tag{3-6}$$

This algorithm accounts for the fact that when $i \neq j$, two permutations produce the same ketone. The number-average molecular weight of the feed salts ($\overline{M}^S$) is

$$\overline{M}^S = \left[\sum_{i=1}^{9} \frac{w_i^S}{M_i^S}\right]^{-1} = \left[\frac{\text{Total grams of salt}}{\text{Total moles of salt}}\right] \tag{3-7}$$

where w_i^S and M_i^S are the weight fraction and the molecular weight of the carboxylate salts present, respectively. For calcium (and other divalent cations) carboxylate salts, one mole of salt produces one mole of ketone. For sodium (and other monovalent cations) carboxylate salts, two moles of salt produces one mole of ketone. Therefore, the theoretical yield for any ketone product mixture is

$$\text{Theoretical yield} = \frac{2}{v} \cdot \frac{\overline{M}^K}{\overline{M}^S} = \left[\frac{\text{Total grams of ketone}}{\text{Total grams of salt}}\right] \tag{3-8}$$

where v is the valence number of the cation. The theoretical yield for the a^{th} ketone is

$$\text{Theoretical yield}_a = \hat{w}_a^K \cdot \frac{2}{v} \cdot \frac{\overline{M}^K}{\overline{M}^S} \tag{3-9}$$

Alternatively, rather than a kinetic model, product composition could be modeled on the basis of thermodynamic stability. Gibbs free energy minimization finds the product composition with the lowest Gibbs free energy. Reactant and product species as well as initial amounts must be defined. The product composition with the lowest Gibbs free energy is found using an element balance around all reaction species. Unlike the random-pairing model, non-expected products can be included in Gibbs free energy minimization as well. Gibbs free energy minimizations were performed using Aspen Plus, V7.3 (Aspen Technology, Inc.) using the NRTL properties method. An input summary of one of the simulations is included in Appendix B.

Using four different R groups (acetate, propionate, butyrate, and valerate), 10 different combinations of "expected ketones" can be produced (i.e., all ketones that would be produced if only the reaction described in Equation 3-1 occurred). Any other ketones or compounds produced from thermal decomposition that were not predicted by the random-pairing model are considered "non-expected products."

3.4. Results and discussion

From the experiment, the composition of expected ketones from the thermal decomposition of calcium salts were compared to the product compositions from the random-pairing model and from Gibbs free energy minimization model in order of increasing ketone molecular weight (Figure 3-1). As expected, the low-molecular-weight calcium salts yielded mostly low-molecular-weight ketones, the high-molecular-weight calcium salts yielded mostly high-molecular-weight ketones, and the equimolar calcium salts yielded mostly ketones in the middle of the molecular weight distribution.

For the low-molecular-weight calcium salts, there are three peaks in the ketone product distribution. The random-pairing model shows the first peak occurs at 2-butanone, the second peak at 3-hexanone, and the third peak at 4-octanone, which agrees with experimental results. The Gibbs free energy minimization model shows the first peak occurring at 2-butanone, the second peak at 3-heptanone, and the third peak at 5-nonanone, which is not consistent with experimental results. In addition to the random-pairing model being a better predictor of experimental ketone product distribution peaks, it tends to predict ketone product compositions that are closer to experimental product compositions than does the Gibbs free energy minimization model.

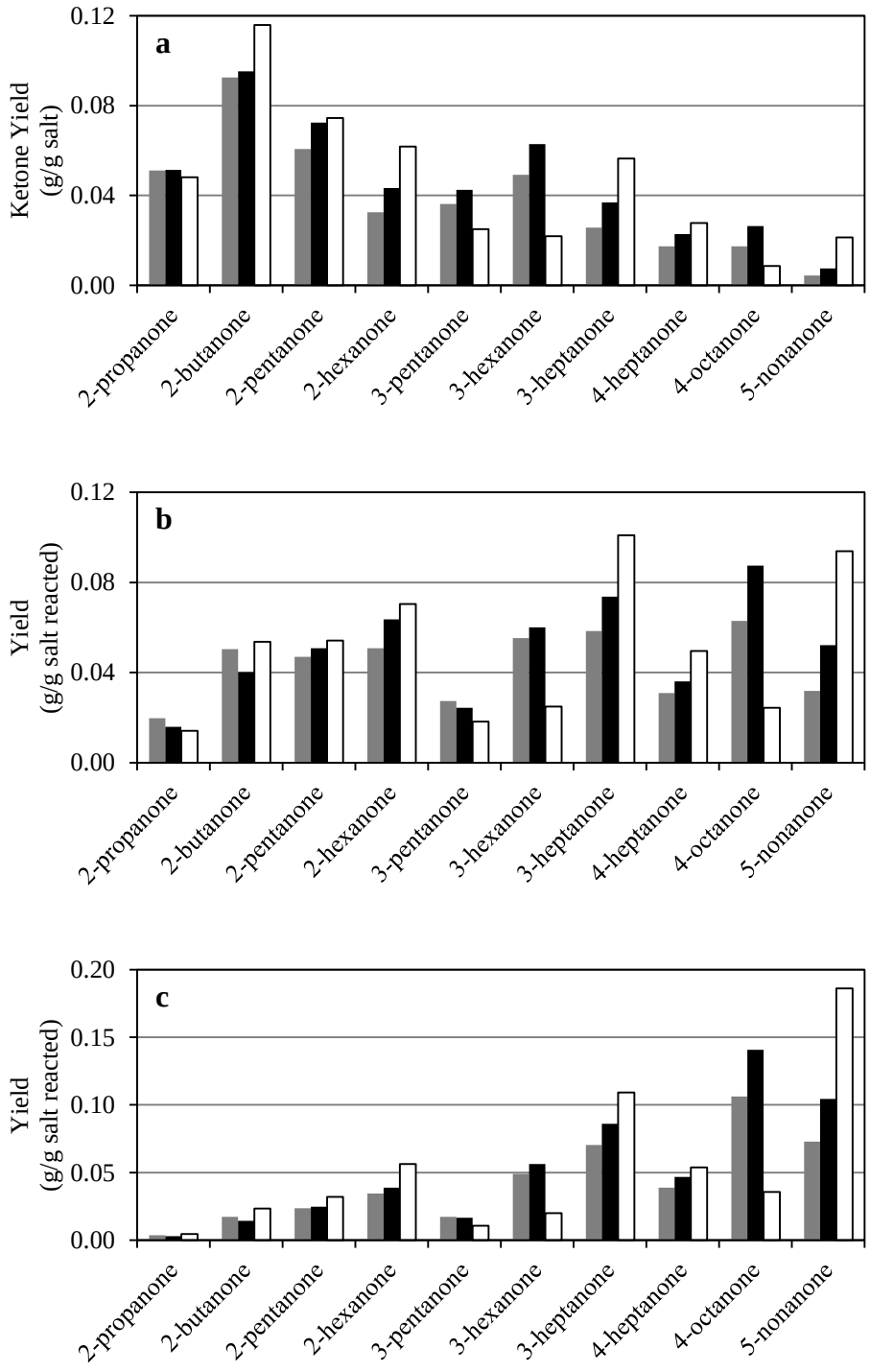

Figure 3-1. Comparison of experimental (■), random pairing (■), and Gibbs free energy minimization (□) distributions of expected ketones for each calcium salt mixture; (a) low-MW Ca salts, (b) equimolar Ca salts, (c) high-MW Ca salts.

For the equimolar calcium salts and the high-molecular-weight calcium salts, there are three peaks in the ketone product distribution. The random-pairing model shows the first peak occurs at 2-hexanone, the second peak at 3-heptanone, and the third peak at 4-octanone for both salt compositions. These both agree with the experimental results. The Gibbs free energy minimization model shows the first peak occurs at 2-hexanone, the second peak at 3-heptanone, and the third peak at 5-nonanone for both salt compositions, which does not agree with the experimental results. Again, for both calcium carboxylate salt compositions, the random-pairing model agrees better with the peaks in the experimental ketone product distribution and better predicts experimental ketone product composition than does the Gibbs free energy minimization model.

For the three different compositions of calcium salts, the random-pairing model fits the experimental results better than the Gibbs free energy model. This is evidence that the thermal decomposition of calcium salts most likely proceeds by random paring. However, even with the random-pairing model there are some significant deviations between the predicted and experimental product compositions of the higher-molecular-weight ketone compositions. This most likely results because high-molecular-weight ketones are less stable at decomposition temperatures and therefore have higher degradation rates. As the calcium salt composition shifts to high-molecular-weight carboxylate salts, which produce more high-molecular-weight ketones, the random-pairing model becomes less reliable.

The findings in this study differ from the findings in Section 2, which show that the random-pairing model did not fit the experimental data as well. It was not possible to

determine whether or not the Gibbs free energy minimization model was better because a direct comparison was not possible, but the trend it predicted was closer to that of the experimental data. In this section, only the low-molecular-weight calcium salt results are compared to the calcium salt results with lime-to-salt ratios of 0–0.00134 in Section 2. This is because the average carboxylate salt molecular weights are similar and it was shown that such small amounts of lime had negligible effects on product composition. In Section 2, there were significant deviations between the predicted and experimental compositions of acetone. The remaining ketone product compositions generally agreed with the random-pairing model. It is not known why such a discrepancy exists.

The compositions of expected ketones from the thermal decomposition of sodium salts were also compared to the product compositions from the random-pairing model and from Gibbs free energy minimization model in order of increasing ketone molecular weight (Figure 3-2). For each sodium salt composition, the peaks in ketone product distribution predicted by random-pairing and Gibbs free energy minimization are similar to peaks predicted for each calcium salt composition. However, the experimental results from the thermal decomposition of sodium salts followed the model results until 2-hexanone. Compositions of high-molecular-weight ketones were much lower than either model. In large part, this was caused by the significantly higher production of tars and heavy oils and hydrocarbons. The fact that the production of tars and heavy oils is so much more than that of hydrocarbons suggest the loss in ketone yield most likely results from product degradation and not a change in reaction or

mechanism. This makes it impossible to determine which model is best for the sodium salts.

Table 3-2 gives yields of all expected ketones for each carboxylate salt mixture. Theoretical yields of expected ketones for the calcium salts were relatively similar with no apparent trend with respect to carboxylate salt composition. For the calcium salts, the average yield of expected ketones was 83.88% of theoretical with a 5.59% difference overall. For the sodium salts, yields of expected ketones were much lower than those for the calcium salts. Further, the yield decreased as the average carboxylate salt molecular weight increased suggesting that high-molecular-weight sodium carboxylate salts have lower expected ketone yields than low-molecular-weight sodium carboxylate salts. For the sodium salts, the average yield of expected ketones was 39.94% of theoretical, less than half of that for calcium salts, with a 43.30% difference overall.

For the calcium salts, liquid product began to appear in the condensers from 170–180 °C. Upon reaching the final reactor temperature, more than 50% of the calcium salts had reacted. This was evident from the amount of liquid product present at 450 °C. For the sodium salts, liquid product began to appear in the condensers from 410–420 °C. The majority of the sodium salts reacted once the final reactor temperature of 470 °C was reached. According to Hurd [16], divaltent salts tend to have better ketone yields than monovalent salts. For alkali metals, ketone yields improve with decreasing atomic number. For alkaline earth metals, ketone yields improve with increasing atomic number.

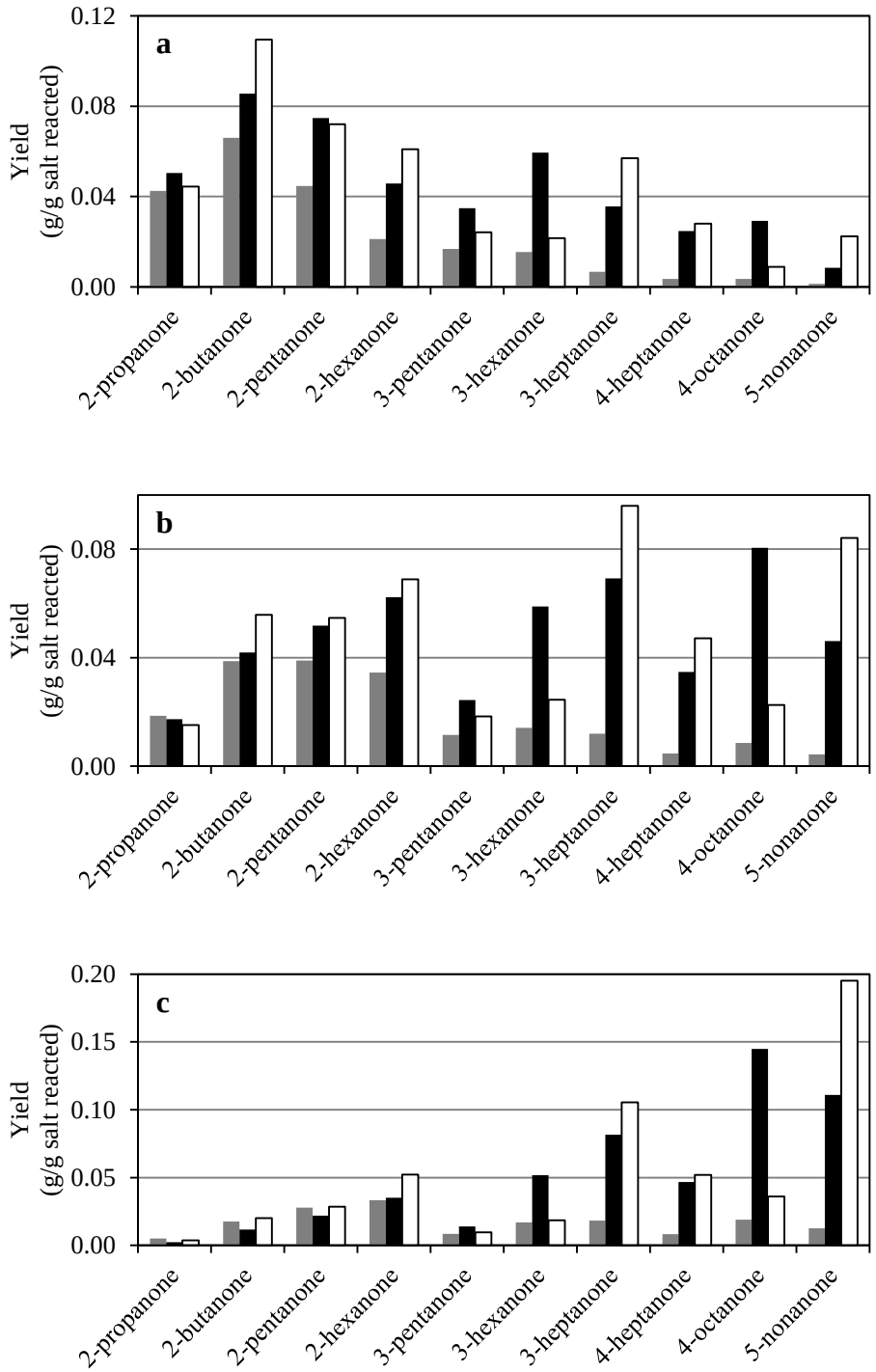

Figure 3-2. Comparison of experimental (■), random pairing (■), and Gibbs free energy minimization (□) distributions of expected ketones for each sodium salt mixture; (a) low-MW Na salts, (b) equimolar Na salts, (c) high-MW Na salts.

Table 3-2. Expected ketone yield analysis for calcium and sodium salts.

Compound Name	Low-MW Ca salts	Equimolar Ca salts	High-MW Ca salts	Low-MW Na salts	Equimolar Na salts	High-MW Na salts
	Yield[d] (g/g salt reacted) × 10^3					
2-propanone	51.11	19.76	3.66	42.49	18.58	5.19
2-butanone	92.53	50.38	17.22	66.07	38.71	17.54
2-pentanone	60.64	47.00	23.57	44.64	39.00	27.77
2-hexanone	32.60	50.83	34.51	21.23	34.51	33.41
3-pentanone	36.25	27.38	17.29	16.79	11.58	8.48
3-hexanone	49.26	55.27	49.09	15.46	14.14	16.91
3-heptanone	25.78	58.40	70.33	6.77	12.01	18.31
4-heptanone	17.39	30.95	38.74	3.64	4.74	8.37
4-octanone	17.42	62.89	106.28	3.55	8.53	18.92
5-nonanone	4.397	31.89	72.79	1.48	4.41	12.60
Total ketone	**387.4**	**434.8**	**433.5**	**222.1**	**186.2**	**167.5**
Theoretical yield (%)	**83.96%**	**86.18%**	**81.49%**	**49.45%**	**38.21%**	**32.16%**

[d] Reported values have been multiplied by 10^3.

Ludlam described calcium carboxylate salts as becoming viscid and semi-transparent, but not quite liquid during thermal decomposition [18], indicating that the crystals must melt before decomposition occurs [34]. This was confirmed using the rotary furnace with viewing port to visually inspect the thermal decomposition and the DSC plot in Figure 3-3a, which shows a sharp melt peak at 350 °C. For calcium carboxylate salt particles, thermal decomposition most likely resembles a heterogeneous shrinking core. The surface of the unreacted layer melts, forming a liquid film. Decomposition occurs in this film, leaving behind a solid layer of calcium carbonate. Sodium carboxylate salts melt well before they thermally decompose. DSC (Figure 3-

3b) shows that they undergo this phase transition from 170–190 °C. This was also confirmed visually using the rotary furnace. For sodium carboxylate salts, thermal decomposition occurs completely in the liquid phase with ketones bubbling out as vapors and sodium carbonate precipitating out as a solid.

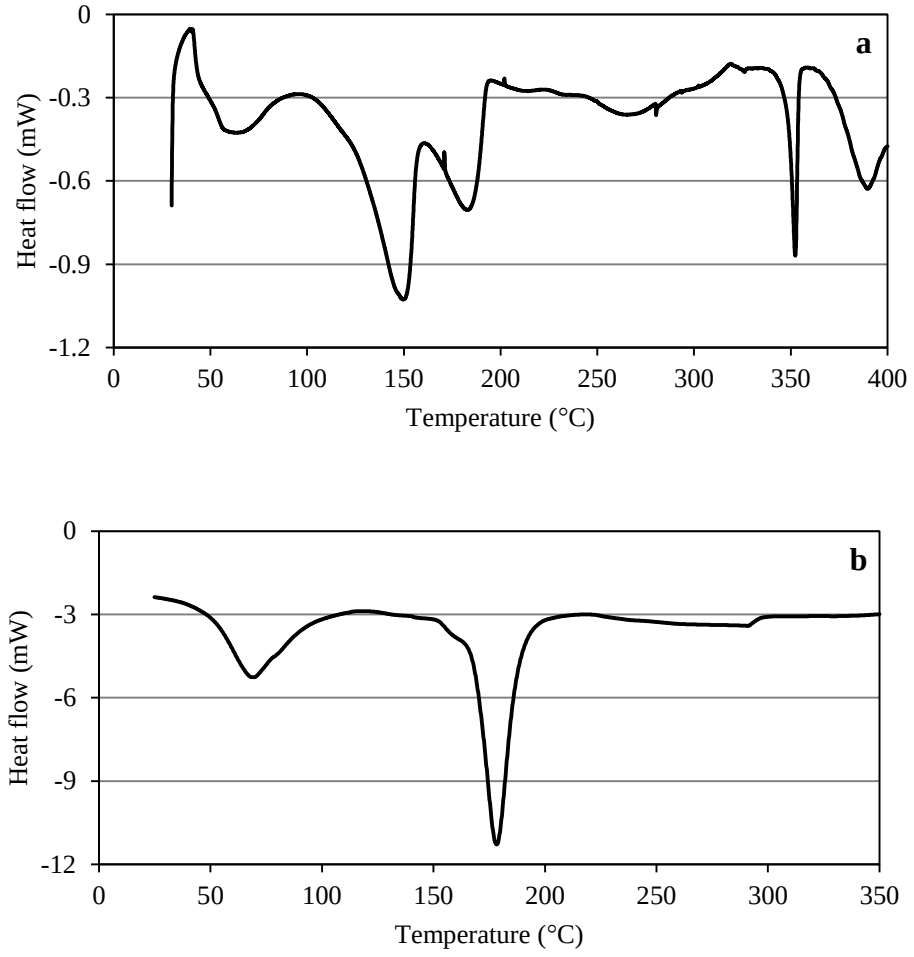

Figure 3-3. DSC plot for (a) low-molecular-weight calcium salts and (b) low-molecular-weight sodium salts.

Analysis of non-expected product yields (Table 3-3) shows that the majority of expected ketone yield loss occurred because of the production of tars and heavy oils. The yield of tars and heavy oils increased with the average carboxylate salt molecular weight. It is assumed that the tars and heavy oils result from ketone degradation, which occurs at the reactor temperature (450–470 °C) [42, 43]. Ketone degradation can produce intermediates that oligomerize into longer chain byproducts. Ketone degradation was minimized by rapidly cooling the product as it exited the reactor and by maintaining a vacuum (~0.4 kPa). Calcium and sodium carbonate that form as the reaction proceeds could form a solid matrix that impedes newly formed ketones from exiting the liquid film into the vapor space. This could be especially significant towards the end of the decomposition when the amount of carbonates are much more than the amount of carboxylate salts, thus allowing for ketone degradation. The fact that sodium salts thermally decompose at much higher temperatures could partially explain why they produce approximately four times as much tars and heavy oils.

Table 3-3. Non-expected product yield analysis for calcium and sodium salts.

Compound	Low-MW Ca salts	Equimolar Ca salts	High-MW Ca salts	Low-MW Na salts	Equimolar Na salts	High-MW Na salts
	Yield[d] (g/g salt reacted) × 10^3					
Non-expected ketones	4.519	4.448	2.607	2.593	3.137	4.652
Other oxygenates						
Acids	–	0.1348	–	–	–	–
Aldehydes	0.1221	0.1348	–	0.1108	0.2137	0.4229
Esters	–	0.08984	0.2209	–	–	–
Ethers	0.4514	–	–	–	–	–
Alcohols	0.1628	0.3144	0.2209	0.2709	0.2631	0.4017
Hydrocarbons						
Aromatics	0.3257	0.5391	0.2650	1.945	0.4461	5.201
Olefins	2.261	2.531	5.179	19.87	38.91	37.09
Paraffins	4.462	5.477	7.592	4.723	20.11	18.78
Other						
Hydrogen	0.7556	1.400	1.768	4.626	5.703	7.007
Carbon monoxide	3.126	2.050	2.064	22.91	–	–
Carbon dioxide	0.9768	0.06052	0.06240	0.1575	4.661	4.665
Tars and heavy oils	57.03	52.32	80.61	194.8	233.2	280.6
Unknowns	4.685	3.731	1.769	2.739	4.845	6.322
Total non-expected products	78.88	73.23	102.4	254.8	311.5	365.1

[d] Reported values have been multiplied by 10^3.

Another significant loss in expected ketone yield was from the production of hydrocarbons. As with tars and heavy oils, the hydrocarbon yield increased as the average carboxylate salt molecular weight increased. Sodium salts produced 5 times as many hydrocarbons as the calcium salts. This could be because the higher thermal decomposition temperature of sodium salts leads to more ketone degradation and, it could be because the decomposition mechanism shifts from a more concerted mechanism to more of a free radical mechanism. The majority of the hydrocarbons produced from calcium salts were in the form of paraffins. The majority of hydrocarbons produced from sodium salts were in the form of olefins. The production of olefins from

sodium salts was approximately 9.5 times higher than that from calcium salts, and the production of paraffins from sodium salts was approximately 2.5 times higher than that from calcium salts. The production of hydrogen from sodium salts was also higher, approximately four times as much, than from calcium salts. The increased production of both olefins and hydrogen is strong evidence that the higher decomposition temperature of sodium salts leads to more thermal cracking.

There was no significant trend between the production of carbon dioxide and carboxylate salt composition, or the production of carbon monoxide and carboxylate salt composition. It is assumed that all carbon dioxide and carbon monoxide produced resulted from ketone degradation, because neither calcium carbonate nor sodium carbonate decomposes at the reactor temperature [35, 44]. Analysis of gas samples revealed small amounts of oxygen, which could have reacted with the product to form carbon dioxide and carbon monoxide. Degradation of some of the ketones themselves could have also led to carbon dioxide production [36-38]. This is evident by fact that both carbon dioxide and paraffin production were higher for the thermal decomposition of sodium salts.

Thermal decomposition of calcium and sodium salts produced similar amounts of non-expected ketones and other oxygenates. There was no significant trend between either carboxylate salt composition and production or cation species and production. The trends mentioned above suggest that high-molecular-weight carboxylate salts form tars and heavy oils as well as well as hydrocarbons and hydrogen more readily than low-molecular-weight carboxylate salts. Of those three products, tars and heavy oils are the

most prevalent. The production of hydrocarbons, hydrogen, and tars and heavy oils from sodium salts are also approximately 4 times higher than from calcium salts. These results, along with others in the literature, suggest that carboxylate salts with divalent cations give higher expected ketone yields, and thus lower non-expected product yields, than carboxylate salts with monovalent cations.

3.5. Conclusions

For the thermal decomposition of calcium salts, the random-pairing model matched the ketone product distribution more closely than the Gibbs free energy minimization model. Both models agree with the experimental data for low-molecular-weight ketone composition and both show some deviations from the experimental data for high-molecular-weight ketone composition. However, the random-pairing model follows the trends in ketone product distribution and deviates less from the experimental data than Gibbs free energy minimization. For the sodium salts, it is not possible to determine which model fits the experimental data better because large amounts of degradation products are formed. Calcium salts begin thermally decomposing at much lower temperatures (170–180 °C) than do sodium salts (410–420 °C). For calcium salts, the expected ketone yield was not significantly affected by carboxylate salt composition. For sodium salts, the expected ketone yield decreased with increasing average carboxylate salt molecular weight. The average expected ketone yield for sodium salts was less than half that for calcium salts. The loss in expected ketone yield was primarily caused by the increased production in tars and heavy oils and hydrocarbons. These byproducts are most likely the result of product degradation. Tars and heavy oils were

the predominant byproduct and increased with average carboxylate salt molecular weight for both calcium and sodium salts; however, sodium salts produced 4 times more tars and heavy oils than did the calcium salts. Hydrocarbons also increased with average carboxylate salt molecular weight for both calcium and sodium salts, with sodium salts producing 9 times more hydrocarbons than calcium salts. Because of poor ketone yields and large production of tars and heavy oils, sodium carboxylate salts would not be recommended for use in a commercial-scale MixAlco™ biorefinery.

4. MODELING THE KINETICS OF THERMAL DECOMPOSITION OF SODIUM CARBOXYLATE SALTS*

4.1. Introduction

Using the MixAlco™ process, the thermal decomposition of carboxylate salts is a critical step in converting biomass into useful chemicals and fuels. Kinetic models and parameters for these decompositions are necessary to design and size commercial-scale reactors. The carboxylate salts are thermally decomposed to yield their corresponding ketones, as shown in Equation 4-1.

$$M^+(RCOO^-) + M^+(R'COO^-) \xrightarrow{\Delta} RCOR' + M_2CO_3 \quad (4\text{-}1)$$

For purposes of this study, M^+ is a sodium ion, but generally can be any alkali metal or half of any alkaline earth metal.

*Reprinted from Biomass and Bioenergy, 45, Landoll M, Holtzapple MT, Kinetics study of thermal decomposition of sodium carboxylate salts, 202–195, Copyright (2012), with permission from Elsevier.

The aim of this study is to first properly model the thermal decomposition of a simple carboxylate salt (sodium acetate) and then apply that model to the thermal decomposition of a mixture of reagent-grade carboxylate salts similar to that produced by the MixAlco™ process. Finally, the model is tested using actual carboxylate salts from a MixAlco™ fermentation. The first step was to determine the activation energy (E_A) for the thermal decomposition of all three salt types using three isoconversional methods. Next, functions of conversion were proposed to model each of the thermal decompositions using three isothermal models. The use of reagent-grade salts eliminated reactions associated with impurities found in fermentation salts, allowing measured kinetics to be attributed solely to the thermal decomposition of the carboxylate salts.

4.2. Materials and methods

4.2.1. Preparation of salts

In this section, any solid mixture of sodium carboxylate salts will be described as *sodium salts*. Anhydrous sodium acetate (Mallinckrodt Chemicals, AR (ACS), 99.0%) was used for this study. It was ground with mortar and pestle and sieved into a particle size range of 150–212 µm. The sodium acetate was then dried at 105 °C for 24 h and placed in a desiccator.

Reagent-grade sodium salts were prepared by mixing the corresponding reagent-grade carboxylic acids with equimolar amounts of reagent-grade sodium carbonate in deionized water, resulting in a solution of pH 8.5. These acid and corresponding salt profiles are typical of what has been reported for anaerobic mixed-culture fermentation [12-14]. A 2-L aliquot of this solution was evaporated in a glass beaker. The precipitated

reagent-grade sodium salts were collected, weighed, and dried at 105 °C for at least 24 h. The sodium salts were ground with mortar and pestle and washed with chloroform to remove any residual acids. The sodium salts were separated into the same particle size range as sodium acetate and then dried at 105 °C for an additional 24 h and placed in a desiccator. Acid and corresponding salt compositions were verified by gas chromatography (Table 4-1).

Fermentation sodium salts were prepared using clarified broth from a MixAlco™ fermentation buffered with sodium carbonate (Terrabon, Inc, Houston, TX). Clarification was performed using a proprietary process involving ultra-filtration and reverse osmosis. The broth was adjusted to pH 9 by adding excess sodium carbonate and was then evaporated to collect the fermentation sodium salts. The fermentation sodium salts were ground and separated into a particle range in the same manner as the reagent-grade sodium salts. Acid and corresponding salt compositions were verified by gas chromatography (Table 4-1).

Table 4-1. Acid and corresponding salt profiles of reagent-grade and fermentation sodium salts.

		Reagent-grade salts		Fermentation salts	
Carbon number	Acid	Acid (wt. %)	Salt (wt. %)	Acid (wt. %)	Salt (wt. %)
2	Acetic	37.48	40.46	45.13	47.68
3	Propionic	14.75	14.97	19.77	19.63
4	Isobutyric	1.43	1.39	1.33	1.27
4	Butyric	12.23	11.87	18.25	17.33
5	Isovaleric	2.60	2.44	3.22	2.95
5	Valeric	10.43	9.79	6.69	6.14
6	Caproic	13.44	12.28	4.20	3.75
7	Heptanoic	5.63	5.04	1.11	0.97
8	Octanoic	2.01	1.77	0.31	0.27

4.2.2. Thermal decomposition

Thermal gravimetric analysis (TGA) decompositions were performed in a Netzsch TG 209 C thermal analyzer, located in room 610 in the Brown Engineering Building at Texas A&M University. Samples were weighed (5–10 mg) into 100-µL aluminum sample pans. A purge gas of N_2 at a flow rate of 20 mL/min was used for all runs. For isothermal runs, the temperature was ramped up to the set temperature at a rate of 20 °C/min. Non-isothermal runs used heating rates of 1, 2, 4, 8, and 16 °C/min. A blank sample pan was also run at each heating rate as a baseline and subtracted from the corresponding sample run to account for thermal drift.

A Carbolite HTR 11/75 rotary reactor furnace with a viewing panel was used to visually inspect the decomposition reaction. Samples of 30 g were placed in the reaction vessel and a purge gas of N_2 at a flow rate of 50 mL/min was used for all runs. All runs in the rotary reactor furnace used a heating rate of 10 °C/min.

4.2.3. Solids analysis

Samples of reagent-grade and fermentation sodium salts were weighed (0.3 g) and dissolved with 2 mL of 3-M phosphoric acid. The mixture was then diluted to 10 mL with deionized water. Solutions of dissolved sodium salts were mixed with equal parts of a 1.162 g/L solution of 4-methyl-valeric acid (internal standard) and 3-M phosphoric acid. Acid analysis was performed using an Agilent 7890A gas chromatograph (GC) system equipped with a flame ionization detector (FID), and an Agilent DB-FFAP: J&W 123-3232 column. Injection volume was 0.2 µL and inlet temperature was 230 °C. Carrier gas was helium at 103 kPa (gauge) at a flow rate of 3.78 mL/min. The

temperature profile was 40 °C for 2 min, ramped to 200 °C at 20 °C/min, and held for 2.5 min. Outlet temperature was 230 °C. The run lasted for 12.5 min. Carboxylate salt compositions and the amount of sodium salts per amount of solid (salt content) were calculated from the acid compositions of the solutions reported by the GC (Table 4-1). Solids remaining in the sample pan after thermal decomposition were not analyzed for composition.

4.3. Theory/calculations

All kinetic analysis was based on the rate equation shown in Equation 4-2

$$\frac{dX}{dt} = k\,f(X) \tag{4-2}$$

where t is time, X is conversion, and k is the rate coefficient given by Equation 4-3

$$k = A\ \exp\left(-\frac{E_A}{RT}\right) \tag{4-3}$$

where T is absolute temperature, R is the ideal gas constant, A is the frequency factor, and E_A is the activation energy. The normalized weight of reactant (W) can be used in place of X. The equation for W is given by

$$W = \frac{m - m_f}{m_0 - m_f} = (1 - X) \tag{4-4}$$

where m is the weight of the sample at a given t, m_0 is the initial weight of the sample, and m_f is the final weight of the sample. W will range from 1 to 0 as the decomposition proceeds forward, which is the opposite of X. Using W as a metric of conversion instead of X eliminates the need for a correction coefficient from global weight-loss kinetic analysis [45]. Substituting Equations 4-3 and 4-4 into Equation 4-2 gives

$$-\frac{dW}{dt} = A\ \exp\left(-\frac{E_A}{RT}\right) f(W) \tag{4-5}$$

If a linear heating rate is used, then

$$\frac{dT}{dt} = \alpha \tag{4-6}$$

where α is the heating rate.

Several isoconversional methods were used: Friedman (FR) method [46, 47], Li-Tang (LT) method [48-50], and Vyazovkin (V) non-linear procedure [51-53]. The Friedman method is a differential method based on Equation 4-7.

$$\ln\left[-\frac{dW}{dt}\right] = \ln[A \cdot f(W)] - \frac{E_A}{RT} \tag{4-7}$$

The Li-Tang method is based on taking the logarithm of Equation 4-5, multiplying by dW, and integrating to give Equation 4-8.

$$\int_{W_0}^{W} \ln\left[-\frac{dW}{dt}\right] dW = (W - W_0)\ln[A] + \int_{W_0}^{W} \ln[f(W)]dW - \frac{E_A}{R}\int_{W_0}^{W} \frac{dW}{T} \tag{4-8}$$

The Vyazovkin procedure is an integral method based on minimizing the condition shown in Equation 4-9.

$$\sum_{i}^{n}\sum_{i\neq j}^{n}\left[\frac{I(E_{A,W}, T_{W,i})\ \alpha_j}{I(E_{A,W}, T_{W,j})\ \alpha_i}\right] = \min \tag{4-9}$$

where

$$I(E_A, T) = \frac{E_A}{R} p(x) \tag{4-10}$$

and n is the number of heating rates used for the procedure. The function $p(x)$ is the temperature integral, which is substituted by an approximation. Several temperature

integration approximation integrals are available (e.g., the Doyle approximation [54] and the Coats-Redfern approximation [55]). For this study, the fourth rational expression of the Senum and Yang approximation [56] (Equation 4-11) was used, because it is the best approximation over the entire x ratio range [57]

$$p(x) \cong \frac{e^{-x}}{x}\left(\frac{x^3 + 18x^2 + 88x + 96}{x^4 + 20x^3 + 120x^2 + 240x + 120}\right) \tag{4-11}$$

where

$$x = \frac{E_A}{RT} \tag{4-12}$$

Each of these isoconversional methods allow the dependence of E_A on W to be evaluated without a prior knowledge of the explicit form of $f(W)$. For thermal decompositions where more than one reaction or mechanism occurs, E_A represents an overall or "global" E_A which is a measure of all reactions/mechanisms occurring at a given value of W. For the Friedman method, E_A is calculated from the slopes of the plots of $\ln(-dW/dt)$ versus $1/T$ for each value of W. For the Li-Tang method, E_A is calculated from the slopes of the plots of $I\{\ln(-dW/dt)\}$ versus $I\{1/T\}$ for each value of W, where $I\{\}$ denotes the negative definite integral from 1 to W. Figure 4-1 and 4-2 show the plots generated for the Friedman and Li-Tang methods, respectively.

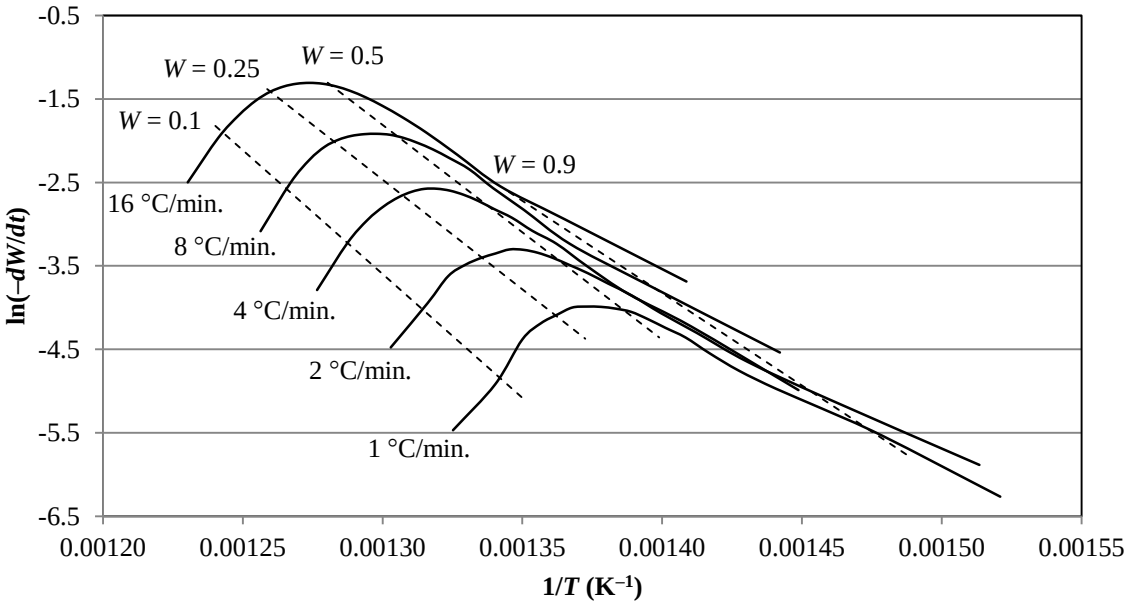

Figure 4-1. Friedman method plot for reagent-grade sodium salts. Slopes of dashed lines are used to calculate E_A at each W.

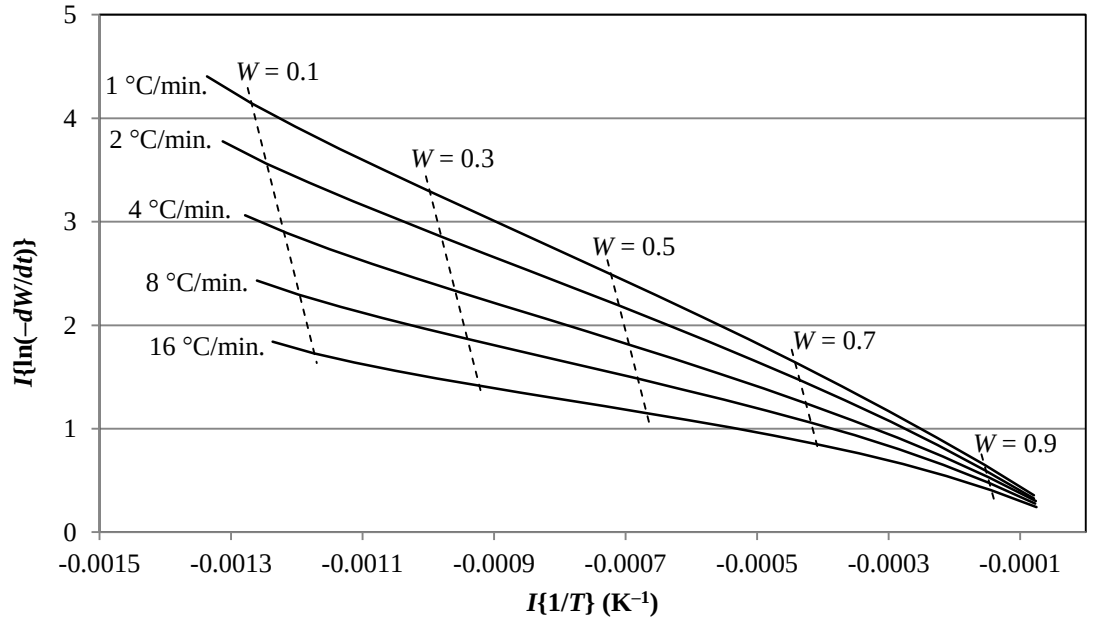

Figure 4-2. Li-Tang method plot for reagent-grade sodium salts. $I\{\}$ denotes the negative definite integral from 1 to W. Slopes of dashed lines are used to calculate E_A at each W.

For the Vyazovkin method, E_A is varied until the left-hand side is minimized. The smallest theoretical value possible is given by

$$\text{Theoretical min} = n(n-1) \tag{4-13}$$

Five different heating rates were used in this study, therefore 20 is the theoretical minimum. If four different heating rates were used, 12 would be the theoretical minimum.

There are many functions of W that model different types of thermal decompositions of solids [58]. The most common are listed in Table 4-2.

Table 4-2. Expressions of $f(W)$ for the most common models of thermal decomposition of solids.

Model	$f(W)$
n^{th}-order	W^n
Exponential law	$(1-W)$
Power law	$n(1-W)^{(n-1)/n}$
Prout-Tompkins	$W(1-W)$
Avrami-Erofeev	$nW[-\ln(W)]^{(n-1)/n}$
Uni-dimensional diffusion (parabolic law)	$[2(1-W)]^{-1}$
Bi-dimensional diffusion	$[-\ln(W)]^{-1}$
Tri-dimensional diffusion	$3/2(W)^{2/3}[1-W^{1/3}]^{-1}$
Ginstein-Brouhnstein	$3/2[W^{-1/3}-1]^{-1}$
Sestak-Berggren	$(1-W)^m W^n[-\ln(W)]^p$

In this study, three models were chosen for comparison: n^{th}-order, Avrami-Erofeev, and Sestak-Berggren. The n^{th}-order model (Equation 4-14) is the simplest model and is most commonly used in the literature, especially in initial kinetic studies.

$$f(W) = W^n \tag{4-14}$$

where n is the reaction order. With respect to W, the integrated form ($g(W)$) of Equation 4-14 is given by Equation 4-15.

$$g(W) = \frac{W^{1-n} - 1}{n - 1} \tag{4-15}$$

The Avrami-Erofeev (A-E) model (Equation 4-16) was originally developed to describe the kinetics of random nucleation and growth of nuclei on thermally decomposing crystals [58-61]. It was chosen for comparison because it describes sigmoid decomposition curves.

$$f(W) = nW[-\ln(W)]^{(n-1)/n} \tag{4-16}$$

With respect to W, the integrated form of Equation 4-16 is given by Equation 4-17.

$$g(W) = [-\ln(W)]^{1/n} \tag{4-17}$$

The Sestak-Berggren (S-B) model (Equation 4-18) was developed to be a general model that could be used to model any type of thermal decomposition [62-65].

$$f(W) = (1 - W)^m W^n [-\ln(W)]^p \tag{4-18}$$

The three exponents allow Equation 4-18 to account for a number of different mechanisms (such as n^{th}-order kinetics, autocatalysis, diffusion, etc.). For example, if m and p are set to zero, Equation 4-18 becomes Equation 4-14 and models n^{th}-order

kinetics. If p is set to zero, it can model autocatalysis. There is no analytical solution to the integrated form of Equation 4-18.

To check the goodness of fit for each model, experimental values were compared to each of the model values using standard error (θ), given by Equation 4-19.

$$\theta = \sqrt{\frac{\Sigma\left(\frac{dW/dt_{exp} - dW/dt_{mod}}{dW/dt_{exp}}\right)^2}{N}} \tag{4-19}$$

where *exp* denotes experimental values, *mod* denotes values from the models, and N is the total number of measurements from all isothermal runs. For this equation, a perfect fit would yield a θ of zero.

Figure 4-3 diagrams the procedure used to determine the kinetic parameters and function of W for the thermal decomposition of carboxylate salts. Carboxylate salts were thermally decomposed with TGA both isothermally, using several different temperatures, and non-isothermally, using multiple linear heating rates. The three isoconversional methods were chosen to determine the dependency of E_A on W using data from the non-isothermal runs. Each method used a different approach to determine E_A at a given W. The results of each method were compared to check for similarity in trends of E_A vs. W. At each value of W, E_A from each of the methods were averaged to give an average $\bar{E}_A$ as a function of W ($\bar{E}_A$ (W)). Values of $\bar{E}_A$ at each W from 0.95–0.05 were then averaged to give an overall average $\hat{E}_A$.

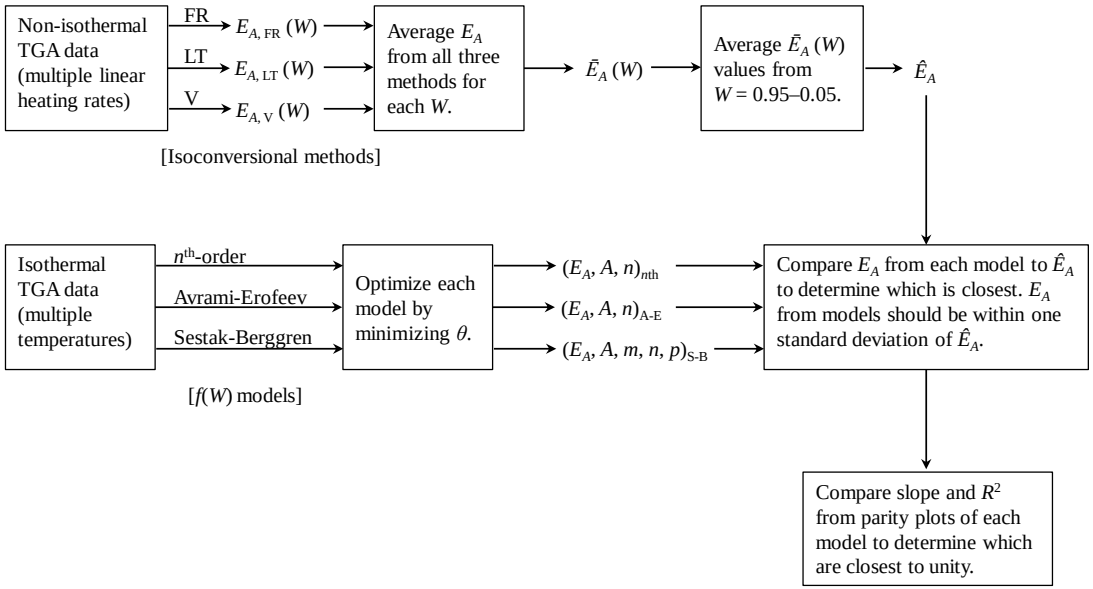

Figure 4-3. Flow diagram of procedure used to determine dependence of E_A on W using Friedman (FR), Li-Tang (LT), and Vyazovkin (V) methods as well as to optimize n^{th}-order, Avrami-Erofeev (A-E), and Sestak-Berggren (S-B) models and indentify which is best for the thermal decomposition of carboxylate salts.

The three $f(W)$ models were compared to the isothermal data and optimized for best fit. To be considered a viable model, its E_A value had to be within one standard deviation of its respective $\hat{E}_A$ value. The ideal model had the lowest value of θ, a parity plot slope and R^2 value closest to unity, and an E_A closest to its respective $\hat{E}_A$. This procedure is the recommended by multiple researchers who are experts in the field and follows the same methodology as ASTM E1641–07, Standard Test Method for Decomposition Kinetics by Thermogravimetry, and E2070–08, Standard Test Method for Kinetic Parameters by Differential Scanning Calorimetry Using Isothermal Methods.

4.4. Results and discussion

The following sections describe the phase behavior of the sodium carboxylate salts as well as non-isothermal and isothermal decompositions.

4.4.1. Phase behavior

Sodium acetate and both the reagent-grade and fermentation sodium salts melt before the onset of thermal decomposition. Visual inspection of the sodium salts during heating showed sodium acetate melting at approximately 325–330 °C and the reagent-grade and fermentation sodium salts both melting at approximately 225–230 °C.

4.4.2. Non-isothermal decomposition

Figures 4-4 through 4-8 show the thermal decomposition curves for reagent-grade sodium acetate, reagent-grade sodium salts, and fermentation sodium salts for all five heating rates used in this study. Sodium acetate begins decomposing at approximately 350 °C, whereas reagent-grade and fermentation sodium salts both begin decomposing at approximately 290 °C. For both reagent-grade and fermentation sodium

salts, there is a discontinuity in the curves that begins at a W of approximately 0.10; the discontinuity is greater for fermentation sodium salts. The discontinuity indicates that a different reaction or mechanism becomes predominant. The sodium acetate curve is continuous throughout the entire decomposition. Heating rates of 1, 2, 4, 8, and 16 °C/min were used for each of the three isoconversional methods employed. The same methods and heating rates were used for the decomposition of all three sodium salt types.

Figure 4-9 shows how E_A varies with W for each isoconversional method used for each sodium salt type. For each value of W, only E_A values with R^2-values of 0.65 and above were considered for the Friedman and Li-Tang methods and E_A values with a minimization value of 22 or less for the Vyazovkin method. For sodium acetate, the three isoconversional methods showed varying trends of E_A with respect to W; however, when the average of the E_A values for each W was taken, the standard deviation was less than 5%. For reagent-grade and fermentation sodium salts, the trends of E_A vs. W for the three isoconversional methods were similar. For each sodium salt type, Table 4-3 shows the average of the three E_A values from the three isoconversional methods ($\bar{E}_A$ (W)) for selected values of W. It also contains the $\hat{E}_A$ and corresponding standard deviations for each sodium salt type.

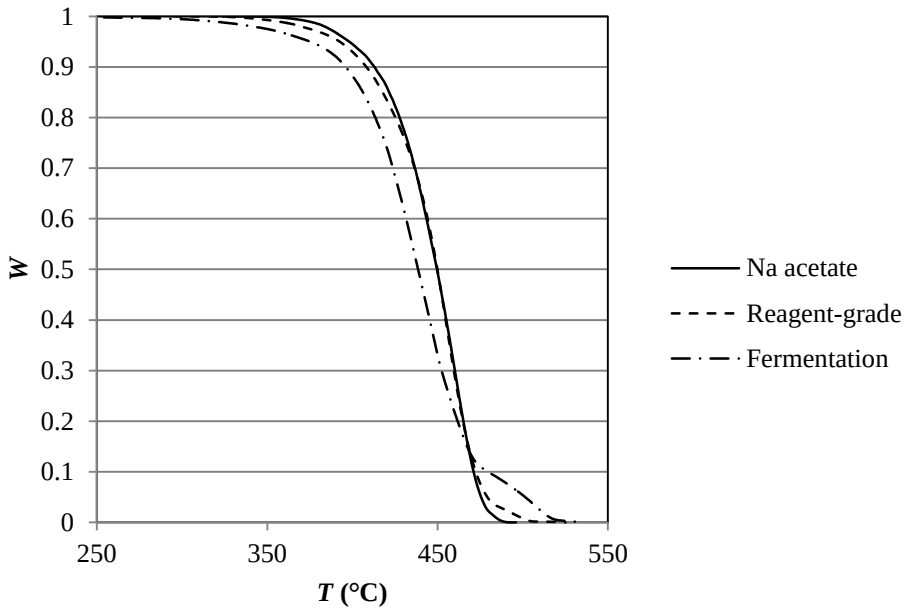

Figure 4-4. Thermal decomposition curves for sodium acetate, reagent-grade sodium salts, and fermentation sodium salts at a heating rate of 1 °C/min.

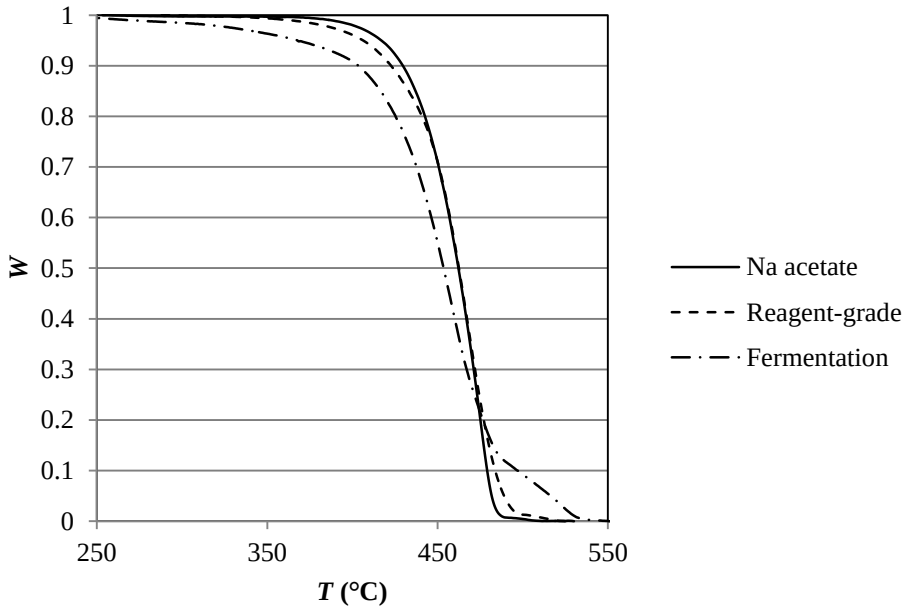

Figure 4-5. Thermal decomposition curves for sodium acetate, reagent-grade sodium salts, and fermentation sodium salts at a heating rate of 2 °C/min.

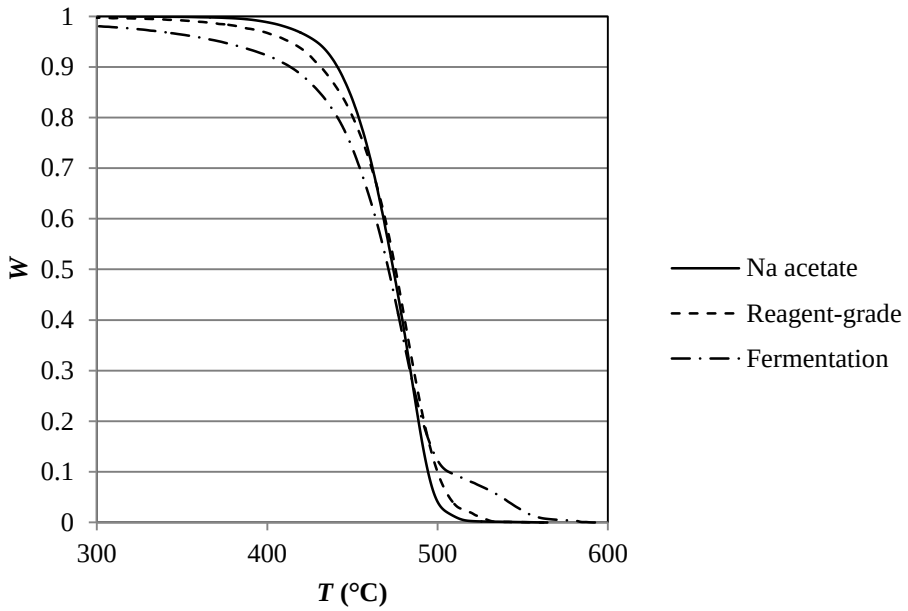

Figure 4-6. Thermal decomposition curves for sodium acetate, reagent-grade sodium salts, and fermentation sodium salts at a heating rate of 4 °C/min.

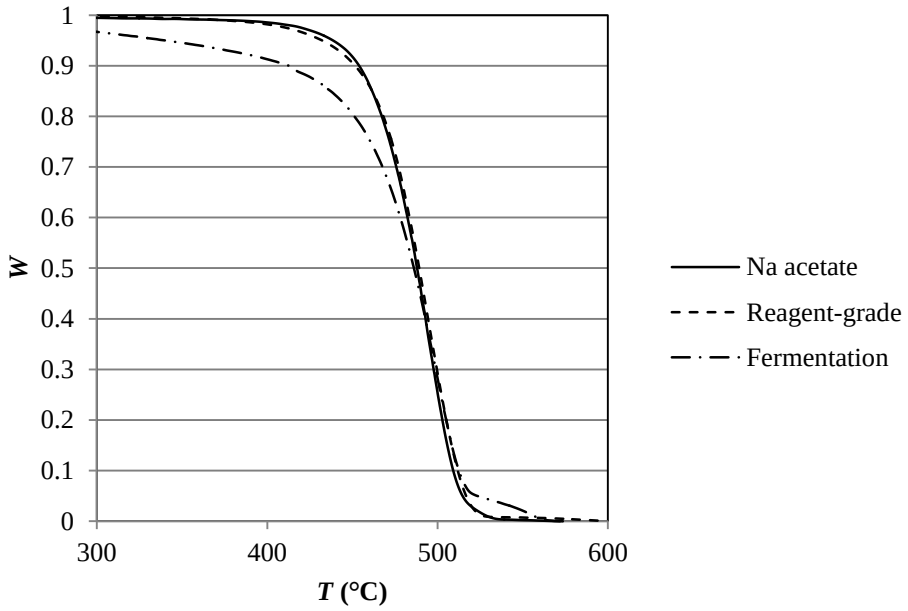

Figure 4-7. Thermal decomposition curves for sodium acetate, reagent-grade sodium salts, and fermentation sodium salts at a heating rate of 8 °C/min.

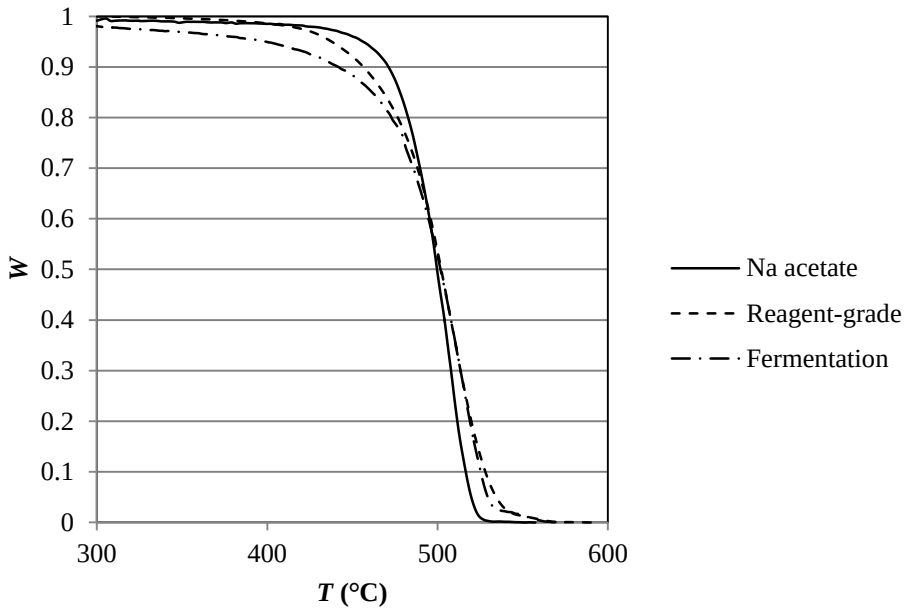

Figure 4-8. Thermal decomposition curves for sodium acetate, reagent-grade sodium salts, and fermentation sodium salts at a heating rate of 16 °C/min.

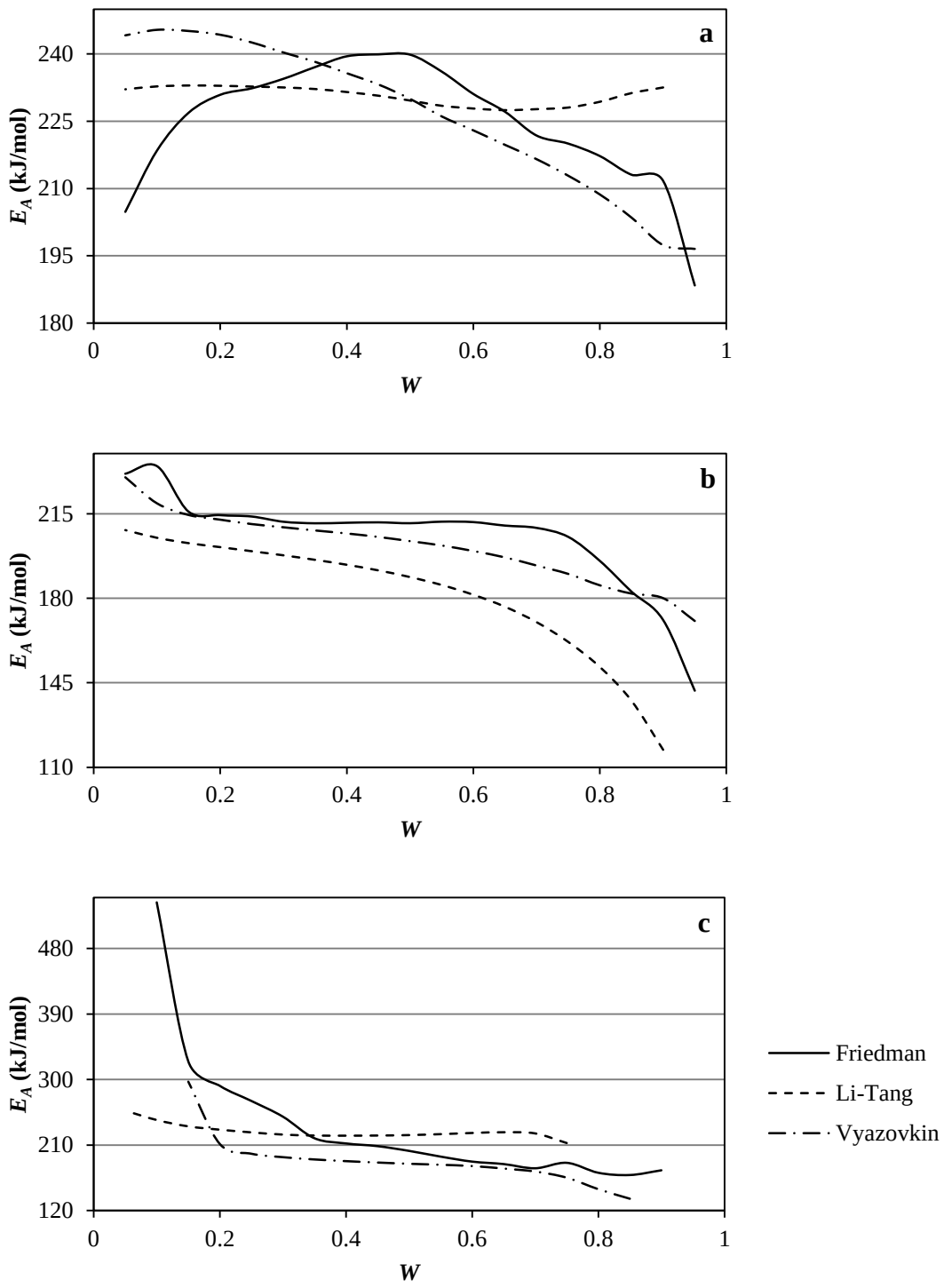

Figure 4-9. Dependence of E_A on W for (a) sodium acetate, (b) reagent-grade sodium salts, and (c) fermentation sodium salts.

Table 4-3. Dependence of $\bar{E}_A$ on W for each sodium salt type.

	$\bar{E}_A$ (W) (kJ/mol)		
W	Sodium acetate	Reagent-grade salts	Fermentation salts
0.95	192.46	156.17	–
0.90	213.87	156.10	175.29
0.85	215.95	167.42	152.52
0.80	218.42	177.48	160.62
0.75	220.31	185.83	187.81
0.70	222.02	190.95	192.54
0.65	224.78	194.52	196.36
0.60	227.30	197.53	198.29
0.55	230.21	199.71	200.64
0.50	233.16	201.19	203.29
0.45	234.61	202.81	205.82
0.40	235.58	204.01	207.63
0.35	235.84	205.04	210.85
0.30	235.78	206.31	222.19
0.25	235.89	208.03	231.98
0.20	236.03	209.40	244.60
0.15	235.00	211.08	285.85
0.10	232.20	219.72	393.78
0.05	227.03	223.33	257.17
$\hat{E}_A$	226.65	195.61	218.18
Standard deviation	11.11	19.25	54.56

For all three sodium salt types, $\bar{E}_A$ (W) increases as thermal decomposition proceeds forward. The $\hat{E}_A$ of sodium acetate is significantly higher than the $\hat{E}_A$ for both reagent-grade and fermentation sodium salts. This suggests that E_A for the decomposition of higher molecular weight sodium salts is lower than that of sodium acetate and presumably E_A decreases with increasing molecular weight. The increased $\hat{E}_A$ for fermentation sodium salts over the $\hat{E}_A$ for reagent-grade sodium salts most likely results from impurities. Contributing to this increase is the spike in $\hat{E}_A$ around $W = 0.1$. This most likely results from the onset of impurity decomposition. A thermal decomposition in which E_A values vary significantly with W indicates that multiple reactions and/or mechanisms occur at different times throughout the reaction. This suggests that the thermal decomposition of sodium acetate proceeds by more than one mechanism. Most likely, it starts as a decomposition mechanism and then gradually shifts to a diffusion or product degradation mechanism as the amount of sodium carbonate surpasses the amount of sodium acetate. For the case of reagent-grade and fermentation sodium salts, dependence of E_A on W is expected. Because multiple species are present, multiple reactions occur at different rates during the decomposition as temperature increases. In addition, multiple mechanisms are likely present in the decomposition of reagent-grade sodium salts and even more so for fermentation sodium salts, because of the presence of impurities.

4.4.3. Isothermal decomposition

Isothermal decompositions were used to evaluate $f(W)$ for each sodium salt type. Sodium acetate decompositions were performed at 400, 410, and 420 °C, and the range

of W used for modeling was from 0.95–0.05. Reagent-grade sodium salts decompositions were performed at 390, 400, and 410 °C, and the range of W used for modeling was from 0.95–0.05. Fermentation sodium salts decompositions were performed at 380, 390, and 400 °C, and the range of W used for modeling was from 0.95–0.15. Figure 4-10 shows the isothermal decomposition curves for each of the sodium carboxylate salt types at each temperature. Each of the three models was fit to the experimental data. For the n^{th}-order and Avrami-Erofeev models, Equations 4-15 and 4-17 were plotted against t, respectively, and k was determined from the slope of the resulting line. Values of n were found by minimizing θ. Because the Sestak-Berggren model does not have an analytical solution for its integrated form, Equation 4-18 was combined with Equations 4-3 and 4-5 and the natural log was taken of both sides, resulting in Equation 4-20.

$$\ln\left(-\frac{dW}{dt}\right) = \ln(k) + m\ln(1-W) + n\ln(W) + p\ln[-\ln(W)] \tag{4-20}$$

Values of k were determined from the intercept of Equation 4-20 (i.e., $\ln(k)$), whereas m, n, and p were found by minimizing θ. Values of E_A and A were calculated using the k values from the three isothermal runs and Equation 4-3.

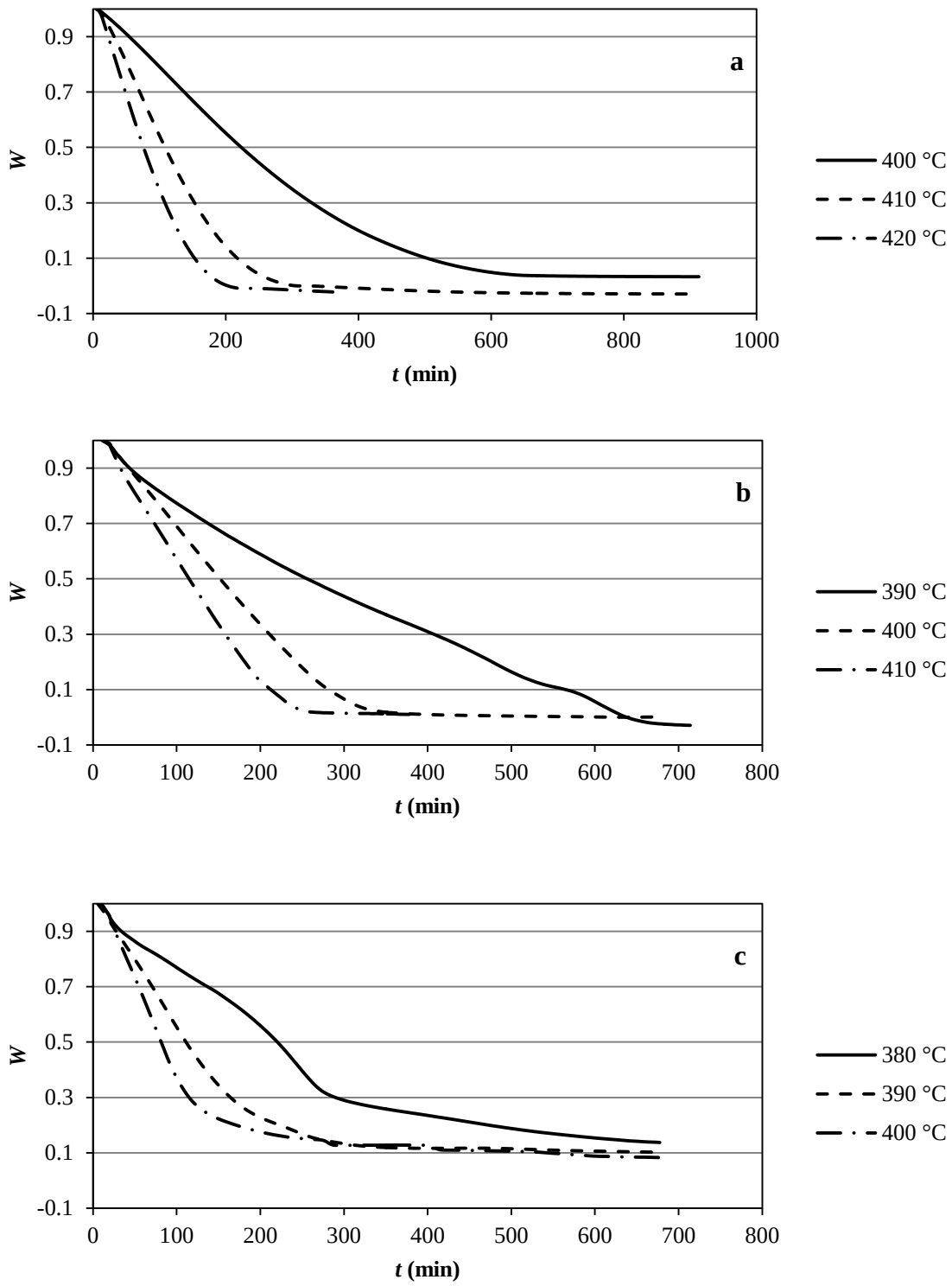

Figure 4-10. Isothermal decomposition curves for (a) sodium acetate, (b) reagent-grade sodium salts, and (c) fermentation sodium salts.

Table 4-4 gives the kinetic parameters for sodium acetate, reagent-grade sodium salts, and fermentation sodium salts. Figure 4-11 shows how dW/dt varies with W using the three isothermal models for each of the three sodium salt types. For sodium acetate, the Avrami-Erofeev and the Sestak-Berggren models fit the experimental data equally well because θ for both models was very similar. However, E_A for the Sestak-Berggren model is a much closer fit to the one determined using the isoconversional methods ($\hat{E}_A$). For the reagent-grade sodium salts, the n^{th}-order and Sestak-Berggren models have very similar values of θ and both give values of E_A similar to $\hat{E}_A$ of reagent-grade salts; however, the Sestak-Berggren model is slightly closer to the $\hat{E}_A$ of reagent-grade salts. For the fermentation sodium salts, the Sestak-Berggren model fits the best because it has the lowest θ and the value of E_A is closest to $\hat{E}_A$ of fermentation sodium salts.

Table 4-4. Kinetic parameters for the thermal decomposition of the three sodium salt types.

Model	Average E_A (kJ/mol)	Average A (min^{-1})	m	n	p	θ
Sodium acetate						
n^{th}-order	243.95 ± 0.22	2.75×10^{16}	–	0.55	–	0.1574
Avrami-Erofeev	242.79 ± 0.22	2.32×10^{16}	–	1.66	–	0.1144
Sestak-Berggren	228.28 ± 0.18	1.29×10^{15}	–4.14	2.12	4.14	0.1137
Reagent-grade sodium salts						
n^{th}-order	207.00 ± 0.20	4.29×10^{13}	–	0.30	–	0.1350
Avrami-Erofeev	209.77 ± 0.21	7.27×10^{13}	–	2.18	–	0.2414
Sestak-Berggren	192.06 ± 0.16	2.36×10^{12}	–1.44	0.75	1.31	0.1319
Fermentation sodium salts						
n^{th}-order	171.95 ± 0.29	3.20×10^{11}	–	1.38	–	0.5921
Avrami-Erofeev	169.00 ± 0.31	1.44×10^{11}	–	0.86	–	0.6891
Sestak-Berggren	211.20 ± 0.19	1.33×10^{14}	–35.90	16.48	35.80	0.2918

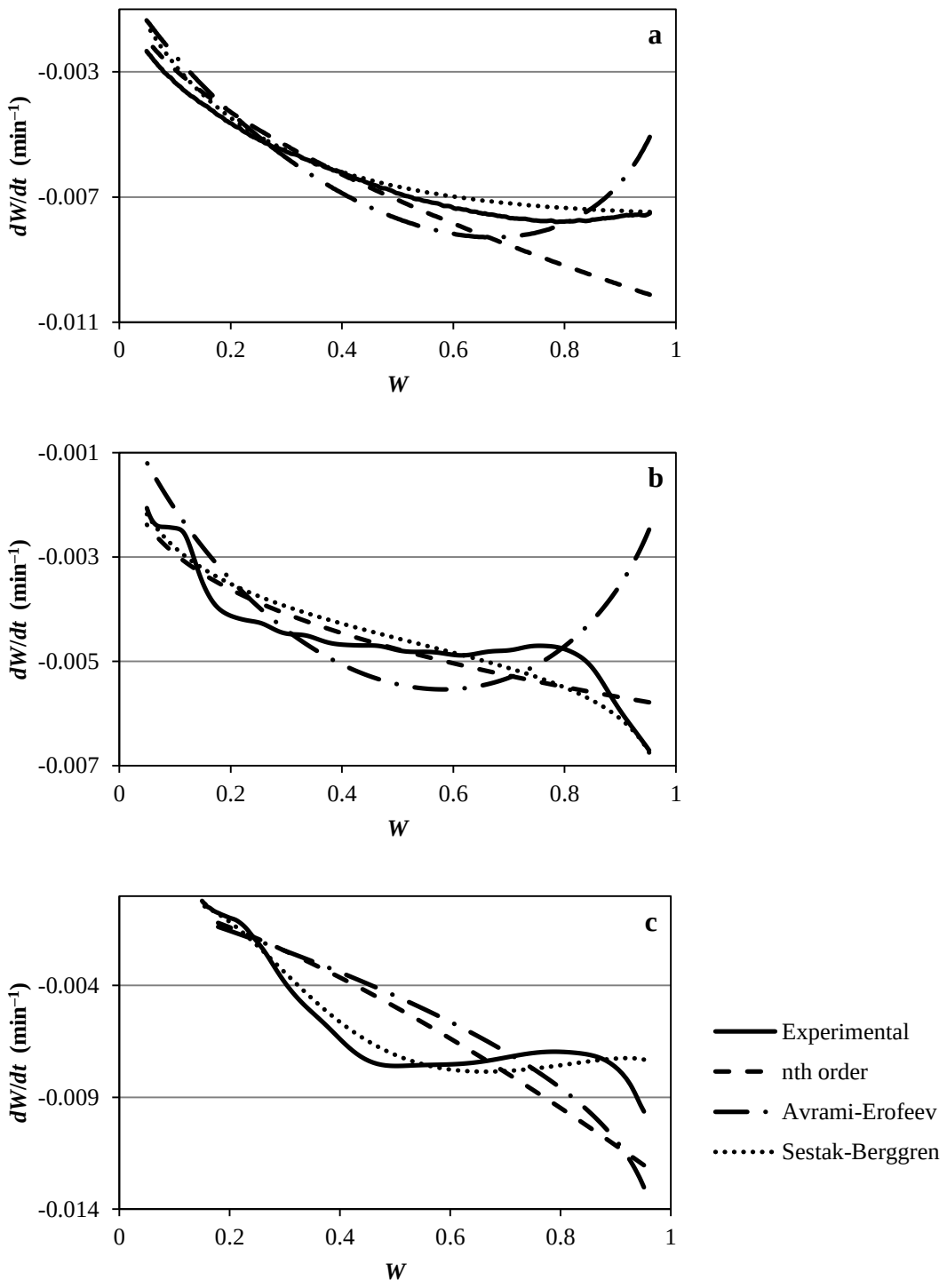

Figure 4-11. Dependence of *dW*/*dt* on *W* for (a) sodium acetate (@ 420 °C), (b) reagent-grade sodium salts (@ 410 °C), and (c) fermentation sodium salts (@ 400 °C).

A case can be made that the Avrami-Erofeev model is suitable for sodium acetate and that the n^{th}-order model is suitable for reagent-grade sodium salts; however, the Sestak-Berggren model fits the fermentation sodium salts best and it fits sodium acetate and reagent-grade sodium salts equally as well, if not slightly better than the other two models. The Sestak-Berggren model is best overall, suitable for sodium carboxylate salts with a wide range of compositions and varying degrees of purity. It is better equipped to handle the complex nature of the thermal decomposition of all three sodium salt types. To illustrate this, Figure 4-12 shows parity plots in which experimental values W_{exp} were plotted against model values W_{mod} from the Sestak-Berggren model for all three isothermal temperatures for each sodium salt type. Table 4-5 gives the slopes and R^2 values for each parity plot from all three models. The Sestak-Berggren model is again shown to be the best overall. All three slopes from the Sestak-Berggren model differ from unity by less than 1% and all three R^2 values are 0.979 and greater. Figures 4-13 to 4-15 compare the time required to achieve W of 0.01, 0.05, and 0.10 for each sodium salt type using the Sestak-Berggren model.

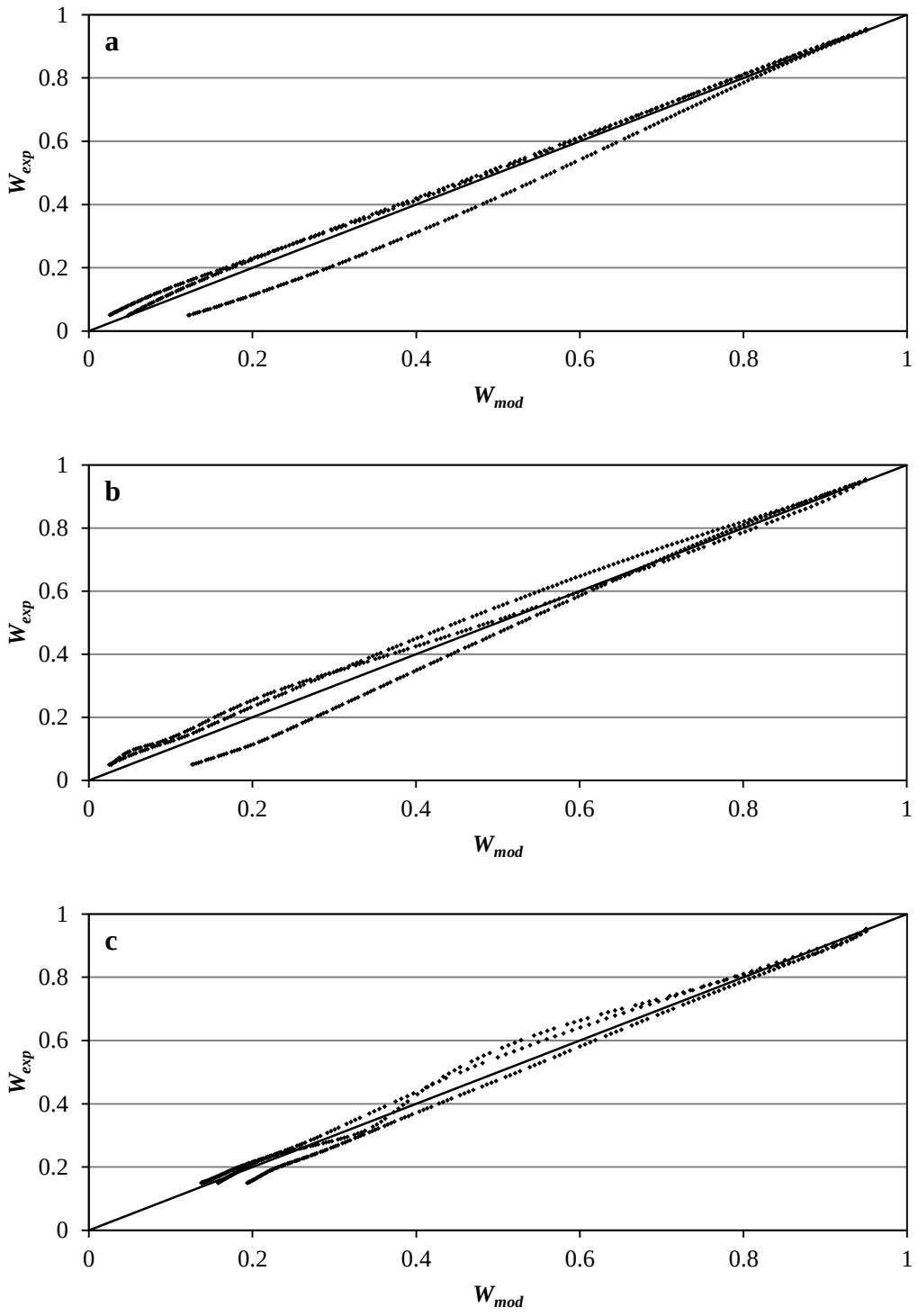

Figure 4-12. Parity plots (W_{exp} vs. W_{mod}) of the Sestak-Berggren model for (a) sodium acetate, (b) reagent-grade sodium salts, and (c) fermentation sodium salts.

Table 4-5. Parameters from parity plots (W_{exp} vs. W_{mod}) of each model for the three sodium salt types.

Model	Slope	R^2
Sodium acetate		
n^{th}-order	1.010	0.983
Avrami-Erofeev	0.929	0.976
Sestak-Berggren	0.995	0.979
Reagent-grade sodium salts		
n^{th}-order	0.992	0.979
Avrami-Erofeev	1.001	0.921
Sestak-Berggren	0.994	0.979
Fermentation sodium salts		
n^{th}-order	1.101	0.958
Avrami-Erofeev	1.098	0.958
Sestak-Berggren	1.007	0.990

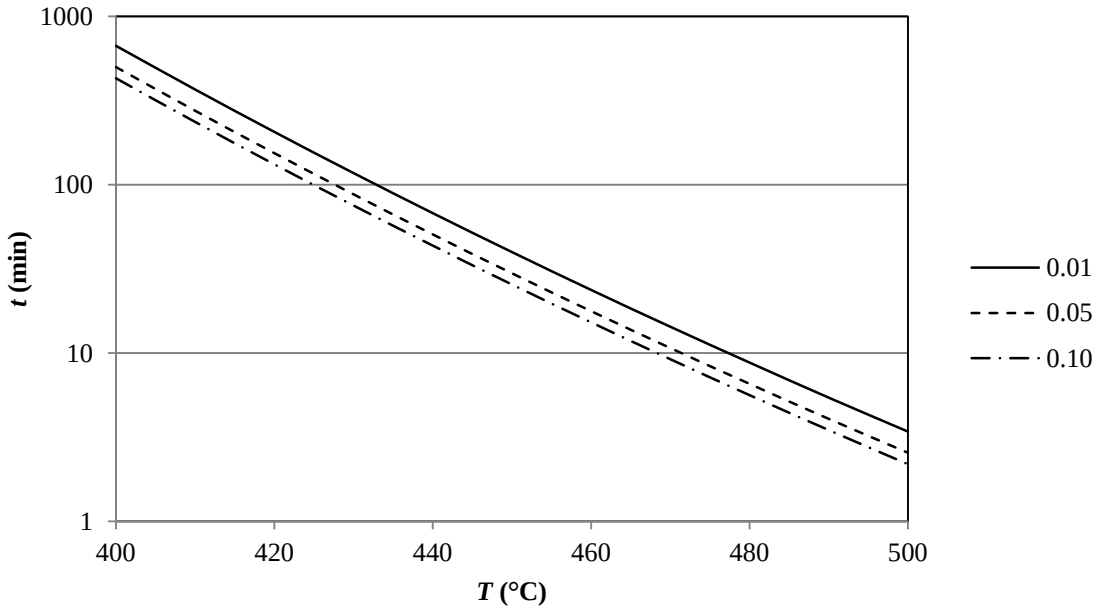

Figure 4-13. Time of thermal decomposition required to achieve *W* of 0.01, 0.05, and 0.10 for sodium acetate.

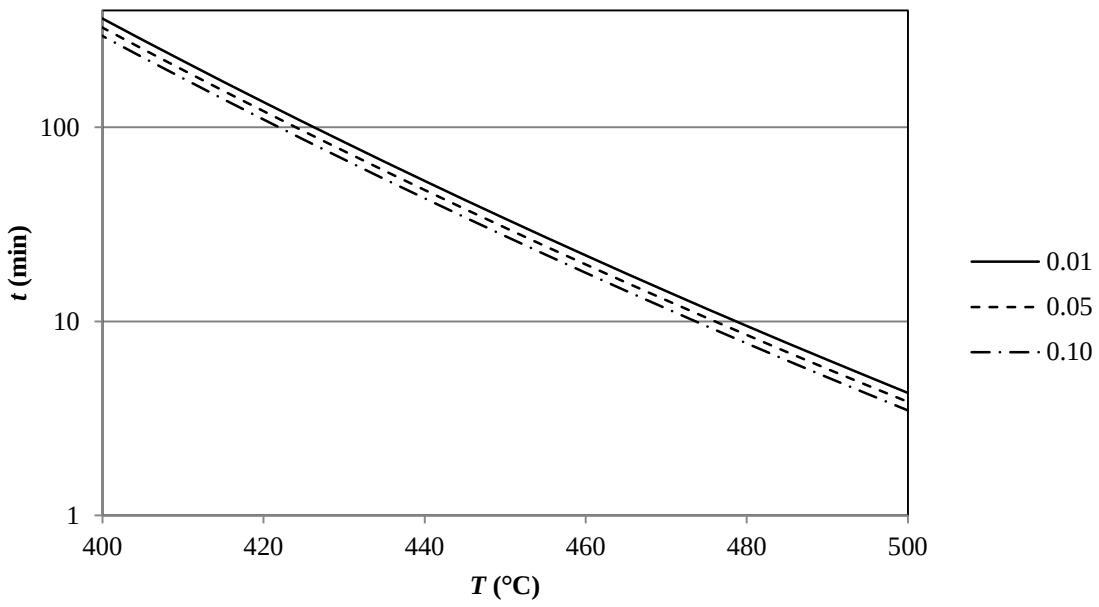

Figure 4-14. Time of thermal decomposition required to achieve *W* of 0.01, 0.05, and 0.10 for reagent-grade sodium salts.

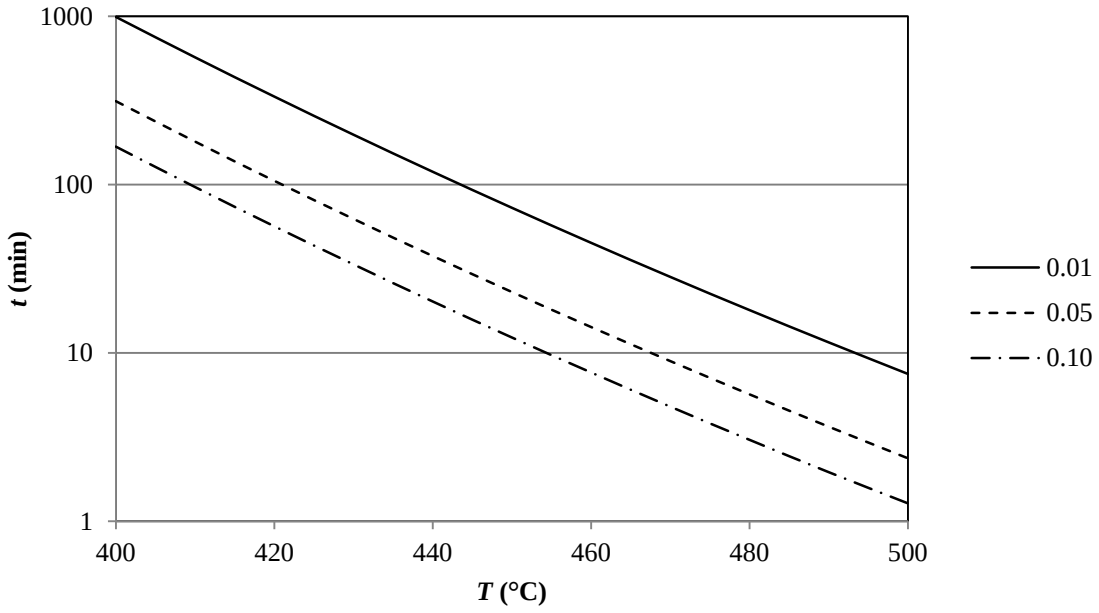

Figure 4-15. Time of thermal decomposition required to achieve *W* of 0.01, 0.05, and 0.10 for fermentation sodium salts.

Two other studies have determined E_A and A for the thermal decomposition of sodium acetate. Reed and Thornley [27] measured weight loss over the course of the thermal decomposition for five isothermal runs with temperatures from 428–452 °C. Afzal et al. [44] measured W using TGA. The data were analyzed using the Coats and Redfern method [55], which is an integral approximation method using a single non-isothermal run with a constant heating rate. The kinetic parameters from both studies are given in Table 4-6. Both studies used n^{th}-order kinetics over limited ranges of W which is not suitable for the complex nature of the thermal decomposition of sodium acetate. In addition, neither study used multiple heating rates to determine how E_A varied with W or determine an average E_A.

Table 4-6. Kinetic parameters of the thermal decomposition of sodium acetate from other studies.

	E_A (kJ/mol)	A (min^{-1})	Reaction order	Range of W
Reed and Thornley	161.92	7.21×10^9	2	1.0–0.25
Afzal et al.	173.55 ± 0.26	–	2	0.86–0.13

4.5. Conclusions

Using three different isoconversional methods, the $\hat{E}_A$ values were found for sodium acetate, reagent-grade sodium salts, and fermentation sodium salts. The E_A of all three sodium salt types varies with W. In part, this is because of the complex nature of the thermal decomposition of the sodium salts and more so because there are many reacting species in the decomposition of reagent-grade and fermentation sodium salts.

Using isothermal decompositions, three models were tested for each sodium salt type. For each of the three sodium salt types, the Sestak-Berggren model had the lowest value of θ and gave E_A values closest to the values of $\hat{E}_A$. This implies that the Sestak-Berggren model is most suitable for modeling sodium carboxylate salts with a variety of compositions and degrees of purity.

5. MODELING THE KINETICS OF THERMAL DECOMPOSITION OF CALCIUM CARBOXYLATE SALTS

5.1. Introduction

Using the MixAlco™ process, the thermal decomposition of carboxylate salts is a critical step in converting biomass into useful chemicals and fuels. Kinetic models and parameters for these decompositions are necessary to design and size commercial-scale reactors. The carboxylate salts are thermally decomposed to yield their corresponding ketones, as shown in Equation 5-1.

$$M^{+}(RCOO^{-}) + M^{+}(R'COO^{-}) \xrightarrow{\Delta} RCOR' + M_2CO_3 \quad (5\text{-}1)$$

For purposes of this study, M^{+} is a calcium ion, but generally can be any alkali metal or half of any alkaline earth metal.

The aim of this study is to first properly model the thermal decomposition of a simple carboxylate salt (calcium acetate) and then apply that model to the thermal decomposition of a mixture of reagent-grade carboxylate salts similar to that produced by the MixAlco™ process. Finally, the model is tested using actual carboxylate salts from a MixAlco™ fermentation. The first step was to determine the activation energy (E_A) for the thermal decomposition of all three salt types using three isoconversional methods. Next, functions of conversion were proposed to model each of the thermal decompositions using three isothermal models. The use of reagent-grade salts eliminated reactions associated with impurities found in fermentation salts, allowing measured kinetics to be attributed solely to the thermal decomposition of the carboxylate salts.

5.2. Materials and methods

5.2.1. Preparation of salts

In this section, any solid mixture of calcium carboxylate salts will be described as *calcium salts*. Calcium acetate hydrate (Alfa Aesar, Ward Hill, MA, 97.0%) was used for this study. It was ground with mortar and pestle and sieved into a particle size range of 25–45 μm. The calcium acetate was then dried at 105 °C for 24 h and placed in a desiccator. The moisture content after drying was 16.5%, which was in the form of hydrated crystalline structure.

Reagent-grade calcium salts were prepared by mixing the corresponding reagent-grade carboxylic acids with equimolar amounts of reagent-grade calcium hydroxide in deionized water, resulting in a solution of pH 8.5. These acid and corresponding salt profiles are typical of what has been reported for anaerobic mixed-culture fermentation [12-14]. A 2-L aliquot of this solution was evaporated in a glass beaker. The precipitated reagent-grade calcium salts were collected, weighed, and dried at 105 °C for at least 24 h. The calcium salts were ground with mortar and pestle and washed with chloroform to remove any residual acids. The calcium salts were separated into the same particle size range as calcium acetate and then dried at 105 °C for an additional 24 h and placed in a desiccator. Acid and corresponding salt compositions were verified by gas chromatography (Table 5-1).

Fermentation calcium salts were prepared using clarified broth from a MixAlco™ fermentation buffered with calcium carbonate (Terrabon, Inc, Houston, TX). Clarification was performed using a proprietary process involving ultra-filtration and

reverse osmosis. The broth was adjusted to pH 9 by adding excess calcium hydroxide and was then evaporated to collect the fermentation calcium salts. The fermentation calcium salts were ground and separated into a particle range in the same manner as the reagent-grade calcium salts. Acid and corresponding salt compositions were verified by gas chromatography (Table 5-1).

Table 5-1. Acid and corresponding salt profiles of reagent-grade and fermentation calcium salts.

		Reagent-grade salts		Fermentation salts	
Carbon number	Acid	Acid (wt. %)	Salt (wt. %)	Acid (wt. %)	Salt (wt. %)
2	Acetic	54.13	56.21	64.90	66.74
3	Propionic	15.55	15.41	8.44	8.29
4	Isobutyric	0.96	0.92	1.31	1.24
4	Butyric	11.05	10.60	17.18	16.31
5	Isovaleric	0.69	0.64	0.68	0.63
5	Valeric	6.13	5.74	1.46	1.35
6	Caproic	7.60	6.98	4.12	3.74
7	Heptanoic	3.31	2.99	0.96	0.86
8	Octanoic	0.56	0.50	0.96	0.84

5.2.2. Thermal decomposition

Thermal gravimetric analysis (TGA) decompositions were performed in a Mettler-Toledo TGA/DSC 1, located in room 1417 in the 1972 Wing of the Chemistry Building at Texas A&M University. Samples were weighed (5–10 mg) into 100-µL aluminum sample pans. A purge gas of Ar at a flow rate of 20 mL/min was used for all runs. For isothermal runs, the temperature was ramped up to the set temperature at a rate of 20 °C/min. Non-isothermal runs used heating rates of 2, 4, 8, and 16 °C/min. A blank sample pan was also run at each heating rate as a baseline and subtracted from the corresponding sample run to account for thermal drift.

A Carbolite HTR 11/75 rotary reactor furnace with a viewing panel was used to visually inspect the decomposition reaction. Samples of 30 g were placed in the reaction vessel and a purge gas of N_2 at a flow rate of 50 mL/min was used for all runs. All runs in the rotary reactor furnace used a heating rate of 10 °C/min.

5.2.3. Solids analysis

Samples of reagent-grade and fermentation calcium salts were weighed (0.3 g) and dissolved with 2 mL of 3-M phosphoric acid. The mixture was then diluted to 10 mL with deionized water. Solutions of dissolved calcium salts were mixed with equal parts of a 1.162 g/L solution of 4-methyl-valeric acid (internal standard) and 3-M phosphoric acid. Acid analysis was performed using an Agilent 7890A gas chromatograph (GC) system equipped with a flame ionization detector (FID), and an Agilent DB-FFAP: J&W 123-3232 column. Injection volume was 0.2 µL and inlet temperature was 230 °C. Carrier gas was helium at 103 kPa (gauge) at a flow rate of 3.78 mL/min. The

temperature profile was 40 °C for 2 min, ramped to 200 °C at 20 °C/min, and held for 2.5 min. Outlet temperature was 230 °C. The run lasted for 12.5 min. Carboxylate salt compositions and the amount of calcium salts per amount of solid (salt content) were calculated from the acid compositions of the solutions reported by the GC (Table 5-1). Solids remaining in the sample pan after thermal decomposition were not analyzed for composition.

5.3. Results and discussion

The formulas and calculations used in the kinetic analysis of the thermal decomposition of calcium salts are detailed in Section 4.3. The following sections describe the phase behavior of the calcium carboxylate salts as well as non-isothermal and isothermal decompositions.

5.3.1. Phase behavior

Calcium acetate and both the reagent-grade and fermentation calcium salts melt at the onset of thermal decomposition. Visual inspection of the calcium salts during heating showed calcium acetate becomes viscid but not fully liquid during the thermal decomposition, which occurs at approximately 435–445 °C. The reagent-grade and fermentation calcium salts behave similarly at approximately 330–350 °C.

5.3.2. Non-isothermal decomposition

Figures 5-1 through 5-4 show the thermal decomposition curves for calcium acetate, reagent-grade calcium salts, and fermentation calcium salts for all four heating rates used in this study. These thermal decomposition curves show that the calcium acetate sample begins to lose significant weight at approximately 350 °C, and the

reagent-grade and fermentation calcium salts samples both begin to lose significant weight at approximately 320 °C. For calcium acetate and the fermentation calcium salts, there is a discontinuity in the curves that begins at a *W* of approximately 0.25. For the reagent-grade calcium salts, there is a discontinuity that begins at a *W* of approximately 0.10. These discontinuities indicate that a different reaction or mechanism becomes predominant.

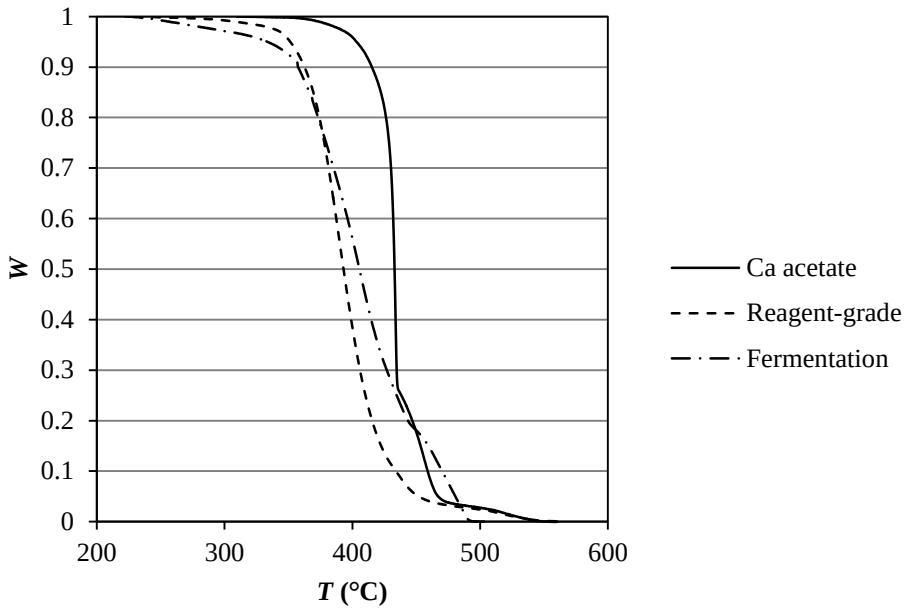

Figure 5-1. Thermal decomposition curves for calcium acetate, reagent-grade calcium salts, and fermentation calcium salts at a heating rate of 2 °C/min.

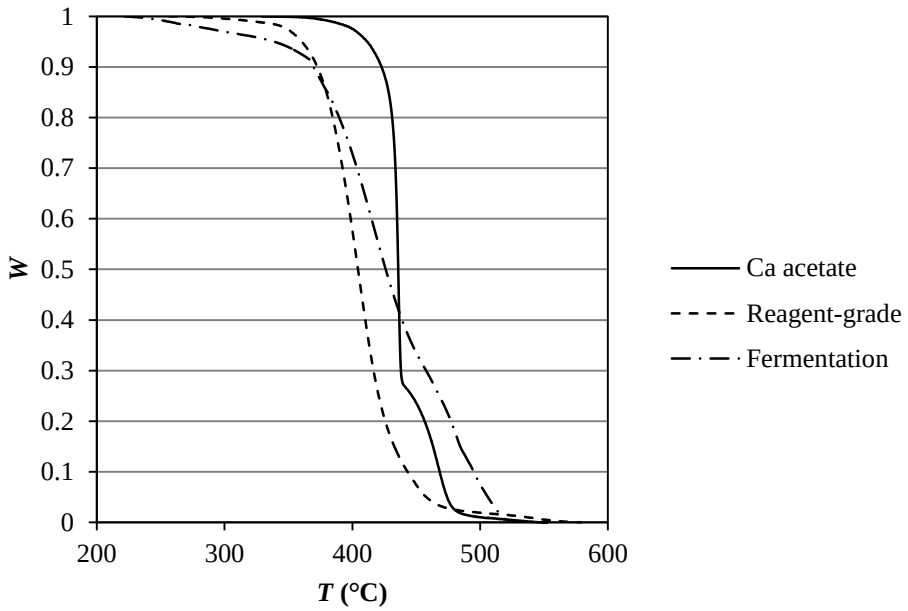

Figure 5-2. Thermal decomposition curves for calcium acetate, reagent-grade calcium salts, and fermentation calcium salts at a heating rate of 4 °C/min.

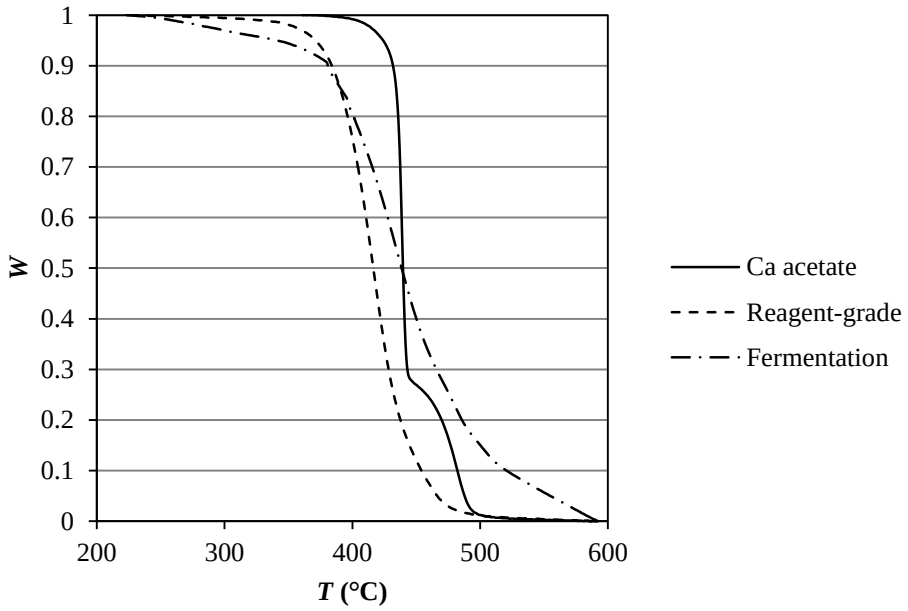

Figure 5-3. Thermal decomposition curves for calcium acetate, reagent-grade calcium salts, and fermentation calcium salts at a heating rate of 8 °C/min.

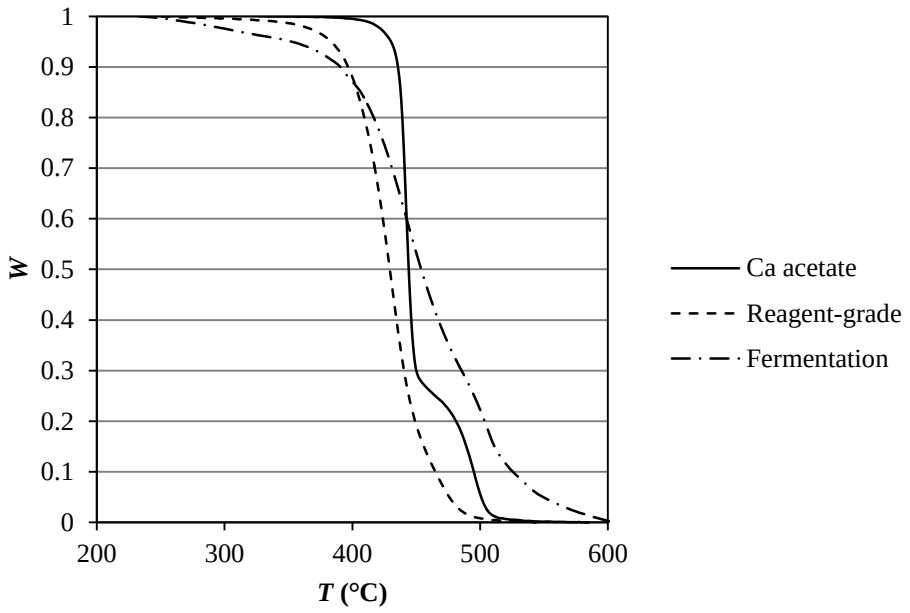

Figure 5-4. Thermal decomposition curves for calcium acetate, reagent-grade calcium salts, and fermentation calcium salts at a heating rate of 16 °C/min.

Heating rates of 2, 4, 8, and 16 °C/min were used for each of the three isoconversional methods employed. The same methods and heating rates were used for the decomposition of all three calcium salt types. Figure 5-5 shows how E_A varies with W for each isoconversional method used for each calcium salt type. For each value of W, only E_A values with R^2-values of 0.85 and above were considered for the Friedman and Li-Tang methods and E_A values with a minimization value of 13 or less for the Vyazovkin method. Of the three calcium salt types, calcium acetate displays the largest variation in E_A during thermal decomposition. All three isoconversional methods show similar trends of E_A with respect to W and indicate that E_A highly depends on W for calcium acetate. All three isoconversional methods show similar trends of E_A vs. W for the reagent-grade and fermentation calcium salts. For both the reagent-grade and fermentation calcium salts, E_A values are much less variable, each having a standard deviation of approximately 19% of the respective $\hat{E}_A$. In addition, E_A significantly depends on W only at the beginning and ends of thermal decomposition for the reagent-grade and fermentation calcium salts. For each calcium salt type, Table 5-2 shows the average of the three E_A values from the three isoconversional methods for selected values of W ($\bar{E}_A$ (W)). It also contains the $\hat{E}_A$ and corresponding standard deviations for each calcium salt type.

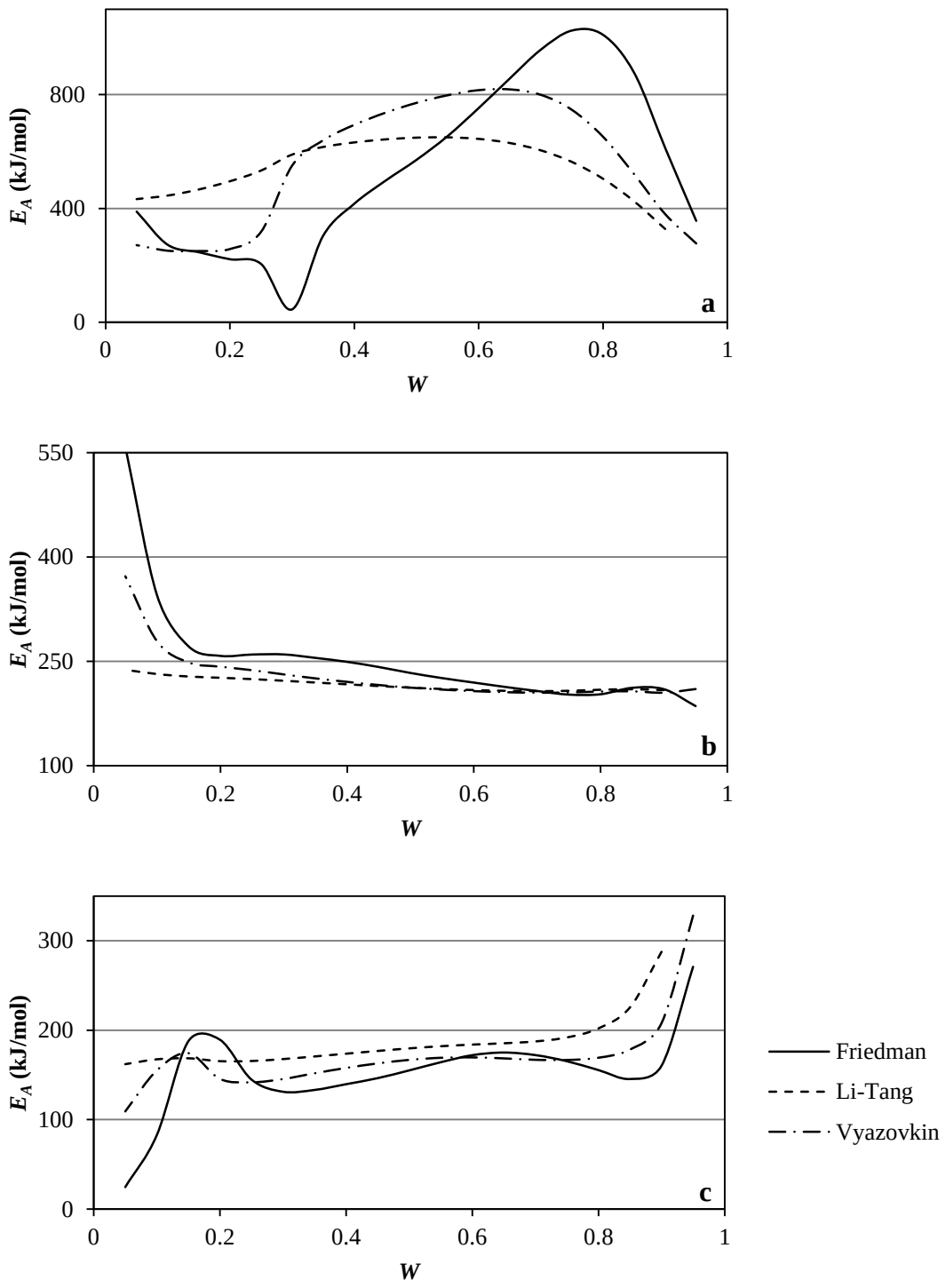

Figure 5-5. Dependence of E_A on W for (a) calcium acetate, (b) reagent-grade calcium salts, and (c) fermentation calcium salts.

Table 5-2. Dependence of $\bar{E}_A$ on W for each calcium salt type.

	$\bar{E}_A$ (W) (kJ/mol)		
W	Calcium acetate	Reagent-grade salts	Fermentation salts
0.95	285.83	203.57	299.50
0.90	440.37	207.86	218.60
0.85	607.75	209.60	183.13
0.80	722.23	206.17	175.56
0.75	778.28	205.05	174.66
0.70	786.91	206.49	175.54
0.65	768.09	208.81	176.32
0.60	737.34	211.82	175.21
0.55	700.33	215.20	171.83
0.50	663.27	219.23	167.20
0.45	625.21	224.08	162.04
0.40	580.60	228.92	157.08
0.35	627.63	233.33	151.91
0.30	569.57	237.73	148.13
0.25	351.84	240.51	150.75
0.20	324.72	242.18	166.81
0.15	321.02	249.30	176.88
0.10	322.96	285.13	161.24
0.05	364.28	389.45	162.05
$\hat{E}_A$	556.75	232.87	176.55
Standard deviation	179.78	43.15	33.55

For calcium acetate, $\bar{E}_A$ (W) increases steeply and then decreases as thermal decomposition proceeds forward. For the reagent-grade calcium salts, $\bar{E}_A$ (W) increases slightly at first and then steeply at the end as thermal decomposition proceeds forward. For the fermentation calcium salts, $\bar{E}_A$ (W) decreases as thermal decomposition proceeds forward. The $\hat{E}_A$ of calcium acetate is significantly higher than the $\hat{E}_A$ for both reagent-grade and fermentation calcium salts. This suggests that E_A for the decomposition of higher molecular weight calcium salts is lower than that of calcium acetate and presumably E_A decreases with increasing molecular weight. The decreased $\hat{E}_A$ for fermentation calcium salts from that of reagent-grade calcium salts most likely results from impurities.

A thermal decomposition in which E_A values vary significantly with W indicates that multiple reactions and/or mechanisms occur at different times throughout the reaction. This suggests that the thermal decomposition of calcium acetate proceeds by more than one mechanism. Most likely, it resembles that of a heterogeneous shrinking core described in Sections 2.4 and 3.4. It begins as a decomposition mechanism on the particle surface as it melts and thermal decomposition begins to occur in the resulting liquid layer. As the thermally decomposing liquid layer moves inward, a porous outer layer of calcium carbonate remains. This causes the mechanism to gradually resemble one of diffusion, because the product vapors must migrate out of the calcium carbonate layer to leave the particle. The apparent E_A of a reaction decreases as it becomes diffusion limited. E_A for both calcium acetate and fermentation calcium salts decreases towards the end of decomposition, suggesting diffusion becomes more predominant. For

the case of reagent-grade and fermentation calcium salts, E_A is expected to depend on W. Because multiple species are present, multiple reactions occur at different rates during the decomposition as temperature increases. In addition, multiple mechanisms are likely present in the decomposition of reagent-grade calcium salts and even more so for fermentation calcium salts, because of the presence of impurities.

5.3.3. Isothermal decomposition

Isothermal decompositions were used to evaluate $f(W)$ for each calcium salt type. Calcium acetate decompositions were performed at 390, 400, 410, and 420 °C, and the range of W used for modeling was from 0.95–0.10. Both the reagent-grade and fermentation calcium salts decompositions were performed at 390, 400, and 410 °C, and the range of W used for modeling was from 0.95–0.05. Figure 5-6 shows the isothermal decomposition curves for each of the calcium carboxylate salt types at each temperature. Each of the three models was fit to the experimental data. For the n^{th}-order, Avrami-Erofeev, and Sestak-Berggren models, values of k, E_A, and A were determined using the method described in Section 4.4. Values of m, n, and p were found by minimizing θ.

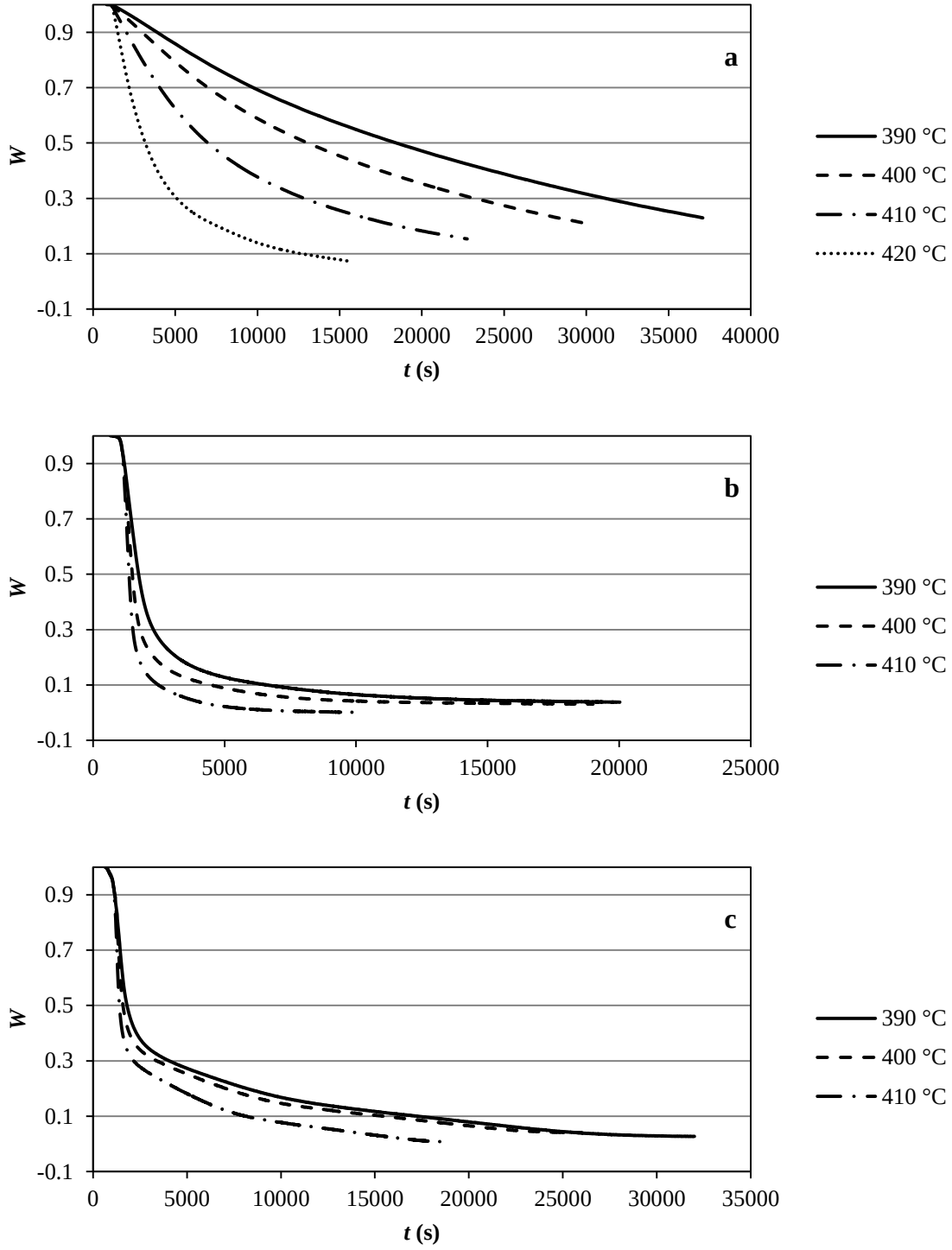

Figure 5-6. Isothermal decomposition curves for (a) calcium acetate, (b) reagent-grade calcium salts, and (c) fermentation calcium salts.

Figure 5-7 shows how dW/dt varies with W using the three isothermal models for each of the three calcium salt types. Table 5-3 gives the kinetic parameters for calcium acetate, reagent-grade calcium salts, and fermentation calcium salts. For calcium acetate, the n^{th}-order and the Sestak-Berggren models fit the experimental data equally well because θ for both models was very similar. However, E_A for all three models is less than half of the one determined using the isoconversional methods ($\hat{E}_A$). It could be that only the E_A at the beginning and/or the end of thermal decomposition was measured using the isothermal methods for calcium acetate. For the reagent-grade calcium salts, the n^{th}-order and Sestak-Berggren models also have very similar values of θ, but the Sestak-Berggren model gives an E_A closer to the $\hat{E}_A$ of reagent-grade calcium salts. For the fermentation calcium salts, the Avrami-Erofeev model has the lowest θ and the Sestak-Berggren model has the highest. However, the Sestak-Berggren model has the closest values of E_A to the $\hat{E}_A$ of fermentation calcium salts.

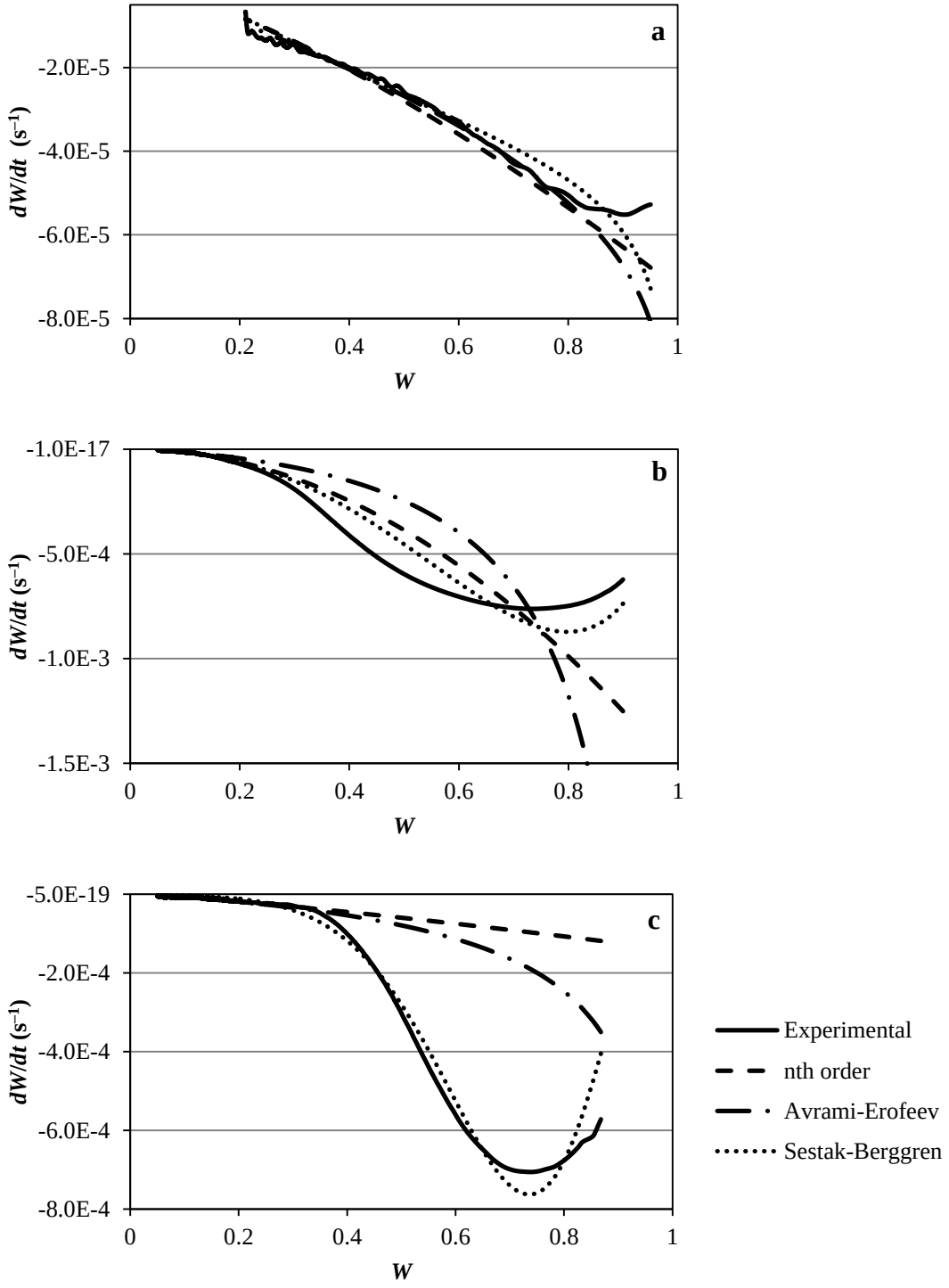

Figure 5-7. Dependence of *dW*/*dt* on *W* for (a) calcium acetate (@ 400 °C), (b) reagent-grade calcium salts (@ 390 °C), and (c) fermentation calcium salts (@ 390 °C).

Table 5-3. Kinetic parameters for the thermal decomposition of the three calcium salt types.

Model	Average E_A (kJ/mol)	Average A (s^{-1})	m	n	p	θ
Calcium acetate						
n^{th}-order	215.45 ± 0.21	5.25×10^{12}	–	1.38	–	0.1395
Avrami-Erofeev	193.59 ± 0.17	8.24×10^{10}	–	0.85	–	0.1949
Sestak-Berggren	240.14 ± 0.23	2.12×10^{14}	–9.88	5.14	9.62	0.1472
Reagent-grade calcium salts						
n^{th}-order	293.04 ± 0.23	2.26×10^{20}	–	2.00	–	0.1575
Avrami-Erofeev	296.86 ± 0.24	1.99×10^{20}	–	0.51	–	0.3530
Sestak-Berggren	246.44 ± 0.04	1.84×10^{17}	6.25	0.31	–5.50	0.1686
Fermentation calcium salts						
n^{th}-order	126.68 ± 0.24	1.39×10^{6}	–	1.24	–	0.2742
Avrami-Erofeev	129.26 ± 0.23	3.20×10^{6}	–	0.63	–	0.2613
Sestak-Berggren	200.54 ± 0.15	4.40×10^{15}	51.13	–14.63	–48.18	0.3526

A case can be made that the n^{th}-order and Sestak-Berggren models are both suitable for calcium acetate and reagent-grade calcium salts, even though neither model gives an E_A value close to the $\hat{E}_A$ for the calcium salts. For the fermentation calcium salts, it appears that both the n^{th}-order and Avrami-Erofeev models fit best, but the Sestak-Berggren model gives the closest E_A value to the $\hat{E}_A$ of fermentation calcium salts. From the values in Table 5-3, it is very difficult to determine which model is best for each calcium salt type and especially difficult to determine which is best overall.

To better determine which model is best, parity plots were made in which experimental values W_{exp} were plotted against model values W_{mod} of each isothermal temperature for each calcium salt type. Table 5-4 gives the slopes and R^2 values for each parity plot from all three models. From this table, it is apparent that the n^{th}-order and Sestak-Berggren model fit the experimental data from calcium acetate equally well. The n^{th}-order model has a slope slightly closer to unity, but the Sestak-Berggren model has a

slightly higher R^2 value. For the reagent-grade and fermentation calcium salts, the Sestak-Berggren model fits the experimental data best. Figure 5-8 shows parity plots from the Sestak-Berggren model for all three isothermal temperatures for each calcium salt type. Because it fits calcium acetate equally well and fits reagent-grade and fermentation calcium salts the best, the Sestak-Berggren model is best overall. It is the most suitable for calcium carboxylate salts with a wide range of compositions and varying degrees of purity and it is better equipped to handle the complex nature of the thermal decomposition of all three calcium salt types. Figures 5-9 to 5-11 compare the time required to achieve W of 0.01, 0.05, and 0.10 for each calcium salt type using the Sestak-Berggren model.

Table 5-4. Parameters from parity plots (W_{exp} vs. W_{mod}) of each model for the three calcium salt types.

Model	Slope	R^2
Calcium acetate		
n^{th}-order	1.004	0.953
Avrami-Erofeev	1.025	0.934
Sestak-Berggren	0.960	0.966
Reagent-grade calcium salts		
n^{th}-order	0.981	0.973
Avrami-Erofeev	0.978	0.918
Sestak-Berggren	1.019	0.995
Fermentation calcium salts		
n^{th}-order	0.553	0.903
Avrami-Erofeev	0.715	0.948
Sestak-Berggren	1.005	0.983

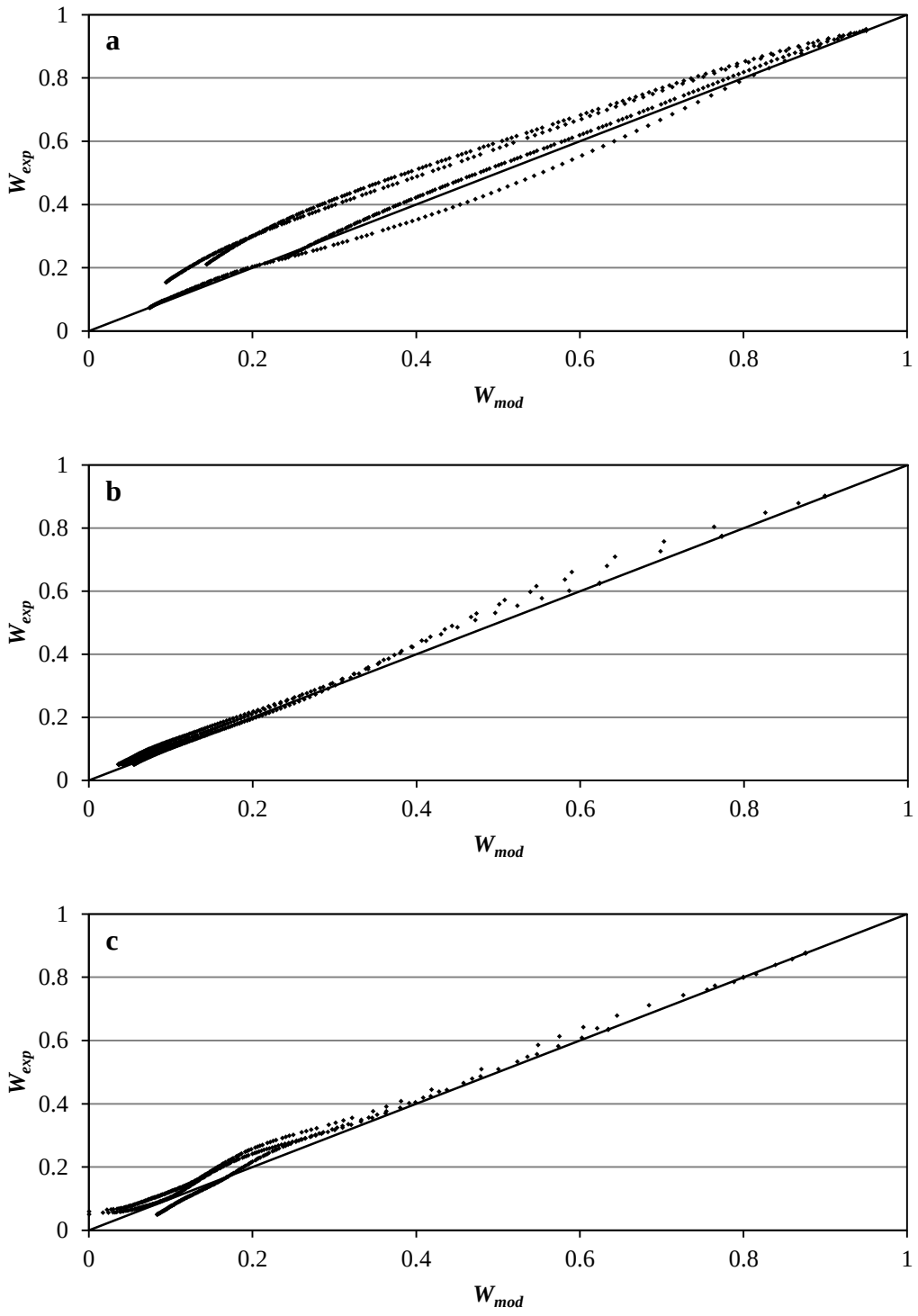

Figure 5-8. Parity plots (W_{exp} vs. W_{mod}) of the Sestak-Berggren model for (a) calcium acetate, (b) reagent-grade calcium salts, and (c) fermentation calcium salts.

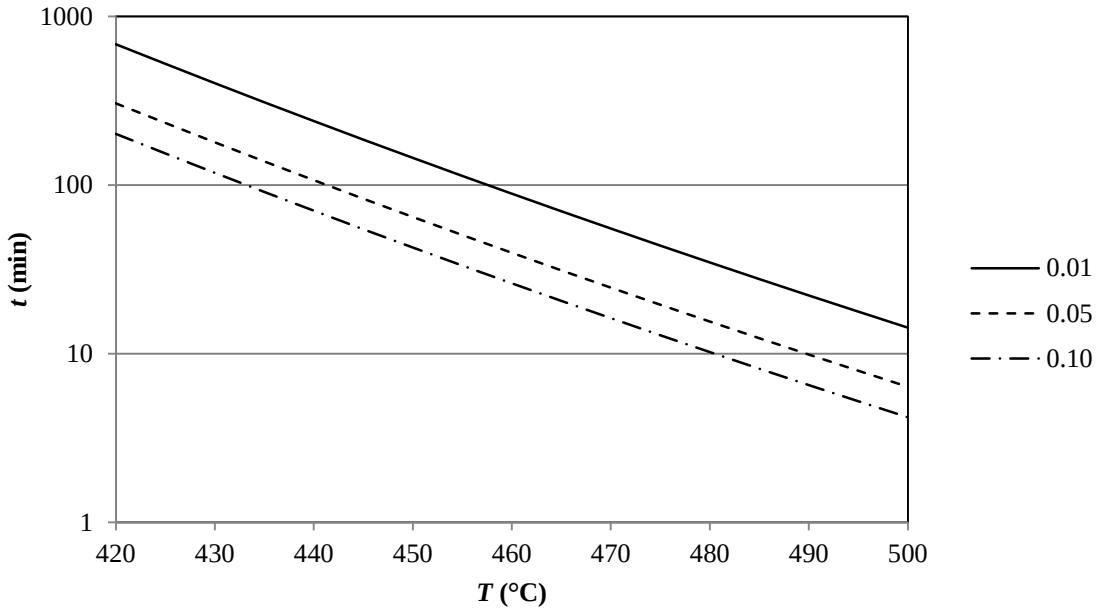

Figure 5-9. Time of thermal decomposition required to achieve *W* of 0.01, 0.05, and 0.10 for calcium acetate.

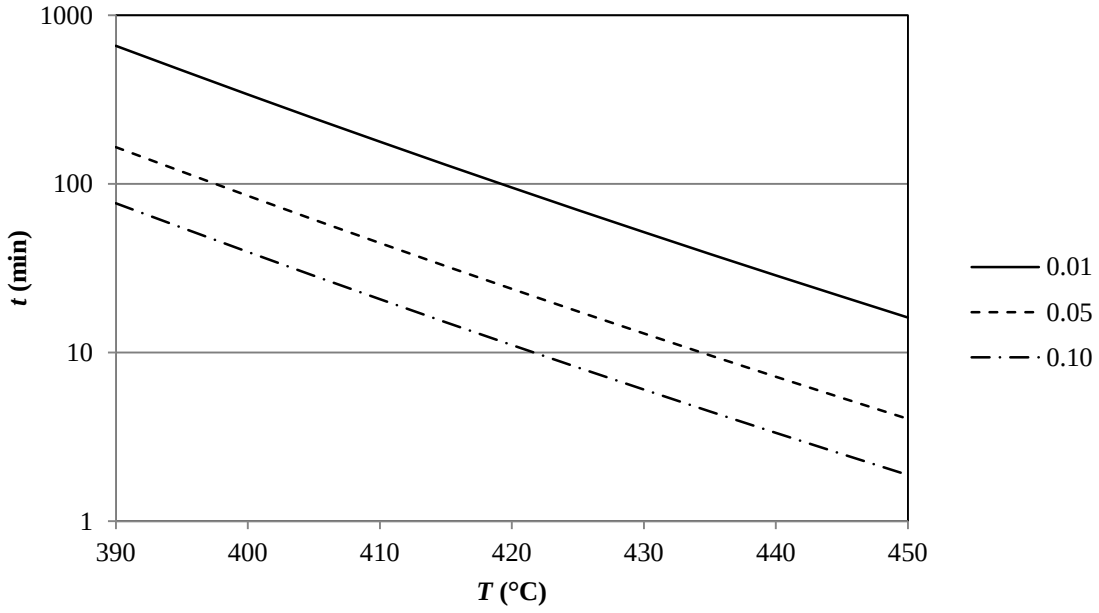

Figure 5-10. Time of thermal decomposition required to achieve *W* of 0.01, 0.05, and 0.10 for reagent-grade calcium salts.

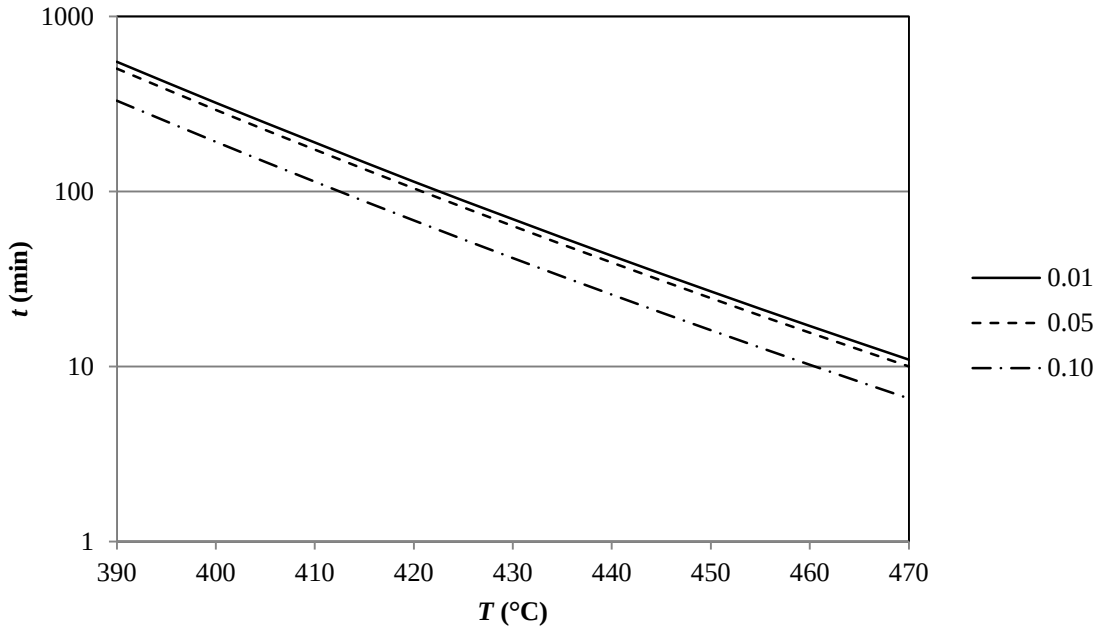

Figure 5-11. Time of thermal decomposition required to achieve *W* of 0.01, 0.05, and 0.10 for fermentation calcium salts.

Several studies have previously attempted to determine the kinetic parameters of the thermal decomposition of calcium acetate and other calcium carboxylate salts. Mu and Perlmutter [35] studied the thermal decomposition of calcium acetate using TGA. Only one run was used at a heating rate of 1 °C/min. Using a simple differential method and n^{th}-order kinetics, the data were fit to a linear form of Equation 5-2.

$$-\frac{dW}{dt} = A \exp\left(-\frac{E_A}{RT}\right) W^n \tag{5-2}$$

To maintain linearity, the thermal decomposition had to be split into two regimes. The first regime was between W of 0.98 and 0.63, and the second between 0.63 and 0.02. Table 5-5 gives the resulting kinetic parameters. Both regimes were found to be 2nd order. The presence of two different regimes suggests a change in mechanisms as the reaction proceeds. A single E_A cannot be used to describe the thermal decomposition over the entire range of W because E_A varies with W. Mu and Perlmutter even admit that not all of the solid decompositions studied follow simple n^{th}-order kinetics because of diffusional resistance in the solid reactant and product.

Table 5-5. Kinetic parameters of the thermal decomposition of calcium carboxylate salts from other studies.

	Calcium carboxylate salt			
	Calcium acetate	Calcium propionate	Calcium butyrate	Fermentation calcium salts
Yeh				
Yield (%)	71.3 ± 16.9	77.5 ± 10	72.3 ± 3.4	96.8 ± 5.8
E_A (kJ/mol)	247.72	105.01	64.16	46.01
A (min^{-1})	1.402×10^{17}	2.332×10^{7}	9348.8	485.36
Reaction order	1	1	1	1
Adelson				
Yield (%)	93.1 ± 0.9	87.5 ± 0.7	94.4 ± 0.9	–
E_A (kJ/mol)	642.6 ± 28.0	2327 ± 162[a] 691.7 ± 73.3[b]	386.5 ± 15.8	–
A (min^{-1})	109.4 ± 0.4	414.7 ± 0.4[a] 121.1 ± 0.2[b]	66.12 ± 0.22	–
Reaction order	1	1	1	–
Mu and Perlmutter				
E_A (kJ/mol)	142.3 ± 2.5[c] 197.9 ± 2.1[d]	–	–	–
A (min^{-1})	1.26×10^{9}[c] 4.16×10^{13}[d]	–	–	–
Reaction order	2	–	–	–

[a] 398 °C and below
[b] 399 °C and above
[c] W: 0.98–0.73
[d] W: 0.73–0.02

Adelson and Yeh, former members of the Holtzapple research group, also separately attempted to determine kinetic parameters for the thermal decompositions of calcium acetate, propionate, and butyrate as well as calcium carboxylate salts from a MixAlco™ fermentation [66, 67]. Both studies measured the accumulation rate of liquid product during thermal decomposition as a measure of conversion using the apparatus described in Section 2.2.2. Table 5-5 summarizes the measured yields and kinetic

parameters. Adelson used one non-isothermal run for calcium acetate, propionate, and butyrate. There was little control over the heating rate, which varied from 0.2–0.7 °C/min and was not very linear in some cases. Using the simple differential method, the data were also fit to a linear form of Equation 5-2. Adelson assumed all calcium salt decompositions to be 1st order. To maintain linearity, he had to split the thermal decomposition of calcium propionate into two regimes. In addition, Adelson conducted two isothermal runs with calcium acetate at 416 and 433 °C for measuring product selectivity. The data from these runs was used to determine the E_A for calcium acetate to be 344.31 kJ/mol, which is approximately half of what he reported in Table 5-5. The E_A reported for the first regime of calcium propionate also seems high for this type of reaction.

Yeh used a series of isothermal runs from 400–500 °C in intervals of approximately 20 °C for each calcium salt type. Using the same linear form of Equation 5-2, he found the order of thermal decomposition for each calcium salt type to be approximately 1.0 and therefore, assumed first-order kinetics for determining E_A and A for each calcium salt type. Yeh had poor temperature control in his experiments, sometimes with as much as 4 °C of variation, and he also used limited ranges of W (0.7–0.2) to determine the kinetic parameters. Yeh's E_A values for calcium propionate, butyrate, and fermentation salts also seemed to be quite low.

Both studies used n^{th}-order kinetics, which is not very suitable for the complex nature of the thermal decomposition of calcium salts, although for calcium acetate, it has

been shown to be as good as the Sestak-Berggren model. In addition, neither study used multiple heating rates to determine how E_A varied with W or to determine an average E_A.

Since these early investigations, the following potential problems with the methods have been identified:

- Conversion was calculated with respect to time by measuring the accumulated volume of liquid product. The fraction of conversion was set equal to the volume fraction and did not consider any gasses evolved during the decomposition or any non-decomposed salts left in the reactor. In addition, equating liquid fraction to the fraction of conversion only holds true if the liquid density remains constant over time. Liquid density was not measured over time to determine if it remained constant.
- Any water vapor and heavier ketones that contacted the dry/ice isopropanol condenser would freeze to the surface, introducing error in the measured liquid fraction.
- The liquid product composition was not determined over time. The liquid was assumed to be pure theoretical product with no presence of byproducts or water from waters of hydration. Analysis of the total liquid product was performed after the reaction was complete for several runs. Liquid product from calcium acetate and propionate and were found to contain 1–5% byproducts. In addition, 99.5% of the liquid product from calcium butyrate was non-theoretical, yet for every value of A and E_A calculated, a 100% theoretical yield was assumed.

- The final degree of conversion of the feed salts was not measured. Instead, it was assumed to go to 100% completion. Using TGA, it is possible to directly measure the mass of the sample over time as it thermally decomposes, eliminating the need to determine it from product measurements over time. TGA also allows temperature and heating rate measurements that are superior to the apparatus used by Adelson and Yeh.

One advantage of the methods used by Adelson and Yeh over using TGA is that the carboxylate salts are thoroughly mixed as they are thermally decomposed which minimizes diffusion effects and product degradation. Attempts are made to keep the samples and particle sizes prepared for TGA small so that diffusion effects are minimized. Another advantage is the ability to collect product samples during or after thermal decomposition. Product vapor could be analyzed if the TGA were used in conjunction with a Fourier-transform infrared (FTIR) spectrometer or a GC-MS.

5.4. Conclusions

Using three different isoconversional methods, the $\hat{E}_A$ values were found for calcium acetate, reagent-grade calcium salts, and fermentation calcium salts. All three calcium salt types have E_A that varies with W. In part, this is because of the complex nature of the thermal decomposition of the calcium salts and more so because there are many reacting species in the decomposition of reagent-grade and fermentation calcium salts.

Using isothermal decompositions, three models were tested for each calcium salt type. For calcium acetate, the n^{th}-order and Sestak-Berggren models seem to work

equally well at modeling the experimental data. Both models have similar values of θ and similar parity plot parameters. The thermal decomposition of calcium acetate is very difficult to study. E_A values from isothermal methods are similar only to the lower $\bar{E}_A$ values from isoconversional methods, not the $\hat{E}_A$ of calcium acetate. For reagent-grade and fermentation calcium salts, the Sestak-Berggren model gives E_A values closest to the respective $\hat{E}_A$ and has parity parameters closest to unity even though it does not have the lowest value of θ. Because the Sestak-Berggren model works best for all three calcium salt types, it is most suitable for modeling calcium carboxylate salts with a variety of compositions and degrees of purity.

6. KETONE REACTOR CONCEPTS AND DESIGNS

6.1. Introduction

For the thermal decomposition of carboxylate salts to be viable step in the MixAlco™ process, it must be a relatively inexpensive continuous process. This section explores reactors used in the past to perform similar thermal decompositions as well as possible reactor designs that address the challenges associated with the continuous thermal decomposition of carboxylate salts from MixAlco™ fermentations. Potential continuous reactor designs and reactor configurations will be presented and discussed. Topics include continuous solids movement through a sealed reactor, phase changes occurring prior to and during decomposition, rapid removal of gaseous products, achieving sufficient heat transfer, and single reactors vs. multiple reactors in series.

After its discovery in 1834, the thermal decomposition of calcium acetate to acetone was the primary industrial process for making acetone until WWI when it was replaced by acetone-producing fermentations, the dehydrogenation of isopropyl alcohol, and the partial oxidation of propane and butane [15]. At the time, it was described as the *dry distillation of acetate of lime*. Acetate of lime referred to the calcium acetate formed by neutralizing pyroligneous acid, an aqueous solution of primarily acetic acid that results from the pyrolysis of wood. Initially, thermal decompositions were performed in batches using fire-heated retorts similar to the one shown in Figure 6-1. A geared stirring arm provided mixing throughout the thermal decomposition. A vapor line connected the retort to a tar and dust trap and then into a condenser. Vapor lines were equipped with

cleaning rods to clear any dust and tar accumulation. The retorts were charged with 300–700 lb_m of calcium acetate and heated to 380 °C. Tar and dust were mostly contained in the trap whereas acetone and water vapor, along with some volatile impurities, were condensed and collected in a storage tank. At the end of the decomposition, steam was blown through the retort to sweep out the remaining vapors. The tar and dust trap was then heated with steam to drive off any remaining acetone.

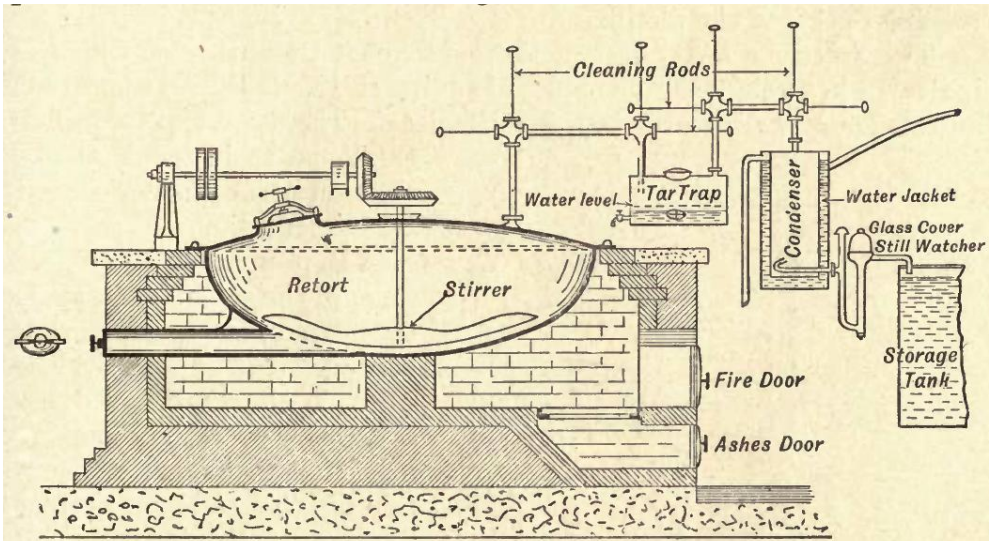

Figure 6-1. Fire-heated retort and collection equipment used for the thermal decomposition of calcium acetate to acetone. Courtesy of Young [32], page 247.

Direct-firing of the outer wall of the retort caused over-heating of the calcium acetate at the inner wall, which increased formation of char, tars, and impurities. To overcome this, retorts such as the one shown in Figure 6-2 were employed. Calcium acetate was placed on trays that were rolled into the retort on wheeled racks. In addition

to eliminating over-heating, it made removal of the residual solids and insertion of fresh calcium acetate faster and cleaner, and it reduced loss of heat.

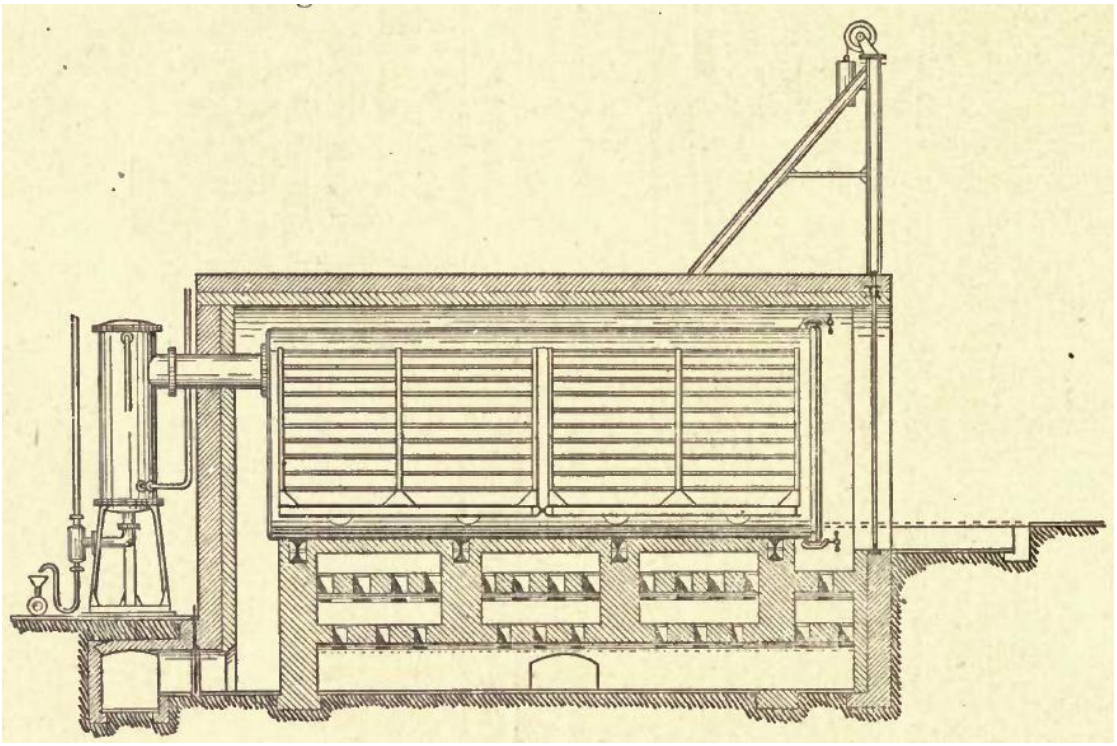

Figure 6-2. Retort with trays on wheeled racks and collection equipment for the thermal decomposition of calcium acetate. Courtesy of Young [32], page 250.

6.2. Continuous reactor design factors

6.2.1. Feeding of carboxylate salts into reactor

Carboxylate salts can be fed into the reactor as either solids or liquids. In the case of feeding solid carboxylate salts, they can have either a crystalline or an amorphous structure with varying degrees of waters of hydration present in the matrix. In the case of feeding liquid carboxylate salts, they are actually in a very concentrated aqueous phase. If the solution is at or above saturation, a slurry will be present.

Feeding liquids is easier than solids because it requires less sophisticated equipment to seal against outside conditions and to meter the flow. Depending on the carboxylate salt composition and water content, the liquid feed can be so viscous that a specialized pump is necessary, or that a minimum water content must be maintained to keep viscosity low. Feeding liquids also introduces more water into the reactor than solids. This additional water must be heated and vaporized, thus significantly increasing reactor heat duty. In addition, the water must be separated from the ketone product after collection. Because of the high reactor temperatures, excess water tends to flash immediately upon entering the reactor, initially generating large amounts of steam that can entrain unreacted solids and remove them from the reactor through the vapor outlets.

Feeding solids introduces much less water into the reactor, thus reducing the heat duty and the amount of water separation from the ketone product. However, solids are much harder to feed and to meter the flow, which requires more sophisticated solids-handling equipment. Because product vapor can escape through the solids-loading mechanisms, they must be delivered in sealed hoppers, which are subject to channeling and bridging without proper agitation. At least two feed hoppers are required for continuous operation so that one delivers solids to the loading mechanism while the other(s) were charged with solids. Valves between each of the hoppers and loading mechanism are necessary to switch between hoppers. Solids entering into the reactor must be kept at temperatures above the product condensation point, otherwise liquids will condense on the solids impeding their ability to flow properly and causing them to cake on the loading mechanism surfaces. Additionally, purge gases on the hopper are

necessary to keep product vapors from migrating into the hopper and condensing. Such a purge gas would not be necessary if a vacuum were employed in the reactor.

6.2.2. Phase changes in the reactor

As mentioned in Section 3, the process of thermally decomposing carboxylate salts undergoes phase changes. Whether fed as a liquid or a solid, once the carboxylate salts enter the reactor, excess water begins to vaporize immediately. All excess water is removed from the salts at approximately 190–210 °C. At that point, the carboxylate salts are either a crystalline solid (in the case of calcium carboxylate salts) or a wax-like amorphous solid (in the case of sodium carboxylate salts). It is important to note that higher molecular weight calcium carboxylate salts form amorphous solids as well. Impurities in the feed, along with rapid dehydration, can also keep the carboxylate salts from forming crystals. As the temperature of the carboxylate salts continues to quickly rise, they begin to melt. Melting points can vary widely depending on cation and carboxylate salt composition. Some carboxylate salts will melt completely before thermal decomposition begins (i.e., sodium carboxylate salts) whereas others will begin to thermally decompose before they have fully melted (i.e., calcium carboxylate salts). Regardless, a liquid phase of carboxylate salts is necessary for thermal decomposition to occur. During this melt/thermal decomposition step, the carboxylate salts can become very viscid and sticky and can coat the interior surfaces of the reactor. This diminishes the effectiveness of the heat transfer surface in the reactor. This viscid and sticky phase also negatively affects ketone yields. Ketone vapors form in the liquid layer as it thermally decomposes and must migrate into the vapor space to be removed from the

reactor. As the viscosity of the liquid layer and its thickness increase, so does the degree of ketone degradation. Degradation products can include tars and heavy oils that can further impede ketone vapors as they are formed. As thermal decomposition proceeds, the carbonates of the carboxylate salts begin to form and precipitate out of the decomposing liquid phase, which forms a paste-like mixture. This solid-liquid mixture can also coat the interior surfaces of the reactor, further impeding heat transfer into the reactor and the transfer of ketone vapors into the vapor space to be removed from the reactor. As the thermal decomposition reaches completion, the residual solids are composed mostly of solid carbonates with small amounts of liquid tars and heavy oils and non-volatile impurities. Large amounts of tars and heavy oils in the residual solids can hinder its flowability. Tars and heavy oils can stick to the heating surfaces of the reactor along with the carbonates and non-volatile impurities and continue to react, forming a layer of char that can be very hard to remove. In addition, this layer greatly reduces the heat transfer into the reactor.

6.2.3. Removal of product vapors and solids from the reactor

Once fully reacted, residual solids can be removed by gravity or mechanically. If the residual solids are flowable and not sticky, they can be removed by gravity through an outlet opening. If the residual solids are not flowable and/or are sticky, they can stick to the outlet over time and clog it. In this case, some mechanical means of removal is necessary. As with feeding, both methods require that residual solids be removed to a sealed collection container to prevent product vapors from escaping. For continuous operation, two or more such collection containers with valves are required so that one is

collecting the residual solids while the other(s) are being emptied. A purge gas on the collection containers is needed to prevent product vapors from migrating in and condensing. Such a purge gas would not be necessary if a vacuum were being employed in the reactor. In addition, the outlet line must be heated above the product condensation point to inhibit condensation as well.

Immediate removal of the product vapor from the reactor is critical because prolonged exposure to the reactor temperatures causes ketone degradation. Removing product vapor from the reactor also must be done in a way that only the vapor is removed and the liquid/solid reactants and products remain in the reactor. If the vapor flow rate is high enough, liquid and solid particles can be entrained and exit the reactor. Like the residual solids outlet, if the entrained particles are sticky they can stick to the vapor outlet and clog over time, and therefore require some mechanical means of removal. The vapor outlet line(s) also must be heated above the product condensation point. The line(s) must be heated from the reactor to a point along the line where condensing product cannot return to the reactor. If the vapor flow rate is not too high and the entrained particles are not sticky, a sufficiently long vapor outlet line can be used to gravity settle any entrained particles back to the reactor. Otherwise, filtering and/or mechanical cleaning of the vapor lines is necessary.

6.2.4. Rapid removal of product vapor: sweep gas vs. vacuum

To minimize the rate of ketone degradation, it is necessary to keep the partial pressure of the ketone vapor low and to remove it from the high-temperature reactor so it can be cooled rapidly. This is especially true for the high-molecular-weight ketones.

Both sweep gas and vacuum create a low partial pressure of ketone vapor and a pressure gradient to move the product vapor out of the reactor. Ludlam [18] and Young [17] used CO_2 sweep gas whereas Ardagh et al. [21] and Goodwin [19] used N_2 sweep gas. Hurd [16] stated that "fairly high yields of good product" could be achieved with no sweep gas as long as the decomposition temperature did not exceed the decomposition temperature of the product, but even better yields were attained with the use of an inert sweep gas. He also suggested a vacuum when high-molecular-weight ketones were produced. Several industrial practices simply operated at atmospheric conditions with no sweep gas or vacuum. With sweep gas, the product vapor can be moved out of the reactor to be cooled much faster than by using a vacuum. However, because of the higher vapor flow rate, solid particles in the reactor are more likely to become entrained using a sweep gas and enter the condensers. This creates the need for more sophisticated equipment to filter the vapor product as it exits the reactor. Not only does this require more capital, but it increases pressure drop, which inhibits the removal of vapor product from the high-temperature reactor. With a vacuum, less filtering is necessary. Another disadvantage to using a sweep gas is that both the product vapor and the sweep gas must be cooled to condense the product vapor. Not only is there an energy penalty for cooling additional sweep gas, but an extra energy penalty comes indirectly from much lower heat transfer coefficients (15–40 $W/(m^2 \cdot K)$) that are present while cooling the sweep gas and product vapor to condensation point. Using a vacuum, only the product vapor must be cooled and condensed. This requires less cooling duty and has a higher overall heat transfer coefficient (200–400 $W/(m^2 \cdot K)$).

6.3. Reactor designs

An auger, similar to the one shown in Figure 6-3, can be used to move solids in and out of the reactor. A rotary valve could also be used to perform this function. A rotary valve consists of a shaft-driven wheel with several vanes that rotate in a housing with an inlet and outlet. Augers and rotary valves that move solids into the reactor are very difficult to seal, especially at higher temperatures. Sealing the shaft that turns the internal parts is usually accomplished with a mechanical seal. A very small clearance is typically kept between the tips of the vanes or auger flighting and the inner housing wall, which minimizes blow-by of fluids. To better seal against fluid leakage, seals can be added to the tips of the vanes and auger flighting that contact the inner housing. This causes the operating temperature of the augers and rotary valves to be limited by the operating temperature of the seals. In addition, the seals are usually much more susceptible to wear than the rest of the moving components, shortening the operating life. If the carboxylate salts are fed into the reactor as a liquid, then a pump that can handle high-viscosity fluids can be used to transport feed into the reactor.

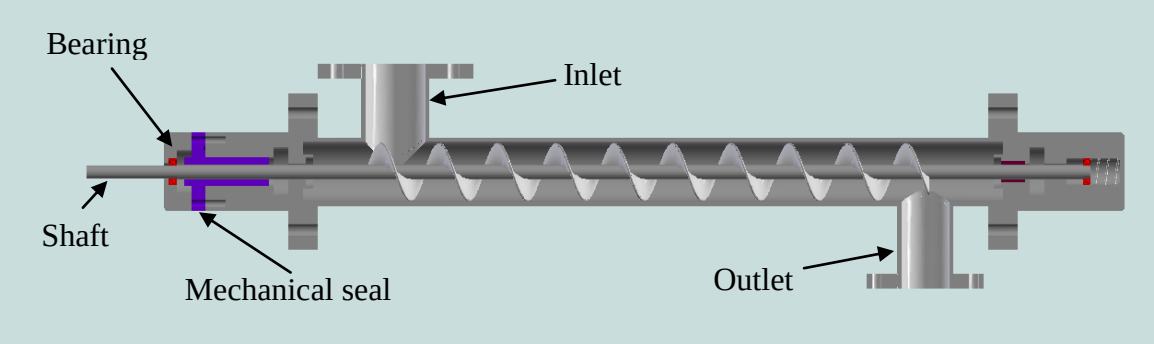

Figure 6-3. Auger for feeding solid carboxylate salts into reactor.

Residual solids can be removed using an auger similar to the one shown in Figure 6-3 or a rotary valve. If the residual solids are sticky and adhere to the auger walls and flighting, a system of parallel augers could be used so that the rotating flighting of one auger "scrapes" and cleans the rotating flighting of the adjacent auger.

Once the carboxylate salts enter the reactor, they must be constantly agitated to maintain flowability and avoid char formation, which impedes heat transfer and increases ketone degradation. In addition, the carboxylate salts must be moved continuously through the reactor or series of reactors. Figures 6-4 and 6-5 show a single-shaft reactor design that could accomplish this. The reactor is a horizontal tube with a shaft containing rows of paddles. A close-up of the paddles is the section view given in Figure 6-6. Four rows of paddles are shown in Figure 6-4 and 6-5, but more or fewer could be used depending on the shaft diameter. Heating is achieved by a jacket around the outside of the tube in which heating media (i.e., high-temperature heating oil or molten salts) is passed. Additionally, heating media passed through the shaft or electric heaters in the shaft could supply heat to the reactor as well. As carboxylate salts are fed into the reactor, they are immediately slung to the reactor wall by the paddles. The shaft is rotated sufficiently fast to keep the carboxylate salts against the reactor wall, forming an annulus as it proceeds through the reactor. As vapors form, they can escape into the center of this annulus and travel to the feed-end where they are removed through the vapor outlet. To aid in this removal, a sweep gas or vacuum may be employed. As the solids reach the end of the reactor, they are removed through the residual solids outlet to an auger or rotary valve.

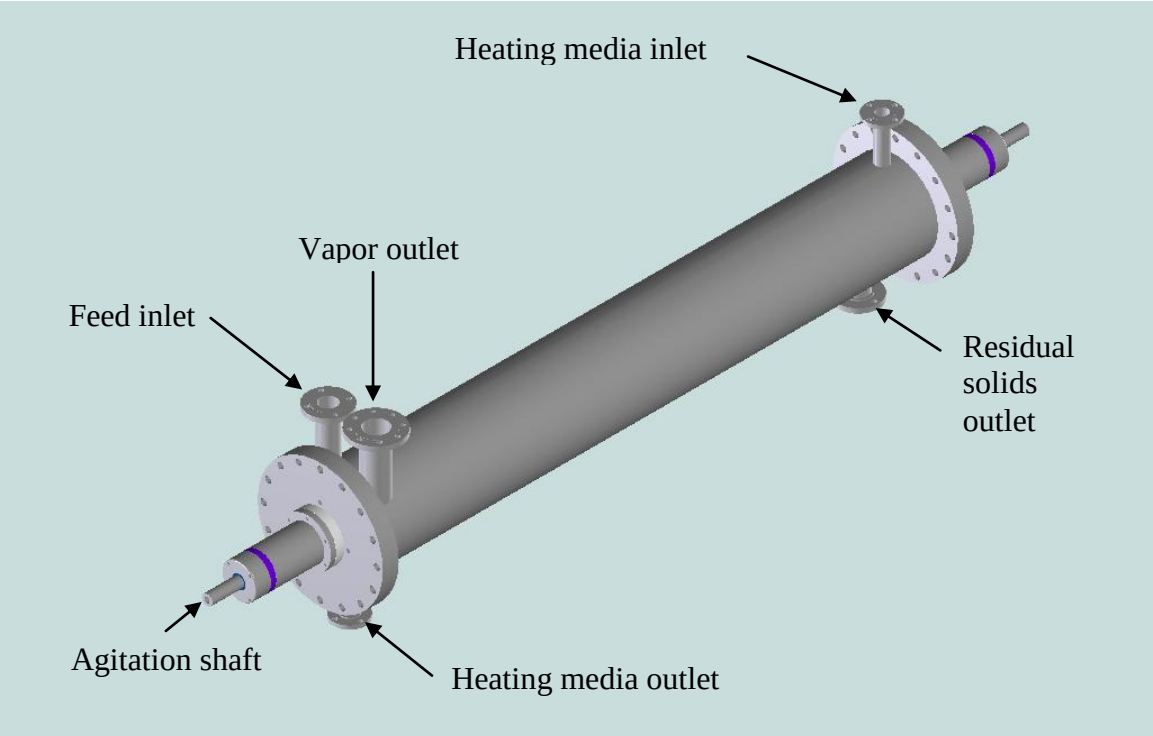

Figure 6-4. Single-shaft ketone reactor.

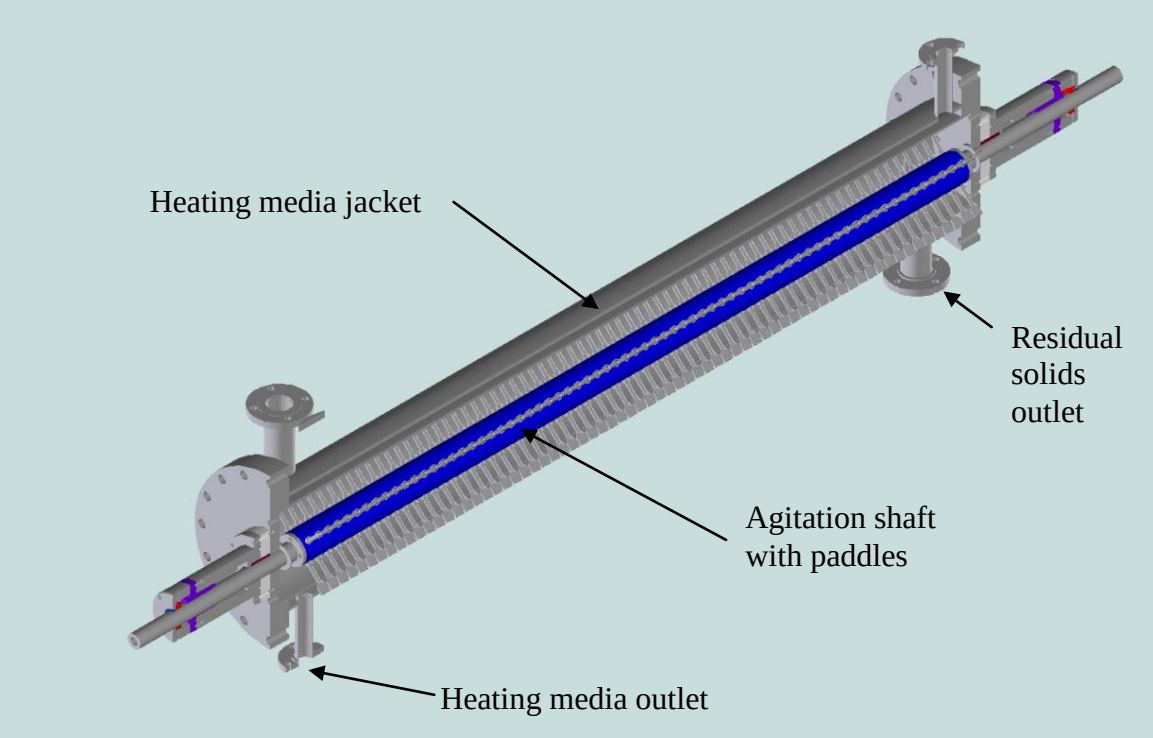

Figure 6-5. Single-shaft ketone reactor section view.

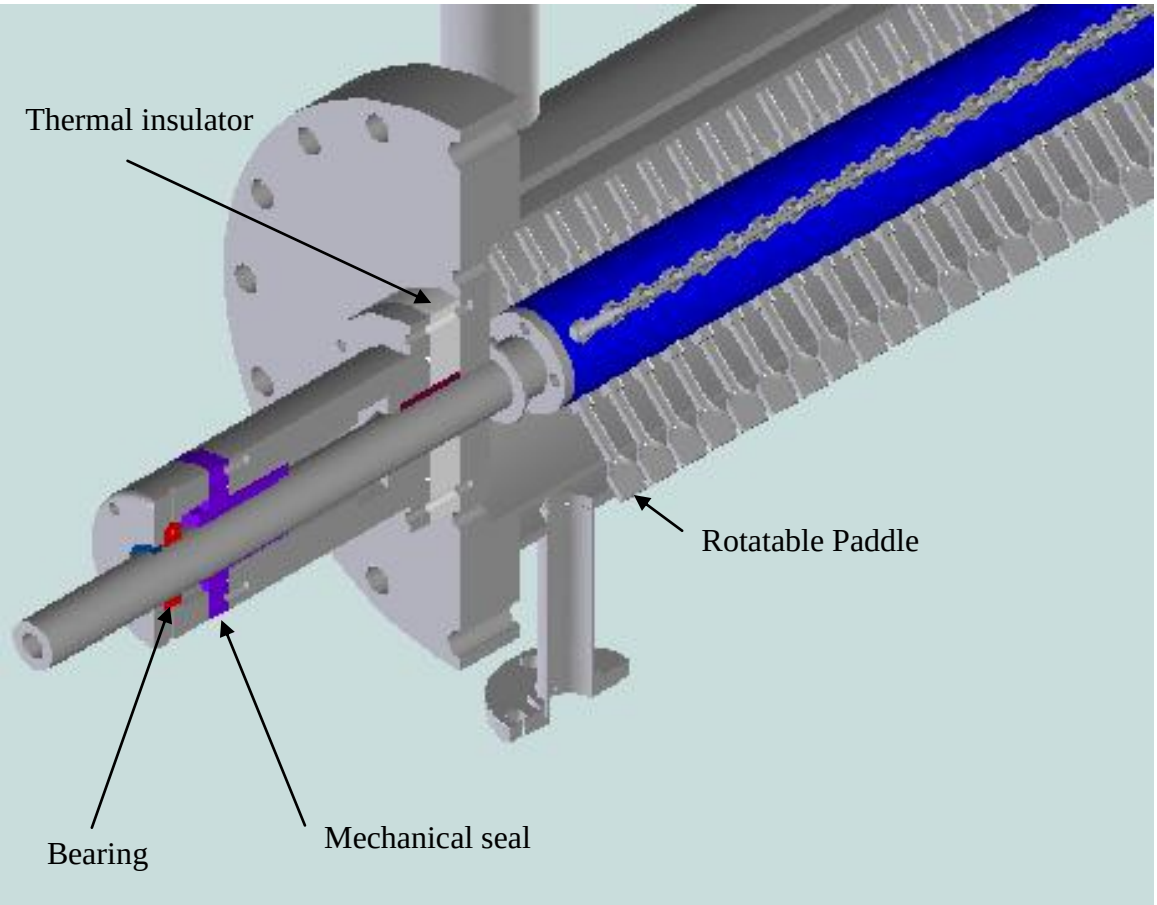

Figure 6-6. Close-up of paddles on single-shaft ketone reactor.

Solids residence time can be adjusted by rotating some or all of the paddles. If less residence time is desired, paddles can be oriented to push the solids through faster; if more residence is desired, paddles can be oriented to provide some back-mixing. A small clearance must be kept between the tips of the paddles and the reactor wall so that if a layer of sticky salts or char forms, the thickness will be minimized. Inert aggregates, such as sand, steel ball bearings, or round zirconium pellets, can be feed with the salts to mechanically abrade deposits and layers that could form on the reactor walls and shaft. The aggregate can be heated before entering the reactor to add thermal mass as well. For

these purposes, Holtzapple et al. [9] suggested passing heated steel shot through a similar type of reactor with the salts.

Mechanical seals are used to seal the shaft as it penetrates the endplates. They are mounted to the endplates along with the bearing assembly. If mounted directly to the endplate, the mechanical seal must be able to operate at the reactor temperatures. If lower operating temperatures are required for the mechanical seal, a thermal insulator (i.e., ceramic) could be placed between the mechanical seal and bearing mount as shown in Figure 6-6. The thermal insulator must have significantly higher thermal resistance than the reactor endplate material. Mechanical seals typically require a fluid to help seal the face, keep debris out of the seal face, and provide cooling. If a sweep gas were being employed in the reactor, it could also serve as the fluid for the mechanical seal, eliminating contamination issues. If a vacuum were employed in the reactor, a viscous liquid must be used with the mechanical seal so that contamination into the reactor is minimized.

A reactor such as the one shown in Figure 6-5 has been built and operated by Terrabon, Inc (Houston, TX) at their research facility, Energy Independence I, in Bryan, TX. It has an inner diameter of 10 in, a length of 6 ft, and a shaft diameter of 4 in. The shaft has two rows of paddles and a maximum rotation rate of 400 rpm. It has operated with calcium carboxylate salts (fed as solids) and sodium carboxylate salts (fed as liquids). Operating data are given in Table 6-1. A tracer study, performed using lithium and copper (II) chloride, showed the residence time was approximately 11.5 min with

sodium carboxylate salts fed at 0.27 kg/min. Terrabon continues to operate and optimize this reactor.

Table 6-1. Operating data from Terrabon's ketone reactor

	Calcium carboxylate salts	Sodium carboxylate salts
Feed rate (kg/min)	0.25–0.30	0.22–0.32
Purity (wt. salt/wt. feed)	0.67–0.74	0.30–0.55
Moisture content (%)	13–16	20–40
Mean reactor temperature (°C)	380–400	380-400
Conversion (*X*)	0.88–0.98	0.91–0.98
Yield (%)	60–65	75–90

One disadvantage of the single-shaft reactor design is that agitation and axial movement of the solids are both affected by the shaft rotation rate. Slowing the rotation rate of the shaft also slows the movement of solids and therefore increases residence time. It also reduces the degree of agitation and perhaps prevents the solids from forming a true annulus. The paddles can be tilted forward or back to adjust residence time without sacrificing shaft speed; however, this is a labor- and time-intensive process that would require the reactor to be shut down and disassembled. By incorporating two shafts, the reactor design shown in Figure 6-7 allows agitation and residence time to be controlled independently while allowing changes during operation. The bottom shaft contains paddles that agitate the solids in chambers whereas the top shaft is equipped with auger flighting to carry the solids from one chamber to the next. The reactor is composed of a larger bottom tube connected to a smaller top tube running parallel to its

axis. The tubes are connected by a narrow slot which runs almost the entire length of each chamber (see close-up section view in Figure 6-8). Not shown is the jacket that surrounds the reactor to hold the heating media. Carboxylate salts enter via the feed inlet and then fall through the narrow slot into the bottom tube where they are agitated with paddles. The paddles can be equipped with wire brushes to scrape the walls and remove sticky salts and char build-up. As with the single-shaft reactor, aggregates can be preheated and fed with the carboxylate salts to avoid build-up on the reactor wall and shaft as well as provide thermal mass. As the paddles pass the slot, centrifugal force flings some of the solids into the top tube where the rotating auger flighting conveys it in the next chamber. Once the solids leave the last chamber, they exit through the residual solids outlet. Vapor exits the reactor through outlets located above each chamber. To prevent solids from leaving through the vapor outlets, filter inserts are placed in each one. The filter media is a porous metal that can withstand the reactor temperatures and have the same radius as the top tube so there is no obstruction to the auger flighting. One disadvantage of the double-shaft reactor is that it is more prone to fouling and clogging by salts that reach a highly viscous state or if char forms in the narrow slots. If this occurs, the reactor must be disassembled and cleaned often, which would be very time and labor intensive. If this were the case, the single-shaft reactor is the preferred choice.

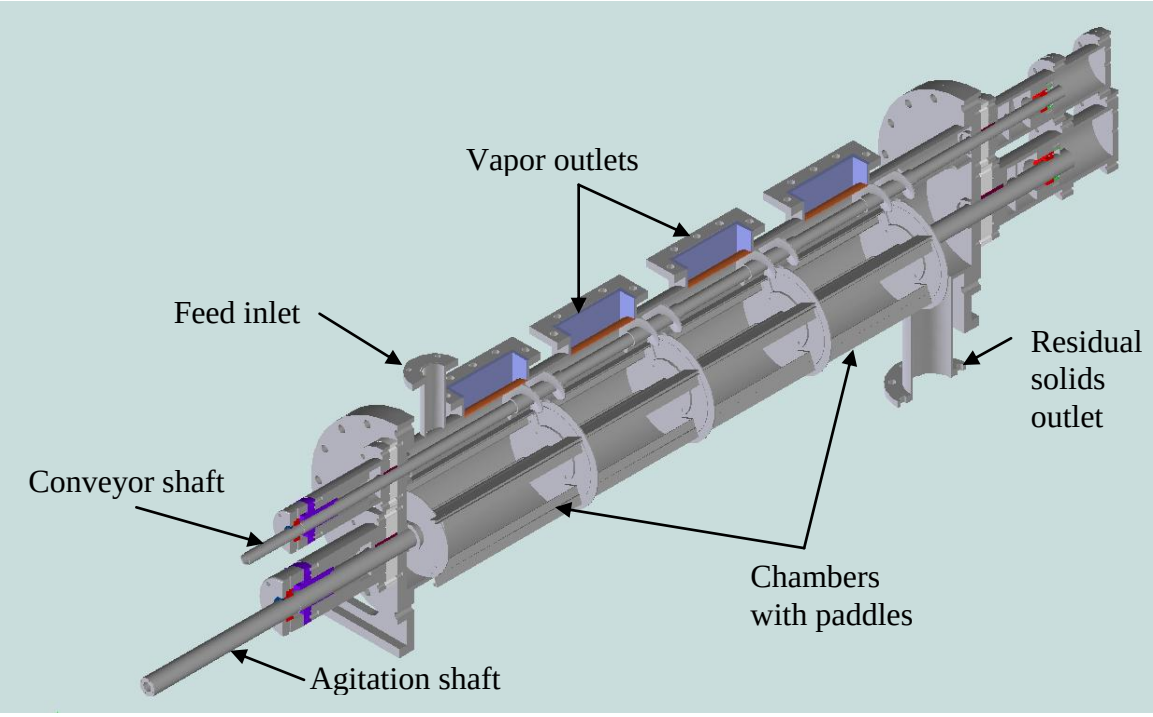

Figure 6-7. Double-shaft ketone reactor shown with four chambers.

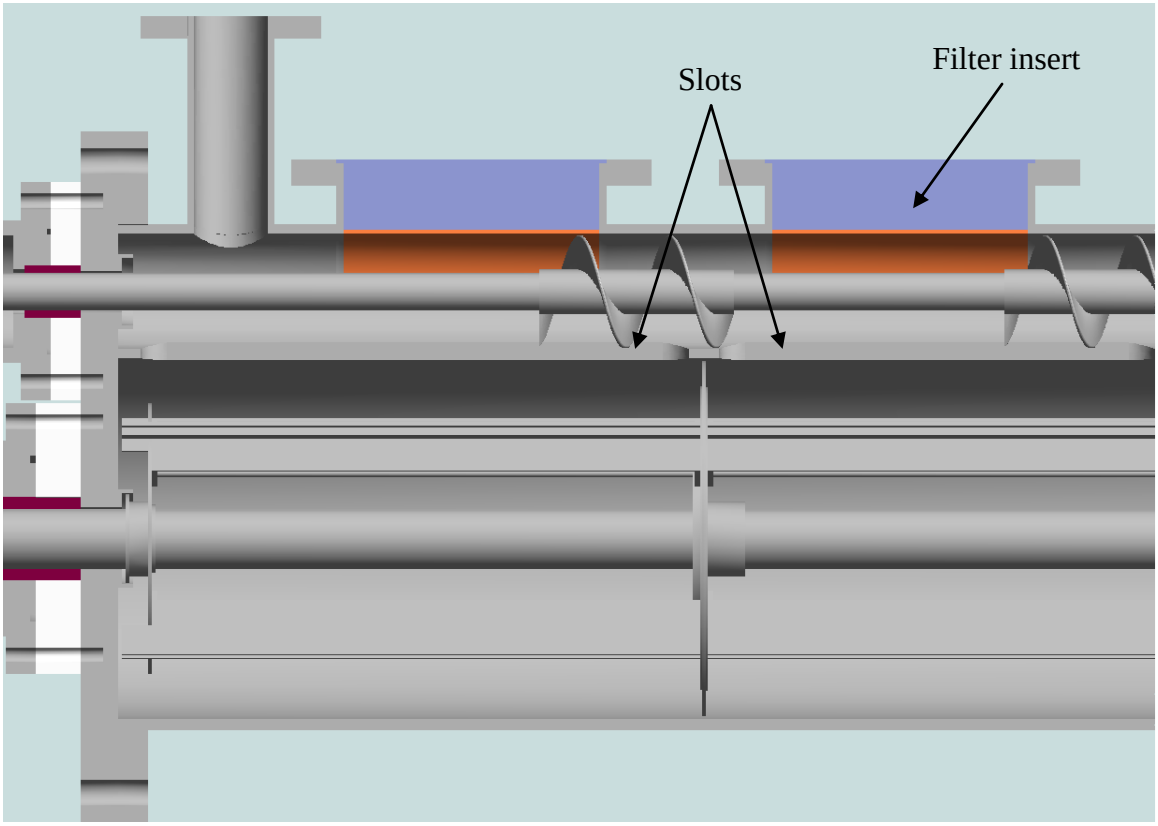

Figure 6-8. Close-up of double-shaft ketone reactor showing slotted access between the agitation chamber and conveyor shaft.

Each chamber in the double-shaft reactor is like a continuous stirred tank reactor (CSTR), so it can be viewed of as a series of CSTRs. The reactor in Figure 6-7 is shown with four chambers, but could be made with fewer or more depending on the desired residence time of each chamber as well as the desired overall residence time. Figure 6-9 shows a prototype of double-shaft reactor with one chamber. It was made of acrylic so that the agitation and conveying of solids could be confirmed visually. It was tested with calcium carbonate. It was able to vigorously agitate and could convey the solids at a rate of up to 3 kg/min.

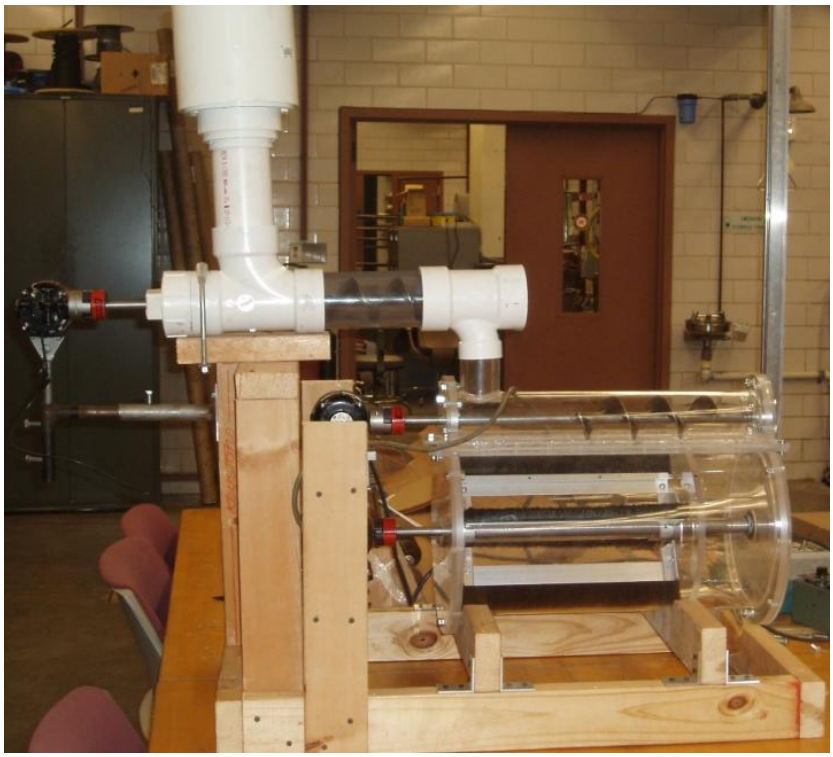

Figure 6-9. Acrylic prototype of double-shaft ketone reactor.

Several reactors could be assembled in series to handle the different phases through which the carboxylate salts might transition during thermal decomposition. The carboxylate salts could first enter a single-shaft reactor to accomplish the dehydration step separate from the thermal decomposition step. If the carboxylate salts were then very viscous or would become viscous upon further heating, they would enter another single-shaft reactor along with heated aggregate so that build-up on the reactor surfaces would be minimized. This second reactor produces the majority of the ketone vapors. An auger or rotary valve would be placed between the first and second reactors to minimize mixing of the resulting vapors.

As the resulting solids formed, they could then be dropped into a double-shaft reactor. The last remaining carboxylate salts need more time to thermally decompose and the double-shaft reactor could provide more residence time with less length of tube. Because of the wire brushes that would scrape the reactor walls, it is also more suited to handle the residual solids and the chars that form. In this configuration, water vapor would be produced in the first reactor and ketone vapor would be produced in the last two, eliminating the need for additional downstream separation.

7. CLARIFICATION OF FERMENTATION BROTH

7.1. Introduction

After the fermentation step in the MixAlco™ process, the exiting broth, which is mostly water, contains small amounts of undigested biomass, cells, extracellular proteins, and non-fermentables (e.g. minerals) in addition to the carboxylic acids. To optimize ketone yields during thermal decomposition, it is necessary to remove as much of these impurities as possible. Some impurities will settle out of the broth, the rest form a suspension and additional separation is needed. To overcome this problem, two methods were tested: filtration and flocculation/coagulation. The broth used in the study was taken from a MixAlco™ fermentation using food scraps as a substrate and nutrient source and ammonium bicarbonate (NH_4HCO_3) as the buffering agent. Acid compositions were verified by gas chromatography (Table 7-1).

Table 7-1. Acid profile of fermentation broth buffered with ammonium bicarbonate.

Acid	Carbon number	Acid (wt. %)
Acetic	2	48.94
Propionic	3	3.48
Isobutyric	4	1.05
Butyric	4	17.31
Isovaleric	5	0.47
Valeric	5	1.76
Caproic	6	0.11
Heptanoic	7	0.87

The first clarification method used membranes to filter the impurities out of the broth. A problem inherent to all membrane and filter separation is fouling (blinding).

Fouling is caused primarily by the formation of a boundary layer that accumulates naturally on the membrane surface during filtration. In addition to reducing flux through the membrane, this boundary or gel layer acts as a secondary membrane that reduces the native design selectivity of the primary membrane. To overcome this, a vibratory shear-enhanced process (VSEP) was used to help eliminate fouling by producing intense shear waves on the face of a membrane. These shear waves are created by vigorously vibrating the membrane element in a direction tangent to the face of the membrane. The shear waves produced by the vibration cause solids and foulants to be lifted off the membrane surface and remixed with the bulk material flowing across it. This high-shear processing exposes the membrane pores for maximum throughput, which is typically 3 to 10 times the throughput of conventional cross-flow systems.

The second clarification method used of flocculants and coagulants. A colloidal suspension arises because of negative or positive charges present on the colloid surfaces. These like charges repel each other and keep the colloids suspended. Many of the impurities present in the broth formed a colloidal suspension. A coagulant carries the opposite charge of the colloid. It neutralizes the charges on the colloid by binding to it, which allows the colloids to form particles, assemble into flocs, and precipitate from the mixture. Flocculants are polymers with ionic side-chains that adsorb to the colloid particles surfaces, thus binding them into agglomerates or clumps that fall out of the mixture. Flocculants destabilize the suspension by both bridging and charge neutralization.

7.2. Material and methods

7.2.1. Filtration

A Pallsep PS10 (Pall Corporation, Port Washington, NY) was used with membranes to perform all filtrations. Seven membranes were used with varying pore sizes and materials (Table 7-2).

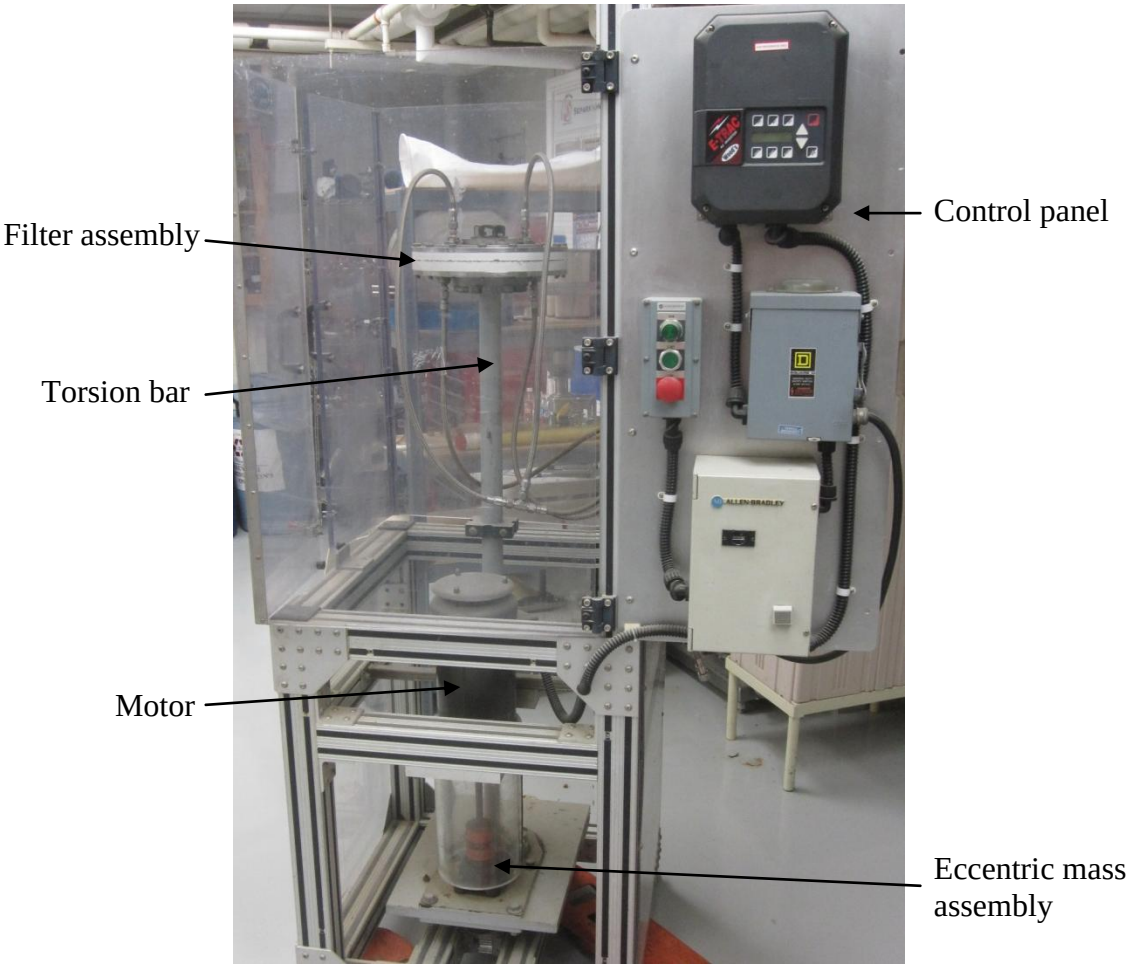

Figure 7-1. Pallsep PS10 located at Cater-Matill Hall, Texas A&M University; College Station, TX.

Table 7-2. Membrane pore sizes and materials.

Membrane pore size	Membrane material
240 Da	TFC polyamide
800 Da	Sulfonated sulfone
20 kDa	Polyethersulfone
50 kDa	Polyethersulfone
100 kDa	Polysulfone
0.1 µm	PTFE on polyester
1 µm	PTFE on rigid polyester

7.2.2. Liquid analysis

Acid compositions of the influent (fermentation broth), permeate, and retentate were determined using the same method described in Section 2.2.5. Purities of the influent and permeate were determined by adding 5-mL samples to pre-weighed crucibles with excess $Ca(OH)_2$ (lime) to convert the carboxylic acids and/or the ammonium carboxylate salts into their corresponding calcium carboxylate salts. Acid concentrations from the GC-FID were used to determine the necessary amounts of lime to be added. The crucibles containing the solutions were placed in a 105 °C oven to dry for 36 h. The weights of the solids were measured and the calculated weight of the calcium carboxylate salts and the excess lime were subtracted to give the weight of the impurities, given in Equation 7-1.

$$\begin{aligned}\text{Impurities (g)} = \text{Total solids (g)} &- \text{Excess lime (g)} \\ &- \text{Calculated calcium carboxylate salts (g)}\end{aligned} \tag{7-1}$$

Each calcium carboxylate salt weight was converted into its ammonium carboxylate salt equivalent. The purity was calculated using Equation 7-2.

$$\text{Purity}\,(\%) = \frac{\text{Theoretical total ammonium carboxylate salts}\,(\text{g})}{\text{Impurities}\,(\text{g}) + \text{Theoretical total ammonium carboxylate salts}\,(\text{g})} \times 100 \quad (7\text{-}2)$$

The amount of energy needed to filter one gallon of fermentation broth was calculated using Equation 17-3.

$$E = \frac{7.25 \times 10^{-6}}{0.6} \Delta P \quad (7\text{-}3)$$

where ΔP is the pressure drop across the filter (lb_f /in^2) and E is the specific energy (kWh/gal). A pump efficiency of 0.6 was assumed.

7.3. Results and discussion

The purity of the influent broth was 73.99%. For membrane filtration using VSEP, Table 7-3 shows the average flow rates and purities attained with each of the membranes tested. These membranes yielded acceptable purities that could be further processed; however, with such low flow rates and high pressures (30–300 psi), they would likely not be economically viable.

Table 7-3. Results of each membrane used to filter fermentation broth.

Membrane pore size	Maximum flow rate	Pressure drop	Purity of permeate (%)	Energy cost (kWh/gal)
1 μm	20 mL/min	20 psi	90.79	2.42×10^{-4}
0.1 μm	12 mL/min	20 psi	90.16	2.42×10^{-4}
100 kDa	8 mL/min	20 psi	90.15	2.42×10^{-4}
50 kDa	7 mL/min	35 psi	90.07	4.23×10^{-4}
20 kDa	6.5 mL/min	35 psi	95.18	4.23×10^{-4}
800 Da	5 mL/min	70 psi	96.51	8.46×10^{-4}
240 Da	3.1 mL/min	60 psi	98.33	7.25×10^{-4}

A coagulating agent (Qemifloc FL 54 CLV) and a flocculating agent (Zetag 7867) were tested for their effectiveness in clarifying fermentation broth. Multiple tests were done to determine the proper pH, temperature, mixing process, and amount of flocculant or coagulant needed to obtain optimum clarity. It was found that a pH of 7 at room temperature (25 °C) was ideal for forming flocs using both agents.

Zetag 7867 is a poly-cationic flocculant that is 40% cationic. It is shipped as an oil-emulsion that must be diluted to at least 1% and allowed to set for a minimum of 30 min to properly activate the polymers. Better activation is achieved by further dilution and longer set periods, which is recommended for liquids with higher percentages of solids. The amount of flocculant added is also crucial because the polymers tend to be less dense than water and too much will cause the flocs to float rather than settle to the bottom. The flocculant must also be added and stirred gently because high shear forces caused by rapid mixing will tear the flocs apart. Using a 0.125% Zetag 7867 solution, 10 mL was gently mixed into 100 mL of fermentation broth at room temperature. Once flocs had formed, the solution sat without mixing for 30 min to allow the flocs to settle. Only a small amount of the colloids came out of the suspension and settled with the flocs. Even though this slightly improved the clarity, a significant amount of the suspension still remained. Further treatments with the flocculant did not improve the clarity any further. The exact purity of the flocculated broth was not measured, but was presumed to be less than 90%.

Qemifloc FL 54 CLV is a cationic coagulant that is 45% polydimethyldiallylammonium chloride in water. Before using, the entire solution must

be diluted to at least 2% and shaken rapidly using vortexing or sonication. This allows proper activation of the polymer as well as proper mixing when added for clarification. For fermentation broth, a concentration as high as 2.5% worked, but 1% was best. The least diluted solution is preferred because the carboxylate salts become diluted as well. When 5 mL of 1% Qemifloc solution was added to 25 mL of fermentation broth and shaken rapidly for 2 min, floc formation was observed and required approximately 8 h of settling time. Further treatment with 10 mL of the 1% Qemifloc solution yielded even better clarity. After centrifugation, the purity of the coagulated broth was 93.23%.

8. CONCLUSIONS

8.1. Summary

8.1.1. Product yields and composition

Upon dewatering, the pH of fermentation broth may be as high as 10 without statistically significant expected ketone yield losses during thermal decomposition. Above pH 10 (i.e., feed salts with lime-to-salt ratios higher than 0.00134), larger amounts of tars and heavy oils and hydrocarbons are produced upon thermal decomposition. This increased production of non-expected products causes losses in expected ketone yields, the majority of which come from tars and heavy oils. In the thermal decomposition of fermentation feed salts, the production of non-expected ketones, acids, hydrocarbons, tar and heavy oils, and other impurities are much higher because of impurities in the fermentation feed salts.

To a first approximation, the random-pairing model predicts expected ketone yields from the thermal decomposition of calcium carboxylate salts typical of a MixAlco™ fermentation; however, there is significant disagreement particularly at low carbon numbers. Gibbs free energy minimization is an alternative approach that appears to follow the experimental data more closely than those of random pairing, although a direct comparison of the data was not possible. For the thermal decomposition of calcium salts comprised of acetate, propionate, butyrate, and valerate, the random-pairing model matched the ketone product distribution more closely than the Gibbs free energy minimization model. Both models agree with the experimental data for low-

molecular-weight ketone composition and both show some deviations from the experimental data for high-molecular-weight ketone composition. However, the random-pairing model follows the trends in ketone product distribution and deviates less from the experimental data than Gibbs free energy minimization. For the sodium salts comprised of acetate, propionate, butyrate, and valerate, it is not possible to determine which model fits the experimental data better because of the high rates of product degradation. Overall it appears that the random-pairing model is best.

Calcium salts begin thermally decomposing at much lower temperatures (170–180 °C) than do sodium salts (410–420 °C). For calcium salts, the expected ketone yield was not significantly affected by carboxylate salt composition. For sodium salts, the expected ketone yield decreased with increasing average carboxylate salt molecular weight. The average expected ketone yield for sodium salts was less than half that for calcium salts. The loss in expected ketone yield was primarily caused by the increased production in tars and heavy oils and hydrocarbons. These byproducts are most likely the result of product degradation. Tars and heavy oils were the predominant byproduct and increased with average carboxylate salt molecular weight for both calcium and sodium salts; however, sodium salts produced 4 times more tars and heavy oils than did the calcium salts. Hydrocarbons also increased with average carboxylate salt molecular weight for both calcium and sodium salts, with sodium salts producing 9 times more hydrocarbons than calcium salts. Because of poor ketone yields and large production of tars and heavy oils, sodium carboxylate salts would not be recommended for use in a commercial-scale MixAlco™ biorefinery.

8.1.2. Kinetics of thermal decomposition

Average E_A values were found for sodium and calcium acetate, mixtures of reagent-grade sodium and calcium salts, and fermentation sodium and calcium salts using three different isoconversional methods that employed TGA curves at different heating rates. For all carboxylate salts and salt mixtures examined, E_A varied significantly with W. In part, this is because of the complex nature of the thermal decomposition of the carboxylate salts and more so because there are many reacting species in the decomposition of reagent-grade and fermentation carboxylate salts. Three models were tested for each carboxylate salt and salt mixture using isothermal decompositions. For each of the three sodium salt types, the Sestak-Berggren model had the lowest value of θ and gave E_A values closest to the ones given by the isoconversional methods. For calcium acetate, the n^{th}-order and Sestak-Berggren models seemed to work equally well at modeling the experimental data. Both models had similar values of θ and similar parity plot parameters. The thermal decomposition of calcium acetate is very difficult to study. E_A values from isothermal methods were similar only to the lower E_A values from isoconversional methods, not the average E_A. For reagent-grade and fermentation calcium salts, the Sestak-Berggren model gave E_A values closest to the ones given by the isoconversional methods and had parity parameters closest to unity even though it did not have the lowest value of θ. The degree of success the Sestak-Berggren model has in modeling the all of the experimental data implies that it is most suitable for modeling carboxylate salts with a variety of compositions and degrees of purity.

8.1.3. Broth clarification and ketone reactor design

Reactor designs of the past used to thermally decompose calcium acetate were reviewed. Phase behavior of carboxylate salts throughout the decomposition process and the potential challenges they pose to feeding carboxylate salts, conveyance of solids, and removal of products were considered. Two designs of continuous reactors were explored along with several configurations between the two. In addition, operating data were given for a continuous ketone reactor in operation.

Flocculation of fermentation broth showed little improvement in purity. Filtration of the fermentation broth was performed using pore sizes from 1 μm – 240 Daltons. Broth purity increased with decreasing pore size, from 90.79–98.33%. Filtration yielded the purest broth, but was energy intensive. Coagulation of the fermentation broth yielded 93.23% purity and required little energy, making it the most desirable method of clarification.

8.2. Future research

8.2.1. Effects of lime on thermal decomposition of calcium carboxylate salts

The thermal decomposition of carboxylate salts with cations other than calcium (i.e., sodium, potassium, magnesium) could be tested to see if the presence of lime affects yield and the production of byproducts.

8.2.2. Modeling product composition from thermal decomposition of carboxylate salts

In addition to calcium and sodium carboxylate salts, carboxylate salts with another monovalent cation (i.e., potassium) and another divalent cation (i.e., magnesium) could be tested and compared to the random-pairing model and the Gibbs

free energy minimization model. Modifications to both models could be implemented. Better agreement between the random-pairing model and experimental data could be achieved by including weighting factors to account for ketones that are kinetically favored. If mechanisms other than those mentioned in Section 2 and 3 could be developed and validated to explain the existence of certain non-theoretical products, the random-pairing model could then be further modified to include these new products as theoretical.

For the sodium carboxylate salts, the Gibbs free energy minimization model could be modified to include the non-theoretical ketones and hydrocarbons, as well as carbon dioxide, carbon monoxide, and hydrogen. If these byproducts are thermodynamically favored, it would help explain their presence in significant quantities from the experimental data. This could be done to other types carboxylate salts where there are significantly large amounts of byproducts.

8.2.3. Kinetics of thermal decomposition of carboxylate salts

In addition to calcium and sodium carboxylate salts, carboxylate salts with other cations (i.e., potassium and magnesium) could be tested using TGA and the methods described in Section 4.3. To determine trends in molecular weight and cations, more individual carboxylate salts (i.e., propionate, butyrate, octanoate, etc.) could be studied in terms of kinetic parameters for their thermal decompositions. Mechanisms that account for the products from the thermal decomposition of individual or mixed carboxylate salts could be developed into a kinetic model and tested. Combinations of mechanisms could be tested by using certain ranges of W for each mechanism. To test

for autocatalysis, carbonates and oxides of the respective carboxylate salts could be added at the beginning of the thermal decomposition to determine if there is a decrease in E_A. Additionally, additives to the thermal decompositions could be tested for improved product yield, decreased activation energy, and lower melting point.

8.2.4. Continuous reactors

Small-scale continuous reactors of various designs could be built and tested with a variety of carboxylate salts. Design parameters that relate length, inner diameter, shaft diameter, shaft rotation rate, and feed rate should be developed. If necessary, these parameters could be developed for different types of salts, but they should be as universal as possible. Different methods for removing and minimizing fouling caused by the various stages of thermal decompositions could be developed and tested. Heating the carboxylate salts through the reactor walls can be problematic because heat transfer from a metal surface to a solid particle is very small. The heat transfer becomes even worse when fouling becomes significant. Different methods of heating the carboxylate salts could be developed (e.g., microwaves, electromagnetic induction, etc.).

REFERENCES

1 McCabe PJ. Energy resources; cornucopia or empty barrel? AAPG Bulletin 1998;82:2110.

2 Sterzinger G. Making biomass energy a contender. Technology Review 1995;98:34.

3 Klass DL. Energy consumption, reserves, depletion, and environmental issues. Biomass for Renewable Energy, Fuels, and Chemicals. San Diego: Academic Press; 1998, p. 1.

4 Hileman B. Case grows for climate change. Chemical & Engineering News 1999;77:16.

5 Ragauskas AJ, Williams CK, Davison BH, Britovsek G, Cairney J, Eckert CA, et al. The path forward for biofuels and biomaterials. Science 2006;311:484.

6 Reddy N, Yang Y. Biofibers from agricultural byproducts for industrial applications. Trends in Biotechnology 2005;23:22.

7 Zhang Y-HP, Lynd LR. Toward an aggregated understanding of enzymatic hydrolysis of cellulose: noncomplexed cellulase systems. Biotechnology and Bioengineering 2004;88:797.

8 Holtzapple M, Granda C. Carboxylate platform: the MixAlco process part 1: comparison of three biomass conversion platforms. Applied Biochemistry and Biotechnology 2009;156:95.

9 Holtzapple M, Davison R, Ross M, Aldrett-Lee S, Nagwani M, Lee C-M, et al. Biomass conversion to mixed alcohol fuels using the MixAlco process. Applied Biochemistry and Biotechnology 1999;79:609.

10 Granda C, Holtzapple M, Luce G, Searcy K, Mamrosh D. Carboxylate platform: the MixAlco process part 2: process economics. Applied Biochemistry and Biotechnology 2009;156:107.

11 Pham V, Holtzapple M, El-Halwagi M. Techno-economic analysis of biomass to fuel conversion via the MixAlco process. Journal of Industrial Microbiology and Biotechnology 2010;37:1157.

12 Chan W, Holtzapple M. Conversion of municipal solid wastes to carboxylic acids by thermophilic fermentation. Applied Biochemistry and Biotechnology 2003;111:93.

13 Thanakoses P, Black AS, Holtzapple MT. Fermentation of corn stover to carboxylic acids. Biotechnology and Bioengineering 2003;83:191.

14 Domke SB, Aiello-Mazzarri C, Holtzapple MT. Mixed acid fermentation of paper fines and industrial biosludge. Bioresource Technology 2004;91:41.

15 Mellan I. Ketones. New York: Chemical Publishing Co., Inc.; 1968.

16 Hurd CD. The pyrolysis of carbon compounds. New York: The Chemical Catalog Company; 1929.

17 Young S. LVIII.—Dibenzyl ketone. Journal of the Chemical Society, Transactions 1891;59:621.

18 Ludlam EB. CXVIII.—The preparation of mixed ketones by heating the mixed calcium salts of organic acids. Journal of the Chemical Society, Transactions 1902;81:1185.

19 Goodwin LF, Sterne ET. Losses incurred in the preparation of acetone by the distillation of acetate of lime. Journal of Industrial & Engineering Chemistry 1920;12:240.

20 Kon GAR. XCII.—The formation and stability of spiro-compounds. part IV. ketones derived from open-chain and cyclic glutaric acids. Journal of the Chemical Society, Transactions 1921;119:810.

21 Ardagh EGR, Barbour AD, McClellan GE, McBride EW. Distillation of acetate of lime. Industrial & Engineering Chemistry 1924;16:1133.

22 Bell J, Reed RI. Isotopic tracer studies of pyrolytic reactions. part I. the formation of acetaldehyde. Journal of the Chemical Society (Resumed) 1952:1383.

23 O'Neill WA, Reed RI. The pyrogenesis of ketones. part I. the formation of the dipropyl ketones. Journal of the Chemical Society (Resumed) 1953:3911.

24 Lee CC, Spinks JWT. The mechanism of the ketonic pyrolysis of calcium carboxylates. The Journal of Organic Chemistry 1953;18:1079.

25 Lee CC, Spinks JWT. The pyrolysis of calcium salts of carboxylic acids. Canadian Journal of Chemistry 1953;31:103.

26 Reed RI. Isotopic studies on the formation of ketones by the catalytic decomposition of certain acids. Journal of the Chemical Society (Resumed) 1955:4423.

27 Reed RI, Thornley MB. The formation of ketones. part III. the pyrolysis of sodium acetate and some sodium dicarboxylates. Journal of the Chemical Society (Resumed) 1957:3714.

28 Nakai R, Sugii M, Nakao H. Isotopic tracer studies of the ketonic pyrolysis of sodium carboxylates. Journal of the American Chemical Society 1959;81:1003.

29 Ötvös L, Noszkó L. Investigation of the pyrolytic decarboxylation of carboxylic acids with 14C mechanism of the formation of camphor from homocamphoric acid. Tetrahedron Letters 1960;1:19.

30 Hites RA, Biemann K. Mechanism of ketonic decarboxylation. pyrolysis of calcium decanoate. Journal of the American Chemical Society 1972;94:5772.

31 Miller AL, Cook NC, Whitmore FC. The ketonic decarboxylation reaction: the ketonic decarboxylation of trimethylacetic acid and isobutyric acid. Journal of the American Chemical Society 1950;72:2732.

32 Young S. Distillation principles and processes. London: Macmillan and Co., Limited; 1922.

33 Moldoveanu SC. Pyrolysis of organic molecules with applications to health and environmental issues. Amsterdam, Oxford: Elsevier; 2010.

34 Valor A, Reguera E, Torres-García E, Mendoza S, Sanchez-Sinencio F. Thermal decomposition of the calcium salts of several carboxylic acids. Thermochimica Acta 2002;389:133.

35 Mu J, Perlmutter DD. Thermal decomposition of carbonates, carboxylates, oxalates, acetates, formates, and hydroxides. Thermochimica Acta 1981;49:207.

36 Waring CE, Mutter WE. The kinetics of the thermal decomposition of gaseous methyl ethyl ketone. Journal of the American Chemical Society 1948;70:4073.

37 Waring CE, Spector M. The mechanism of the thermal decomposition of methyl ethyl ketone. Journal of the American Chemical Society 1955;77:6453.

38 McNesby JR, Davis TW, Gordon AS. Pyrolysis of mixtures of acetone and acetone-d6. Journal of the American Chemical Society 1954;76:823.

39 Johnston J. The thermal dissociation of calcium carbonate. Journal of the American Chemical Society 1910;32:938.

40 Beruto DT, Botter R. Liquid-like H_2O adsorption layers to catalyze the $Ca(OH)_2/CO_2$ solid-gas reaction and to form a non-protective solid product layer at 20°C. Journal of the European Ceramic Society 2000;20:497.

41 Duruz JJ, Michels HJ, Ubbelohde AR. Decomposition reactions of sodium propionate. Journal of the Chemical Society B: Physical Organic 1971:1505.

42 Barry WT, Walters WD. The thermal decomposition of methyl n-butyl ketone. Journal of the American Chemical Society 1957;79:2102.

43 Hurd CD, Kocour C. The ketenic decomposition of methylethyl ketone. Journal of the American Chemical Society 1923;45:2167.

44 Afzal M, Butt PK, Ahmad H. Kinetics of thermal decomposition of metal acetates. Journal of Thermal Analysis and Calorimetry 1991;37:1015.

45 Conesa JA, Marcilla A, Caballero JA, Font R. Comments on the validity and utility of the different methods for kinetic analysis of thermogravimetric data. Journal of Analytical and Applied Pyrolysis 2001;58-59:617.

46 Friedman HL. Kinetics of thermal degradation of char-forming plastics from thermogravimetry. application to a phenolic plastic. Journal of Polymer Science Part C: Polymer Symposia 1964;6:183.

47 Miura K. A new and simple method to estimate $f(E)$ and $k_0(E)$ in the distributed activation energy model from three sets of experimental data. Energy & Fuels 1995;9:302.

48 Li C-R, Tang T. Dynamic thermal analysis of solid-state reactions. Journal of Thermal Analysis and Calorimetry 1997;49:1243.

49 Li C-R, Tang TB. A new method for analysing non-isothermal thermoanalytical data from solid-state reactions. Thermochimica Acta 1999;325:43.

50 Li C-R, Tang TB. Isoconversion method for kinetic analysis of solid-state reactions from dynamic thermoanalytical data. Journal of Materials Science 1999;34:3467.

51 Vyazovkin S, Dollimore D. Linear and nonlinear procedures in isoconversional computations of the activation energy of nonisothermal reactions in solids. Journal of Chemical Information and Computer Sciences 1996;36:42.

52 Vyazovkin S. Advanced isoconversional method. Journal of Thermal Analysis and Calorimetry 1997;49:1493.

53 Vyazovkin S. Evaluation of activation energy of thermally stimulated solid-state reactions under arbitrary variation of temperature. Journal of Computational Chemistry 1997;18:393.

54 Doyle CD. Estimating isothermal life from thermogravimetric data. Journal of Applied Polymer Science 1962;6:639.

55 Coats AW, Redfern JP. Kinetic parameters from thermogravimetric data. Nature 1964;201:68.

56 Senum GI, Yang RT. Rational approximations of the integral of the Arrhenius function. Journal of Thermal Analysis and Calorimetry 1977;11:445.

57 Weber R. Extracting mathematically exact kinetic parameters from experimental data on combustion and pyrolysis of solid fuels. Journal of the Energy Institute 2008;81:226.

58 Galwey AK, Brown ME. Thermal decomposition of ionic solids Amsterdam: Elsevier Science B.V.; 1999.

59 Avrami M. Kinetics of phase change. I general theory. The Journal of Chemical Physics 1939;7:1103.

60 Avrami M. Kinetics of phase change. II transformation-time relations for random distribution of nuclei. The Journal of Chemical Physics 1940;8:212.

61 Avrami M. Granulation, phase change, and microstructure, kinetics of phase change. III. The Journal of Chemical Physics 1941;9:177.

62 Šesták J, Berggren G. Study of the kinetics of the mechanism of solid-state reactions at increasing temperatures. Thermochimica Acta 1971;3:1.

63 Šesták J. Diagnostic limits of phenomenological kinetic models introducing the accommodation function. Journal of Thermal Analysis and Calorimetry 1990;36:1997.

64 Málek J, Criado JM. Is the Šesták-Berggren equation a general expression of kinetic models? Thermochimica Acta 1991;175:305.

65 Koga N. Kinetic analysis of thermoanalytical data by extrapolating to infinite temperature. Thermochimica Acta 1995;258:145.

66 Adelson SK. Pyrolytic decompostion of volatile fatty acid salts. Chemical Engineering. College Station: Texas A&M University; 1994.

67 Yeh H-W. Pyrolytic decomposition of carboxylate salts. Chemical Engineering. College Station: Texas A&M Universtiy; 2002.

APPENDIX A:

INPUT SUMMARY FROM GIBBS FREE ENERGY MINIMIZATION SIMULATION

FOR SIMULATED CALCIUM FEED SALTS IN ASPEN PLUS, V7.2

```
;
;Input Summary created by Aspen Plus Rel. 24.0 at 14:52:26 Wed Apr 20, 2011
;Directory   Filename C:\Users\m0l9510\AppData\Local\Temp\~ap4a00.txt
;


DYNAMICS
   DYNAMICS RESULTS=ON

IN-UNITS SI FLOW='gm/min' MASS-FLOW='gm/min' MOLE-FLOW='mol/min'  &
      VOLUME-FLOW='l/min' PRESSURE=torr TEMPERATURE=C DELTA-T=C  &
      HEAD=meter FLUX='l/sqm-sec' MASS-FLUX='gm/sqcm-s'  &
      PDROP-PER-HT='torr/m' PDROP=torr INVERSE-PRES='1/torr'

DEF-STREAMS MIXCISLD ALL

SIM-OPTIONS
   IN-UNITS MET VOLUME-FLOW='cum/hr' ENTHALPY-FLO='Gcal/hr'  &
      HEAT-TRANS-C='kcal/hr-sqm-K' PRESSURE=bar TEMPERATURE=C  &
      VOLUME=cum DELTA-T=C HEAD=meter MASS-DENSITY='kg/cum'  &
      MOLE-ENTHALP='kcal/mol' MASS-ENTHALP='kcal/kg' HEAT=Gcal  &
      MOLE-CONC='mol/l' PDROP=bar
   SIM-OPTIONS OLD-DATABANK=NO

DESCRIPTION "
   Solids Simulation with Metric Units :
   C, bar, kg/hr, kmol/hr, Gcal, cum/hr.

   Property Method: None

   Flow basis for input: Mass

DATABANKS 'APV72 PURE24' / 'APV72 AQUEOUS' / 'APV72 SOLIDS' /  &
      'APV72 INORGANIC' / NOASPENPCD

PROP-SOURCES 'APV72 PURE24' / 'APV72 AQUEOUS' / 'APV72 SOLIDS' &
       / 'APV72 INORGANIC'
```

```
COMPONENTS
   "CA(ACE)2" CAC4H6O4 /
   "CA(PRO)2" "CA(PROP)2" /
   "CA(BUT)2" "CA(BUT)2" /
   "CA(PEN)2" "CA(PENT)2" /
   CACO3 CACO3-A /
   ACETONE C3H6O-1 /
   2-BUTANO C4H8O-3 /
   2-PENTAN C5H10O-2 /
   2-HEXANO C6H12O-D3 /
   3-PENTAN C5H10O-4 /
   3-HEXANO C6H12O /
   3-HEPTAN C7H14O-E1 /
   4-HEPTAN C7H14O-E2 /
   4-OCTANO C8H16O-D3 /
   5-NONANO C9H18O-E2 /
   WATER H2O

FLOWSHEET
   BLOCK REACTOR IN=SALT OUT=KETONE

PROPERTIES NRTL

PROP-DATA REVIEW-1
   IN-UNITS MET VOLUME-FLOW='cum/hr' ENTHALPY-FLO='Gcal/hr'  &
      HEAT-TRANS-C='kcal/hr-sqm-K' PRESSURE=bar TEMPERATURE=C  &
      VOLUME=cum DELTA-T=C HEAD=meter MASS-DENSITY='kg/cum'  &
      MOLE-ENTHALP='kcal/mol' MASS-ENTHALP='kcal/kg' HEAT=Gcal  &
      MOLE-CONC='mol/l' PDROP=bar
   PROP-LIST DGSFRM / DHSFRM
   PVAL "CA(PRO)2" -333 / -353
   PVAL "CA(BUT)2" -333 / -353
   PVAL "CA(PEN)2" -333 / -353
   PROP-LIST DGSFRM
   PVAL "CA(ACE)2" -333

PROP-DATA NRTL-1
   IN-UNITS MET VOLUME-FLOW='cum/hr' ENTHALPY-FLO='Gcal/hr'  &
      HEAT-TRANS-C='kcal/hr-sqm-K' PRESSURE=bar TEMPERATURE=C  &
      VOLUME=cum DELTA-T=C HEAD=meter MASS-DENSITY='kg/cum'  &
      MOLE-ENTHALP='kcal/mol' MASS-ENTHALP='kcal/kg' HEAT=Gcal  &
      MOLE-CONC='mol/l' PDROP=bar
   PROP-LIST NRTL
```

BPVAL 2-BUTANO WATER 0.0 201.3011000 .3000000000 0.0 0.0 &
0.0 73.30000000 100.0000000
BPVAL WATER 2-BUTANO 0.0 1087.744000 .3000000000 0.0 0.0 &
0.0 73.30000000 100.0000000
BPVAL 2-PENTAN WATER -5.934900000 1958.433200 .2000000000 &
0.0 0.0 0.0 0.0 65.00000000
BPVAL WATER 2-PENTAN 12.19090000 -2447.230200 .2000000000 &
0.0 0.0 0.0 0.0 65.00000000
BPVAL 2-HEXANO WATER -4.093900000 1410.315900 .2000000000 &
0.0 0.0 0.0 10.00000000 50.00000000
BPVAL WATER 2-HEXANO 11.95150000 -1999.085700 .2000000000 &
0.0 0.0 0.0 10.00000000 50.00000000
BPVAL 2-BUTANO 3-PENTAN 0.0 -289.8223000 .3000000000 0.0 &
0.0 0.0 80.31000000 99.40000000
BPVAL 3-PENTAN 2-BUTANO 0.0 382.0600000 .3000000000 0.0 &
0.0 0.0 80.31000000 99.40000000
BPVAL 3-PENTAN WATER 2.783500000 1584.356800 .2000000000 &
0.0 -1.230600000 0.0 3.000000000 162.1000000
BPVAL WATER 3-PENTAN 115.2036000 -6954.594700 .2000000000 &
0.0 -15.44790000 0.0 3.000000000 162.1000000
BPVAL 3-PENTAN 3-HEXANO 0.0 246.3425000 .3000000000 0.0 &
0.0 0.0 101.4000000 123.8000000
BPVAL 3-HEXANO 3-PENTAN 0.0 -202.2620000 .3000000000 0.0 &
0.0 0.0 101.4000000 123.8000000
BPVAL 3-HEXANO WATER -1.825700000 821.2336000 .2000000000 &
0.0 0.0 0.0 20.00000000 30.00000000
BPVAL WATER 3-HEXANO 10.54260000 -1605.540600 .2000000000 &
0.0 0.0 0.0 20.00000000 30.00000000
BPVAL 3-PENTAN 4-HEPTAN 0.0 190.4777000 .3000000000 0.0 &
0.0 0.0 101.4000000 144.1000000
BPVAL 4-HEPTAN 3-PENTAN 0.0 -187.3279000 .3000000000 0.0 &
0.0 0.0 101.4000000 144.1000000
BPVAL 3-HEXANO 4-HEPTAN 0.0 -351.8266000 .4500000000 0.0 &
0.0 0.0 123.4000000 144.1000000
BPVAL 4-HEPTAN 3-HEXANO 0.0 732.7732000 .4500000000 0.0 &
0.0 0.0 123.4000000 144.1000000
BPVAL 4-HEPTAN WATER 252.7309000 -12207.13960 .2000000000 &
0.0 -36.19950000 0.0 0.0 75.00000000
BPVAL WATER 4-HEPTAN 237.5792000 -11507.97750 .2000000000 &
0.0 -33.95300000 0.0 0.0 75.00000000
BPVAL 5-NONANO WATER 11.78610000 -1049.309000 .2000000000 &
0.0 0.0 0.0 10.00000000 50.00000000
BPVAL WATER 5-NONANO 11.74130000 -1035.711100 .2000000000 &
0.0 0.0 0.0 10.00000000 50.00000000

```
   BPVAL ACETONE 2-BUTANO -8.098500000 2364.934300 .3000000000  &
      0.0 0.0 0.0 56.20000000 79.50000000
   BPVAL 2-BUTANO ACETONE 5.102500000 -1083.495700 .3000000000  &
      0.0 0.0 0.0 56.20000000 79.50000000
   BPVAL ACETONE 3-PENTAN 0.0 -222.5506000 .3000000000 0.0  &
      0.0 0.0 56.20000000 101.7000000
   BPVAL 3-PENTAN ACETONE 0.0 276.5292000 .3000000000 0.0 0.0  &
      0.0 56.20000000 101.7000000
   BPVAL ACETONE WATER 6.398100000 -1808.991000 .3000000000  &
      0.0 0.0 0.0 20.00000000 95.10000000
   BPVAL WATER ACETONE .0544000000 419.9716000 .3000000000 0.0  &
      0.0 0.0 20.00000000 95.10000000

DEF-STREAM-C CONVEN MIXED CISOLID

PROP-SET ALL-SUBS
   IN-UNITS MET VOLUME-FLOW='cum/hr' ENTHALPY-FLO='Gcal/hr'  &
      HEAT-TRANS-C='kcal/hr-sqm-K' PRESSURE=bar TEMPERATURE=C  &
      VOLUME=cum DELTA-T=C HEAD=meter MASS-DENSITY='kg/cum'  &
      MOLE-ENTHALP='kcal/mol' MASS-ENTHALP='kcal/kg' HEAT=Gcal  &
      MOLE-CONC='mol/l' PDROP=bar
   PROPNAME-LIS VOLFLMX MASSVFRA MASSSFRA RHOMX MASSFLOW
TEMP  &
      PRES UNITS='kg/cum' SUBSTREAM=ALL
;  "Entire Stream Flows, Density, Phase Frac, T, P"


STREAM SALT
   IN-UNITS MET VOLUME-FLOW='cum/hr' ENTHALPY-FLO='Gcal/hr'  &
      HEAT-TRANS-C='kcal/hr-sqm-K' PRESSURE=bar TEMPERATURE=C  &
      VOLUME=cum DELTA-T=C HEAD=meter MASS-DENSITY='kg/cum'  &
      MOLE-ENTHALP='kcal/mol' MASS-ENTHALP='kcal/kg' HEAT=Gcal  &
      MOLE-CONC='mol/l' PDROP=bar
   SUBSTREAM MIXED TEMP=21. PRES=5. <torr>  &
      MASS-FLOW=12. <gm/min>
   MASS-FRAC WATER 1.
   SUBSTREAM CISOLID TEMP=21. PRES=5. <torr>  &
      MASS-FLOW=88. <gm/min>
   MASS-FRAC "CA(ACE)2" 0.645 / "CA(PRO)2" 0.166 /  &
      "CA(BUT)2" 0.121 / "CA(PEN)2" 0.068

BLOCK REACTOR RGIBBS
   IN-UNITS MET VOLUME-FLOW='cum/hr' ENTHALPY-FLO='Gcal/hr'  &
      HEAT-TRANS-C='kcal/hr-sqm-K' PRESSURE=bar TEMPERATURE=C  &
```

```
      VOLUME=cum DELTA-T=C HEAD=meter MASS-DENSITY='kg/cum'  &
      MOLE-ENTHALP='kcal/mol' MASS-ENTHALP='kcal/kg' HEAT=Gcal  &
      MOLE-CONC='mol/l' PDROP=bar
   PARAM TEMP=450. PRES=5. <torr>
   PROD CACO3 SS / ACETONE / 2-BUTANO / 2-PENTAN /  &
      2-HEXANO / 3-PENTAN / 3-HEXANO / 3-HEPTAN / 4-HEPTAN / &
      4-OCTANO / 5-NONANO / WATER

UTILITY BFW GENERAL
   IN-UNITS MET VOLUME-FLOW='cum/hr' ENTHALPY-FLO='Gcal/hr'  &
      HEAT-TRANS-C='kcal/hr-sqm-K' PRESSURE=bar TEMPERATURE=C  &
      VOLUME=cum DELTA-T=C HEAD=meter MASS-DENSITY='kg/cum'  &
      MOLE-ENTHALP='kcal/mol' MASS-ENTHALP='kcal/kg' HEAT=Gcal  &
      MOLE-CONC='mol/l' PDROP=bar
   COST PRICE=0. <$/kg>
   PARAM UTILITY-TYPE=GENERAL PRES=1. PRES-OUT=50. <psig>  &
      TIN=90. <F> VFR-OUT=1. CALOPT=FLASH
   COMPOSITION WATER 1.

UTILITY CW GENERAL
   IN-UNITS MET VOLUME-FLOW='cum/hr' ENTHALPY-FLO='Gcal/hr'  &
      HEAT-TRANS-C='kcal/hr-sqm-K' PRESSURE=bar TEMPERATURE=C  &
      VOLUME=cum DELTA-T=C HEAD=meter MASS-DENSITY='kg/cum'  &
      MOLE-ENTHALP='kcal/mol' MASS-ENTHALP='kcal/kg' HEAT=Gcal  &
      MOLE-CONC='mol/l' PDROP=bar
   COST PRICE=0.013 <$/tonne>
   PARAM UTILITY-TYPE=WATER PRES=1.25 PRES-OUT=1. TIN=90. <F>  &
      TOUT=120. <F> CALOPT=FLASH

EO-CONV-OPTI

STREAM-REPOR MOLEFLOW MASSFLOW MOLEFRAC MASSFRAC  &
      PROPERTIES=ALL-SUBS

PROPERTY-REP NOPARAM-PLUS
;
;
;
;
;
```

APPENDIX B:

INPUT SUMMARY FROM GIBBS FREE ENERGY MINIMIZATION SIMULATION

FOR EQUIMOLAR SODIUM CARBOXYLATE SALTS IN ASPEN PLUS, V7.3

```
;
;Input Summary created by Aspen Plus Rel. 25.0 at 16:22:26 Thu Apr 12, 2012
;Directory G:\Papers\Product Compostion Model Comparison\Aspen  Filename
C:\Users\m0l9510\AppData\Local\Temp\~ap94e7.txt
;


DYNAMICS
   DYNAMICS RESULTS=ON

IN-UNITS SI FLOW='gm/min' MASS-FLOW='gm/min' MOLE-FLOW='mol/min'  &
       VOLUME-FLOW='l/min' PRESSURE=torr TEMPERATURE=C DELTA-T=C  &
       HEAD=meter FLUX='l/sqm-sec' MASS-FLUX='gm/sqcm-s'  &
       PDROP-PER-HT='torr/m' PDROP=torr INVERSE-PRES='1/torr'

DEF-STREAMS MIXCISLD ALL

DESCRIPTION "
   Solids Simulation with Metric Units :
   C, bar, kg/hr, kmol/hr, Gcal, cum/hr.

   Property Method: None

   Flow basis for input: Mass

 DATABANKS 'APV73 PURE25' / 'APV73 AQUEOUS' / 'APV73 SOLIDS' /  &
       'APV73 INORGANIC' / NOASPENPCD

PROP-SOURCES 'APV73 PURE25' / 'APV73 AQUEOUS' / 'APV73 SOLIDS' &
       / 'APV73 INORGANIC'

COMPONENTS
   "NA(ACE)" C2H3NAO2 /
   "NA(PRO)" "NA(PROP)" /
   "NA(BUT)" "NA(BUT)" /
   "NA(PEN)" "NA(PENT)" /
   NA2CO3 NA2CO3 /
```

```
   "CA(ACE)2" CAC4H6O4 /
   "CA(PRO)2" "CA(PROP)2" /
   "CA(BUT)2" "CA(BUT)2" /
   "CA(PEN)2" "CA(PENT)2" /
   CACO3 CACO3-A /
   ACETONE C3H6O-1 /
   2-BUTANO C4H8O-3 /
   2-PENTAN C5H10O-2 /
   2-HEXANO C6H12O-D3 /
   3-PENTAN C5H10O-4 /
   3-HEXANO C6H12O /
   3-HEPTAN C7H14O-E1 /
   4-HEPTAN C7H14O-E2 /
   4-OCTANO C8H16O-D3 /
   5-NONANO C9H18O-E2 /
   WATER H2O

CISOLID-COMPS "NA(ACE)" "NA(PRO)" "NA(BUT)" "NA(PEN)" NA2CO3  &
      "CA(ACE)2" "CA(PRO)2" "CA(BUT)2" "CA(PEN)2" CACO3

FLOWSHEET
   BLOCK REACTOR IN=SALT OUT=KETONE

PROPERTIES NRTL

PROP-DATA REVIEW-1
   IN-UNITS MET VOLUME-FLOW='cum/hr' ENTHALPY-FLO='Gcal/hr'  &
      HEAT-TRANS-C='kcal/hr-sqm-K' PRESSURE=bar TEMPERATURE=C  &
      VOLUME=cum DELTA-T=C HEAD=meter MASS-DENSITY='kg/cum'  &
      MOLE-ENTHALP='kcal/mol' MASS-ENTHALP='kcal/kg' HEAT=Gcal  &
      MOLE-CONC='mol/l' PDROP=bar
   PROP-LIST DGSFRM / DHSFRM
   PVAL "CA(PRO)2" -333 / -353
   PVAL "CA(BUT)2" -333 / -353
   PVAL "CA(PEN)2" -333 / -353
   PROP-LIST DGSFRM
   PVAL "CA(ACE)2" -333

PROP-DATA NRTL-1
   IN-UNITS MET VOLUME-FLOW='cum/hr' ENTHALPY-FLO='Gcal/hr'  &
      HEAT-TRANS-C='kcal/hr-sqm-K' PRESSURE=bar TEMPERATURE=C  &
      VOLUME=cum DELTA-T=C HEAD=meter MASS-DENSITY='kg/cum'  &
      MOLE-ENTHALP='kcal/mol' MASS-ENTHALP='kcal/kg' HEAT=Gcal  &
      MOLE-CONC='mol/l' PDROP=bar
```

PROP-LIST NRTL
BPVAL 2-BUTANO WATER 0.0 201.3011000 .3000000000 0.0 0.0 &
0.0 73.30000000 100.0000000
BPVAL WATER 2-BUTANO 0.0 1087.744000 .3000000000 0.0 0.0 &
0.0 73.30000000 100.0000000
BPVAL 2-PENTAN WATER -3.665100000 1273.258900 .2000000000 &
0.0 0.0 0.0 31.73000000 193.7300000
BPVAL WATER 2-PENTAN 10.16230000 -1845.002800 .2000000000 &
0.0 0.0 0.0 31.73000000 193.7300000
BPVAL 2-HEXANO WATER -1.868200000 750.4318000 .2000000000 &
0.0 0.0 0.0 31.73000000 195.5300000
BPVAL WATER 2-HEXANO 9.448700000 -1244.305000 .2000000000 &
0.0 0.0 0.0 31.73000000 195.5300000
BPVAL 2-BUTANO 3-PENTAN 0.0 -289.8223000 .3000000000 0.0 &
0.0 0.0 80.31000000 99.40000000
BPVAL 3-PENTAN 2-BUTANO 0.0 382.0600000 .3000000000 0.0 &
0.0 0.0 80.31000000 99.40000000
BPVAL 3-PENTAN WATER -2.748400000 1090.512100 .2000000000 &
0.0 0.0 0.0 31.73000000 193.7300000
BPVAL WATER 3-PENTAN 9.367900000 -1637.873300 .2000000000 &
0.0 0.0 0.0 31.73000000 193.7300000
BPVAL 3-PENTAN 3-HEXANO 0.0 246.3425000 .3000000000 0.0 &
0.0 0.0 101.4000000 123.8000000
BPVAL 3-HEXANO 3-PENTAN 0.0 -202.2620000 .3000000000 0.0 &
0.0 0.0 101.4000000 123.8000000
BPVAL 3-HEXANO WATER -1.825700000 821.2336000 .2000000000 &
0.0 0.0 0.0 20.00000000 30.00000000
BPVAL WATER 3-HEXANO 10.54260000 -1605.540600 .2000000000 &
0.0 0.0 0.0 20.00000000 30.00000000
BPVAL 3-PENTAN 4-HEPTAN 0.0 190.4777000 .3000000000 0.0 &
0.0 0.0 101.4000000 144.1000000
BPVAL 4-HEPTAN 3-PENTAN 0.0 -187.3279000 .3000000000 0.0 &
0.0 0.0 101.4000000 144.1000000
BPVAL 3-HEXANO 4-HEPTAN 0.0 -351.8266000 .4500000000 0.0 &
0.0 0.0 123.4000000 144.1000000
BPVAL 4-HEPTAN 3-HEXANO 0.0 732.7732000 .4500000000 0.0 &
0.0 0.0 123.4000000 144.1000000
BPVAL 4-HEPTAN WATER -1.022800000 760.5935000 .2000000000 &
0.0 0.0 0.0 31.73000000 193.7300000
BPVAL WATER 4-HEPTAN 10.11390000 -1200.776700 .2000000000 &
0.0 0.0 0.0 31.73000000 193.7300000
BPVAL 5-NONANO WATER -.0793000000 609.3645000 .2000000000 &
0.0 0.0 0.0 31.73000000 193.7300000
BPVAL WATER 5-NONANO 12.25860000 -1173.838000 .2000000000 &

```
      0.0 0.0 0.0 31.73000000 193.7300000
   BPVAL ACETONE 2-BUTANO -8.098500000 2364.934300 .3000000000  &
      0.0 0.0 0.0 56.20000000 79.50000000
   BPVAL 2-BUTANO ACETONE 5.102500000 -1083.495700 .3000000000  &
      0.0 0.0 0.0 56.20000000 79.50000000
   BPVAL ACETONE 3-PENTAN 0.0 -222.5506000 .3000000000 0.0  &
      0.0 0.0 56.20000000 101.7000000
   BPVAL 3-PENTAN ACETONE 0.0 276.5292000 .3000000000 0.0 0.0  &
      0.0 56.20000000 101.7000000
   BPVAL ACETONE WATER 6.398100000 -1808.991000 .3000000000  &
      0.0 0.0 0.0 20.00000000 95.10000000
   BPVAL WATER ACETONE .0544000000 419.9716000 .3000000000 0.0  &
      0.0 0.0 20.00000000 95.10000000
   BPVAL 3-HEPTAN WATER -1.215900000 797.4041000 .2000000000  &
      0.0 0.0 0.0 31.73000000 193.7300000
   BPVAL WATER 3-HEPTAN 10.55680000 -1328.926700 .2000000000  &
      0.0 0.0 0.0 31.73000000 193.7300000

DEF-STREAM-C CONVEN MIXED CISOLID

PROP-SET ALL-SUBS
   IN-UNITS MET VOLUME-FLOW='cum/hr' ENTHALPY-FLO='Gcal/hr'  &
      HEAT-TRANS-C='kcal/hr-sqm-K' PRESSURE=bar TEMPERATURE=C  &
      VOLUME=cum DELTA-T=C HEAD=meter MASS-DENSITY='kg/cum'  &
      MOLE-ENTHALP='kcal/mol' MASS-ENTHALP='kcal/kg' HEAT=Gcal  &
      MOLE-CONC='mol/l' PDROP=bar
   PROPNAME-LIS VOLFLMX MASSVFRA MASSSFRA RHOMX MASSFLOW
TEMP  &
      PRES UNITS='kg/cum' SUBSTREAM=ALL
;  "Entire Stream Flows, Density, Phase Frac, T, P"


STREAM SALT
   IN-UNITS MET VOLUME-FLOW='cum/hr' ENTHALPY-FLO='Gcal/hr'  &
      HEAT-TRANS-C='kcal/hr-sqm-K' PRESSURE=bar TEMPERATURE=C  &
      VOLUME=cum DELTA-T=C HEAD=meter MASS-DENSITY='kg/cum'  &
      MOLE-ENTHALP='kcal/mol' MASS-ENTHALP='kcal/kg' HEAT=Gcal  &
      MOLE-CONC='mol/l' PDROP=bar
   SUBSTREAM MIXED TEMP=21. PRES=5. <torr> MASS-FLOW=0. <gm/min>
   MASS-FRAC WATER 1.
   SUBSTREAM CISOLID TEMP=21. PRES=5. <torr>  &
      MASS-FLOW=100. <gm/min>
   MASS-FRAC "NA(ACE)" 0.1969 / "NA(PRO)" 0.2251 / "NA(BUT)"  &
      0.2671 / "NA(PEN)" 0.311
```

```
BLOCK REACTOR RGIBBS
   IN-UNITS MET VOLUME-FLOW='cum/hr' ENTHALPY-FLO='Gcal/hr'  &
      HEAT-TRANS-C='kcal/hr-sqm-K' PRESSURE=bar TEMPERATURE=C  &
      VOLUME=cum DELTA-T=C HEAD=meter MASS-DENSITY='kg/cum'  &
      MOLE-ENTHALP='kcal/mol' MASS-ENTHALP='kcal/kg' HEAT=Gcal  &
      MOLE-CONC='mol/l' PDROP=bar
   PARAM TEMP=450. PRES=5. <torr>
   PROD NA2CO3 SS / ACETONE / 2-BUTANO / 2-PENTAN /  &
      2-HEXANO / 3-PENTAN / 3-HEXANO / 3-HEPTAN / 4-HEPTAN / &
      4-OCTANO / 5-NONANO / WATER

UTILITY BFW GENERAL
   IN-UNITS MET VOLUME-FLOW='cum/hr' ENTHALPY-FLO='Gcal/hr'  &
      HEAT-TRANS-C='kcal/hr-sqm-K' PRESSURE=bar TEMPERATURE=C  &
      VOLUME=cum DELTA-T=C HEAD=meter MASS-DENSITY='kg/cum'  &
      MOLE-ENTHALP='kcal/mol' MASS-ENTHALP='kcal/kg' HEAT=Gcal  &
      MOLE-CONC='mol/l' PDROP=bar
   COST PRICE=0. <$/kg>
   PARAM UTILITY-TYPE=GENERAL PRES=1. PRES-OUT=50. <psig>  &
      TIN=90. <F> VFR-OUT=1. CALOPT=FLASH
   COMPOSITION WATER 1.

UTILITY CW GENERAL
   IN-UNITS MET VOLUME-FLOW='cum/hr' ENTHALPY-FLO='Gcal/hr'  &
      HEAT-TRANS-C='kcal/hr-sqm-K' PRESSURE=bar TEMPERATURE=C  &
      VOLUME=cum DELTA-T=C HEAD=meter MASS-DENSITY='kg/cum'  &
      MOLE-ENTHALP='kcal/mol' MASS-ENTHALP='kcal/kg' HEAT=Gcal  &
      MOLE-CONC='mol/l' PDROP=bar
   COST PRICE=0.013 <$/tonne>
   PARAM UTILITY-TYPE=WATER PRES=1.25 PRES-OUT=1. TIN=90. <F>  &
      TOUT=120. <F> CALOPT=FLASH

EO-CONV-OPTI

STREAM-REPOR MOLEFLOW MASSFLOW MOLEFRAC MASSFRAC  &
      PROPERTIES=ALL-SUBS

PROPERTY-REP NOPARAM-PLUS
;
;
;
;
;
```